Thermal and photostability studies of furosemide and its cyclodextrin mixtures

A thesis submitted in fulfilment of the
requirements for the degree of

MASTER OF SCIENCE

Of

RHODES UNIVERSITY

by

BABALWA BLOSSOM MELANE

March 2002

TABLE OF CONTENTS

LIST OF FIGURES

LIST OF TABLES

LIST OF ABBREVIATIONS

AUFS-absorption unit full scale

BCD -beta-cyclodextrin

CD -cyclodextrin

CRH- critical relative humidity

DMSO-dimethylsulfoxide

DSC -differential scanning calorimetry

DTA -differential thermal analyis

DTG- derivative thermogravimetry

EGA -evolved gas analysis

EMC-equilibrium moisture content

FR -furosemide

FTIR- Fourier transform infrared

GCD - gamma-cyclodextrin

HPLC- high-performance liquid chromatography

HSM- hot-stage microscopy

ICH - International Conference on Harmonisation

IR -infrared

MS-mass spectrometry

NMR-nuclear magnetic resonance

PTFE - polytetrafluroethylene

TA - thermal analysis

TG -thermogravimetry

UV-ultraviolet

UV/vis-ultraviolet-visible

XRD -X-ray diffraction

ACKNOWLEDGEMENTS

Professor Mike Brown, for his supervision, patience, support and encouragement, advancement, development and confidence in taking me as one of his students as well as teaching me to be independent and responsible.

Professor Beverly Glass, for her supervision, support, patience and helping me with the HPLC, as well as her confidence in taking me as one of her students.

Emmanuel Lamprecht, for helping with the instrumentation (TG, DSC, XRD and TG-FTIR) and his tolerance throughout the year and being considerate. Thank-you.

Edith Antunes for her willingness to help.

DAAD and NRF for providing financial assistance.

The friends I came across at Rhodes, for constant friendship, love, support, encouragement, patience and advice, always willing to listen, for showing me that everything is within my reach. To mention but a few: Thandiwsa Kani, Mmosimotsana Lebete, Patrick Hlabela, Robert, X-man, Moses K.Rotich, Vuyani Ngoyi and Vuyelwa Ndlebe, you were all stars and no one could have done it better than you. Then to all my old time friends for always being there supporting and encouraging me.

The rest of my family, my brothers, in particular **Sakhekile,** and my sister **Phumeza,** thanks very much for your support guys, you are stars.

Lastly to my parents, **Nontuthuzelo and Stembiso Melane** for their constant tenacity, love, friendship, support, willingness, guidance and always telling me the stars are always within reach "they can be yours", for my upbringing as well as my existence and inspiration and showing me that durability is a way of life. I thank the **Lord Almighty** in **Jesus Christ's** name for bringing me this far.

dedicated to my parents

Mr and Mrs Melane

ABSTRACT

Furosemide (Lasix®), abbreviated as FR and also known as frusemide, is a drug used for renal problems and treatment of cardiac edema. Various polymorphic forms of furosemide, dependent upon the method of preparation and thermal treatment, have been reported. The main thermal decomposition product of furosemide has been identified as saluamine. The dissolution properties of furosemide have also been reported to be improved by complexation with beta-cyclodextrin. Photostabilities of the different crystal forms have been studied.

Differential scanning calorimetry (DSC) and thermogravimetry (TG) have been used to examine the thermal behaviour of furosemide itself and of its physical and kneaded mixtures with beta-cyclodextrin (BCD) and gamma-cyclodextrin (GCD). There is strong evidence from DSC that complex formation between FR and GCD occurs. This is supported by IR and XRD data. Decreases in the intensity and broadening of the characteristic carbonyl (1660 cm^{-1}) and amine (1588 cm^{-1}) bands in the *kneaded* mixture, compared to the *physical* mixture, were observed with IR. X-ray diffraction results for the 1:3 molar ratio FR/GCD kneaded mixture showed a halo diffraction pattern characteristic of an amorphous solid and did not resemble patterns from the drug, or the gamma-cyclodextrin, or the physical mixture.

Photostability studies have been conducted on solid furosemide and its mixtures with GCD or BCD. An HPLC method was developed to determine the amount of drug remaining after exposure and the presence of any degradants. Results indicated that about 10 % degradation of the drug occurred during exposure for 16 hours at 550 W/m^2, with the appearance of polar degradants.

Although IR and DSC results for the 1:3 molar ratio FR/GCD kneaded mixture showed a probable strong interaction between FR and GCD, the photostability of FR was decreased. The 1:3 molar ratio FR/BCD kneaded mixture showed less photo-degradation than the 1:3 molar ratio FR/GCD mixture under similar conditions, suggesting that inclusion of the drug molecule (FR) is different in the two cyclodextrins.

Chapter 1

1. INTRODUCTION

1.1. Characteristics of furosemide (FR) and its clinical uses

Furosemide [1, 2] is a short-acting loop diuretic, known by the trade name of Lasix® [3] and sometimes referred to as frusemide. It is effective in the treatment of the edema due to hepatic, renal or cardiac failure, as well as edema due to burns. It can also be used to reduce urinary output if the patient has pregnancy complications; for treatment of hypertension, and as an adjunct in hypertensive crisis. Furosemide acts on the kidney to increase the body's loss of water and assorted minerals and electrolytes (e.g. salts of potassium, calcium and magnesium). Accumulation of fluids in the body tissues is thus decreased by removing water through excretion. The drug is available in two forms: as an injectable drug which is used in cases of acute heart-failure crisis; or in oral tablet form which is generally adequate for continued management after stabilization. Its toxicity involves abnormalities in fluid and electrolyte balance. Hyperuricemia and gastrointestinal side-effects are also commonly observed [4].

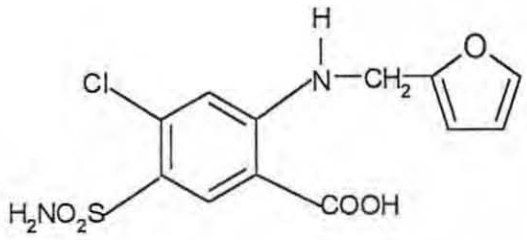

Figure 1.1 Furosemide (FR)

The empirical formula of furosemide (abbreviated to FR) is $C_{12}H_{11}ClN_2O_5S$ and it has a molecular mass of 330.8 g/mol. The elemental composition is C 43.57 %, H 3.35 %, Cl 10.72 %, N 8.47 %, O 24.19 % and S 9.70 %. It is a slightly yellow, crystalline powder, odourless and is almost tasteless.

Aqueous solutions of furosemide [5] have pH's between 8.9 and 9.3. Furosemide is usually characterized more by its pharmacological than its chemical similarities. It is regarded as a derivative of anthranilic acid, or o-aminobenzoic acid (see **Figure 1.4**). Because the drug molecule possesses a free carbonyl group, it is known to be a stronger acid than the thiazide diuretics [6]. The drug is excreted mostly unchanged, although a small amount of metabolism can take place on the furan ring [7]. The drug has a duration of action of about six to eight hours.

Furosemide is slightly soluble in water, chloroform and diethylether and highly soluble in acetone, methanol, dimethyl formamide [8] and solutions of alkali metal hydroxides [9]. The drug is known to be unstable to both heat and light and has to be stored at temperatures of 15-30 ^{0}C and must be protected from light, because exposure of the tablets may cause discolouration. Discoloured tablets are not allowed to be dispensed to patients [5].

The bioavailability of FR has been known to be poor and highly variable in oral dosage forms. This poor bioavailability has been speculated to be due to a variety of reasons; including poor aqueous solubility, site-specific absorption (which has shown that the stomach has a greater absorptive area for furosemide than the intestine, despite the smaller absorptive area in the stomach) and pre-systematic metabolism [10, 11]. Additional reasons include its instability in gastric and or duodenal juices [12], inter-and intra-patient variability, as well as formulation differences [13].

Because the drug is known to be only slightly soluble in water, improvement of its dissolution properties is essential. The *in vitro* dissolution behavior of a drug is closely related to its bioavailability [14]. Proudfoot [15] states that the rate at which a sparingly soluble drug dissolves in the gastrointestinal fluids may be the slowest step in the sequence of events leading to the appearance of the drug intact in the systematic circulation. Drug absorption and bioavailability are also known to depend on how rapidly the drug dissolves in the gastrointestinal fluids. Therefore, factors which influence the rate of dissolution will also influence the bioavailability of the drug.

Noyes-Whitney's equation [13] can be used to describe the process of dissolution in drugs:

$$dm/dt = \{(D\ A) / h\}(C_s-C)$$

where dm /dt = mass rate of dissolution, D = diffusion coefficient of the drug in solution in the gastrointestinal fluids, A = surface area of drug particles in contact with the gastrointestinal fluids, h = thickness of the diffusion layer around the drug particle, C_s = saturation solubility of the drug in the diffusion layer and C = the concentration of the drug in solution in the bulk of the gastrointestinal fluid.

Furosemide is known to absorb ultraviolet light at 275 and 345 nm and to fluoresce at 405 to 417 nm. The fluorescence is pH dependent [10].

Bundgaard, Nørgaard and Nielsen [17] reported that Sturm *et al.* [16] found that the furylmethyl group in the molecule is acid-labile and furosemide has been shown to undergo acid-catalyzed hydrolysis in aqueous solution to yield 4-chloro-5-sulphamoyl-anthranilic acid (saluamine).

Beyers *et al.* [18] reported that decomposition of furosemide occurs before or during melting. The degradation products formed were not described. The main thermal decomposition product of furosemide was also identified as saluamine [18].

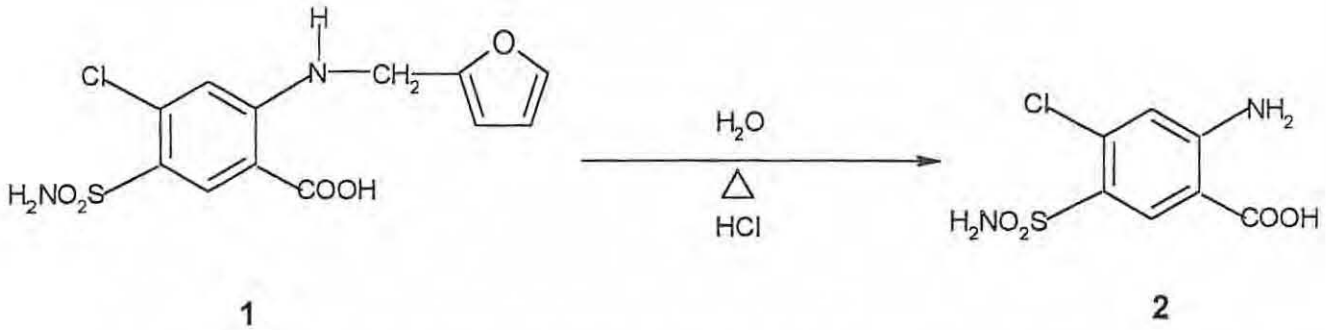

1 2

Figure 1.2 The formation of saluamine (**2**) through acid hydrolysis of furosemide (**1**), as reported by Beyers *et al.* [18].

1.2. Polymorphic forms and thermal behaviour

The melting range of furosemide has been reported to be 217-222 °C [19]. This drug was initially reported by Doherty and York [19] to have two polymorphic forms: Form I and Form II. These two forms were prepared by recrystallization of commercial furosemide, using methanol and ethanol solutions, respectively. DSC curves of the compounds showed two endotherms: the first, around 136-139 °C, is associated with Form I and is reversible (with $\Delta H = 2.2$ kJ/mol, or 67 J/g). The second endotherm corresponds to melting with decomposition. Form II did not show the first endotherm around 136-139 °C. Doherty and York proposed that the weak endotherm around 136-139 °C must be a subtle change in molecular conformation and crystal packing. They recorded a series of variable temperature FTIR spectra and the results obtained suggested that the two forms were discrete crystal structures of FR and that they did not transform on heating to 180 °C, within the experimental conditions used.

NMR data also suggested changes in the molecular conformation of the FR molecule in the crystal Form II that were associated with an altered hydrogen-bonding sequence and a different crystal packing arrangement, in agreement with their IR and XRD data [19].

No thermal route was found for conversion of Form I to Form II. Hot-stage microscopy showed an abrupt disintegration of crystals of Form I around 135-140 °C without any sign of melting [19]

(the extent of the mass loss was not given). Form II has been reported [19] to have a greater dissolution rate in water than Form I. Further research by Abdulla et al. [6] showed that there are three forms of furosemide. FR I was prepared from methanol solution, FR II, which was prepared from 5 % ammonia solution and was shown to be an ammonium salt, and FR III, which was prepared from n-butanol solution.

FR III showed a phase transition at 105 ^{0}C to FR I. The IR spectra of FR I and FR II differ in the regions 3380-3260 cm^{-1} and 1420-1370 cm^{-1}. FR I shows a band at 3380 cm^{-1}, characteristic of the secondary amine group, and two peaks at 3320 cm^{-1} and 3260 cm^{-1} corresponding to the sulfonamide amino group. Spectral changes also occurred in the SO_2 absorption region 1420-1370 cm^{-1}.

Matsuda and Tatsumi [20] obtained further forms of furosemide, Form IV and Form V, on heating the other forms to 180 ^{0}C. The DSC curve for Form IV was reported [20] to have a sharp endotherm at 93 ^{0}C, accompanied by a shoulder at 102 ^{0}C, and followed by a slight endotherm at 143 ^{0}C. The TG curve showed a mass loss of 17.3 % of the total mass between 70-127 ^{0}C, corresponding to the first endotherm. This suggests that desolvation occurs. The XRD pattern of this form, which had been heated once and then cooled, revealed it to be identical with Form I. The second endotherm at 143 ^{0}C was attributed to the resultant Form I undergoing transformation to a higher-temperature stable form. The DSC curve of Form V displayed [20] strong and weak endotherms at 89 and 139 ^{0}C, respectively, with the final melting endotherm at 218 ^{0}C. A 20.5 % loss in total mass over the temperature range from 89-218 ^{0}C, was indicated by the TG curve. It was suggested that the endotherm at 89 ^{0}C was caused by desolvation, thereby demonstrating the close agreement between the observed and theoretical values for a 1:1 dioxane solvate. From XRD results, Form V was shown to be a solvate with dioxane and to be transformed into Form I by desolvation at temperatures above 90 ^{0}C. The weak endotherm of Form V around 139 ^{0}C was found to correspond to that of Form I, indicating transformation of Form I into a higher-temperature stable form. An exotherm around 130 ^{0}C was also reported in the DSC curve for Form I.

The amorphous form of FR, which was also obtained by Matsuda and Tatsumi, was recognized as an unstable form [20]. It was prepared by spray drying. The DSC curve of this form showed an exotherm at about 103-104 ^{0}C and a melting endotherm at 214-215 ^{0}C. The cause of the exotherm was not determined, due to its small size, but it was found to be correlated with the transformation to a higher- temperature stable form, as observed in all the other forms.

XRD analysis of the amorphous form gave a characteristic halo pattern, instead of sharp diffraction peaks. The infrared spectrum gave broad absorptions throughout the entire range, due to the low degree of crystallinity possessed by this form. Matsuda and Tatsumi [20] drew up an interconversion scheme for furosemide, showing the transformation relationships and conditions for stability of these forms. Byrn *et al.* [21] redrew and summarized these interconversion routes. Form I is the most stable form at room temperature (**Figure 1.3**)

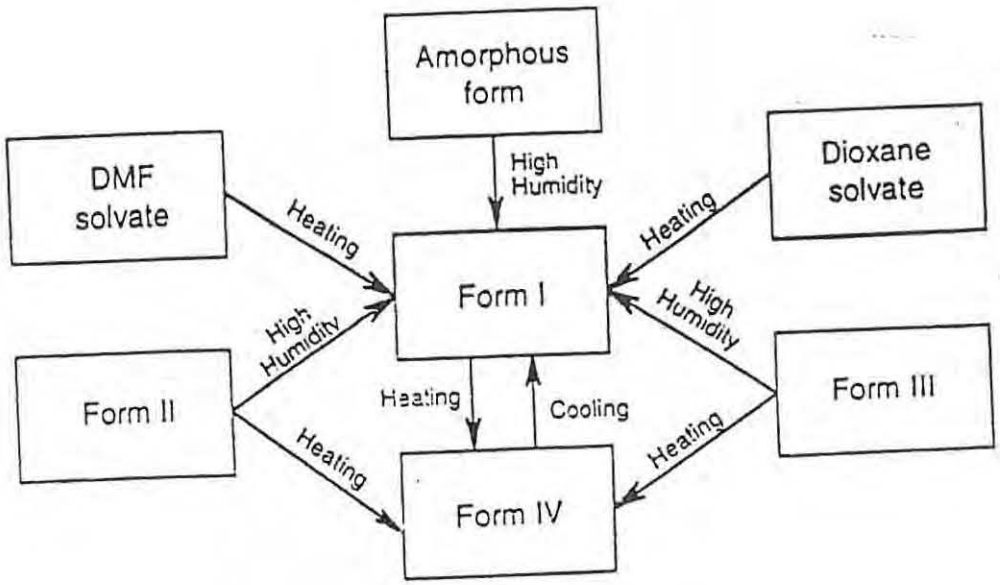

Figure 1.3 Interconversion scheme for furosemide solid forms under various conditions. Redrawn by Byrn *et al.*[21] from the scheme of Matsuda and Tatsumi, [20].

Beyers *et.al.* [18] reported that the main thermal decomposition product of furosemide at high temperatures (218 ^{0}C) was saluamine (4-chloro-4-sulfamoylanthranilic). Saluamine was formed by cleavage of the C-N bond (see **Figure 1. 4**). Cottrell [22] calculated that the experimental activation energy of 200 (±2) kJ mol^{-1}, was well below the expected activation energy of 247 (± 4) kJ mol^{-1} actually needed for the C-N cleavage [22]. This difference was explained as possible weakening of the C-N bond through the inductive effect of the furan ring and the delocalization of the electrons of the aniline nitrogen in the chlorosuphamoyl benzoic acid entity of furosemide [18].

Lamotte *et al.* [23] mentioned that, when some of the inter-and intramolecular bonds that form part of the hydrogen-bond network involving the sulfonamide groups in furosemide disappear, as in the structurally- related decomposition product saluamine, the aqueous solubility increases. Saluamine is approximately 30 times more soluble in water than furosemide, but can still be classified as a poorly water-soluble compound [23]. This poor solubility of saluamine was attributed to the strong hydrogen bonds between the amine and the carbonyl groups that also exist in furosemide [23].

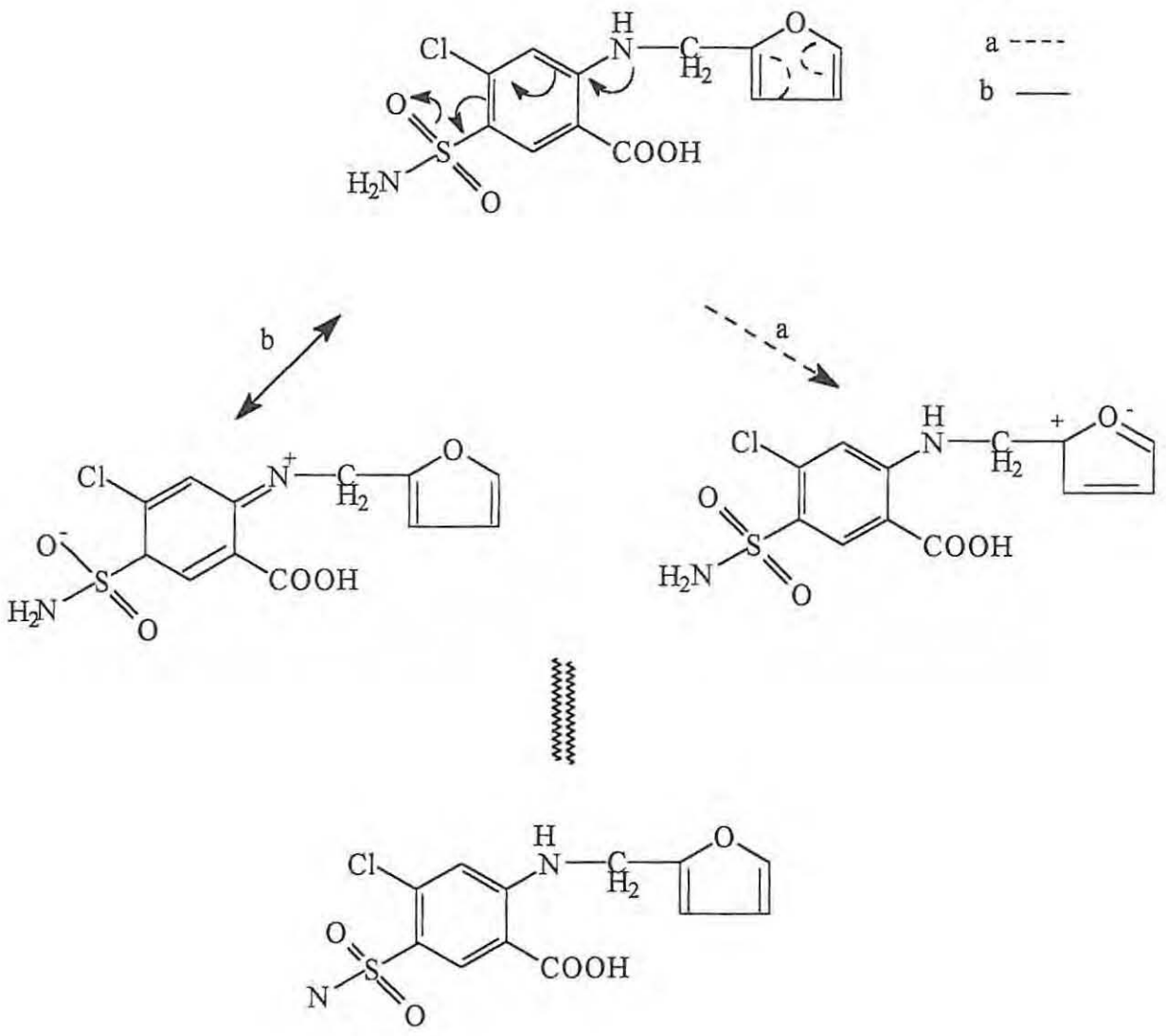

Figure 1.4 The weakening of the C-N bond in furosemide through **(a)** the negative inductive effect of the furan ring on the chlorosuphamoyl entity and **(b)** delocalization of the electrons of the aniline nitrogen in the benzoic acid entity, as reported by Beyers *et al.*[18].

1.3 Photostability of furosemide

Matsuda and Tatsumi [20] studied the photostability of FR tablets prepared from Forms I and III and of a powder sample of Form II. The tablet surfaces were exposed to light from a 400 W mercury vapour lamp and the colour changes, ΔE, of the surfaces with time were measured by colorimetry. The darkening process followed a rate equation of the form:

$$-d\Delta E/dt = k(\Delta E)^n$$

Values of n for all the polymorphic forms were similar (-1.2 to -1.6). Form I was the most stable. Rowbotham *et al.* [24] reported that ultraviolet irradiation of alkaline solutions of furosemide produced 4-chloro-5-sulphoanthranilic acid by oxidation of the sulphamoyl group and hydrolysis of the furfuryl group. Moore and Tomat [25] reported complete dechlorination after UV irradiation in deoxygenated neutral aqueous solutions.

Moore and Sithipitaks [26] reported that when methanol solutions of furosemide were irradiated with 365 nm UV light, photoreduction to N-furfuryl-5-saluamine occurred. Yahya *et al.* [26] have shown that aqueous furosemide solutions, stored in burette administration sets, are stable over a 48 hour period when exposed to direct daylight/ fluorescent strip room lighting, but decomposed with a half-life of about 4 hours when exposed to sunlight.

Neil *et al.* [28] found that furosemide solutions were stable when stored in normal daylight. Bundgaard, Nørgaard and Nielsen [17] suggested that the photostability of furosemide may be a function of the degree of ionization of its carboxylic acid group (i.e. solution pH) such that the un-ionized species, resembling the esters in terms of inductive effect, might be much more unstable towards photolysis than the ionized form. During the development of ester prodrugs of furosemide, they noted the extremely high susceptibility of furosemide esters to undergo photodegradation in aqueous solutions exposed to normal conditions of artificial light or daylight.

1.4 Mixtures of cyclodextrins (CDs) with furosemide

Özdermir and Ordu [29] used DSC to study kneaded and physical mixtures of FR with beta-cyclodextrin (BCD) and reported the following. DSC curves for BCD displayed no peaks in the temperature range between 40 ^{0}C and 300 ^{0}C, while FR exhibited its characteristic endotherm associated with the melting of the drug at 226 ^{0}C. For the kneaded mixtures, the melting endotherm of FR in the DSC curve disappeared and the physical mix had a less intense endotherm. The absence of the peak in the DSC curves may be considered as a strong indication that inclusion of the drug in the BCD cavity had occurred.

IR spectra of the mixtures showed modifications of the carbonyl stretch at 1671 cm^{-1}; the amide stretch at 1596 cm^{-1}; the sulfonamide stretch at 1322 cm^{-1}; and the chloride stretch at 582 cm^{-1}. Mixtures were stored for 9 months and no changes in the aged samples could be identified from the DSC curves.

Chapter 2

2. THERMAL ANALYSIS TECHNIQUES AND THEIR USES

2.1 Thermal analysis techniques

2.1.1 Definition

Thermal analysis (TA) [32] is the term used to describe those analytical techniques that measure some property of a sample as a function of temperature or time while the sample, in a controlled atmosphere, is subjected to a temperature programme. This programme may consist of a series of preselected segments in which the sample is heated or cooled at a constant rate or held at a constant temperature. The atmosphere surrounding the sample is important and may consist of inert or reactive gases.

2.1.2 Differential Scanning Calorimetry, DSC

A differential scanning calorimeter measures the difference between the rate of heat flow (measured in watts (W) or milliwatts (mW)) to the sample and to a reference pan that are subjected to the same temperature programme. If the power supplied is integrated with respect to time, then a quantity of energy is obtained which may be expressed in units of mW s = mJ. If the sample absorbs energy, the enthalpy change is positive and the process is called endothermic. If the sample liberates energy, then the enthalpy change is negative and the process is said to be exothermic.

DSC measurements provide information on thermal events which are characterized by enthalpy changes, such as melting, crystallization, solid-solid transitions and chemical reactions. Because DSC measurements are based on measurements of heat capacity, changes in heat capacity, such as that which occurs at the glass transition, can also be determined.

2.1.3 Differential Thermal Analysis, DTA

This technique is qualitatively similar to DSC, except that DTA instruments measure the temperature difference, ΔT, between the sample and the reference [30, 31]. Because of their simpler construction, more reliable quantitative information can usually be obtained from DSC. DTA instruments can usually be used to higher temperatures than DSC instruments [32].

2.1.4 Thermogravimetry, TG (also referred to as TGA)

In thermogravimetry, the mass of a sample which is subjected to a temperature programme is measured. The measurement is performed in a defined atmosphere, usually in inert conditions (nitrogen), or in an oxidative environment (air or oxygen). The mass is measured with a sensitive electronic balance. Interfering buoyancy or gas-flow effects are compensated for by a blank curve correction. Volatile components formed from the sample are also sometimes analysed by evolved gas analysis (EGA), (see below). TG can provide information on the content of volatile components, such as solvents or water and on decomposition behaviour.

2.1.5 Evolved Gas Analysis, EGA

This is the term given to the investigation of the gases or volatile components that may be liberated from the sample during thermal analysis. The analysis of these components is usually done by combination of the basic thermal analysis technique with a mass spectrometer, or in the gas cell of a FTIR spectrometer coupled to the TA module. Important factors when combining or coupling different analytical methods for detecting and analysing evolved gases or volatiles are: a) the selection of the methods to be combined, b) selection of the coupling method and coupling interface, c) the gas flow conditions in the combined instruments, d) detection limits for the evolved gases, e) the response time and resolution of the gas analysis system, f) the temperature range and type of samples to be analysed, g) correlation between the data acquired from different detector systems, h) interpretation of the results, i) and the possibility of calibration and quantitative work [33].

FTIR allows the whole IR spectrum (400–4000 cm^{-1}) to be scanned several times within one second [34]. TG-FTIR allows for real-time collection of spectra of gases evolved during sample heating, so that one can make assignment of the evolved gases to the detected mass loss [35]. The interface for the coupling of FTIR to the thermobalance has to transfer the gas flow into the gas cell of the spectrometer without pressure changes and losses by condensation and without secondary reactions occurring in the transmission line.

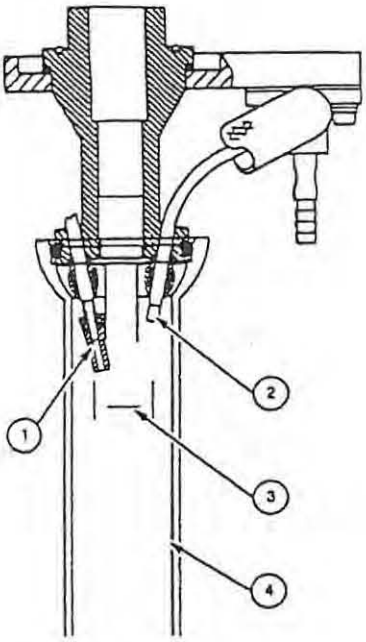

1 Ceramic Nozzle
2 Purge Outlet
3 Furnace
4 Furnace Tube

Figure 2.1 The Perkin-Elmer TG furnace system showing the purge outlet that leads evolved gases to the gas line.

The transfer line is usually made of PTFE (polytetrafluroethylene) and is heated so that gases are carried through this line to a heated IR gas cell without condensation. **Figure 2.1** shows the purge outlet which leads to the transfer line [34]. A gas cell (see **Figure 2.2**) with a long light path ensures high sensitivity and good light transmission through the fumes coming from decomposing samples. Samples are loaded in the same way as they are loaded in TG and there is no need for transfer- line disconnection [33].

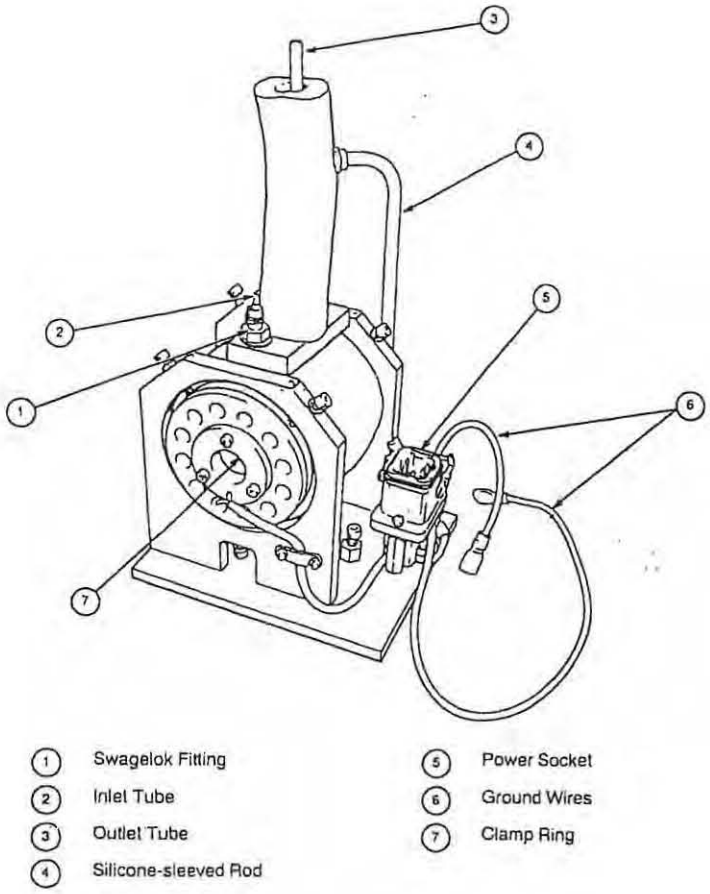

Figure 2.2 The Perkin-Elmer on-line gas cell for evolved gas analysis using TG-FTIR

Factors that should be avoided once the interface has been connected are: loss of gas by condensation at cold spots; low-detection sensitivity due to heavy dilution with the purge gas; low-time and temperature resolution because of long transfer times; mixing of evolved gas by diffusion and by uncontrolled flow conditions, and variation in the purge gas composition [33].

FTIR results are usually presented in a Gram-Schmidt plot (a typical example is shown in **Figure 2.3**). In a Gram-Schmidt plot, the total IR absorption over a set wavelength-range is plotted against time and the plot is comparable, under ideal operating conditions, with the derivative mass-loss versus time (DTG) plot. The TG heating programme enables the time to be related to the temperature. It is necessary to correct for any time-delay that occurs as the evolved gases are passed through the transfer line to the gas cell. Berbenni *et al.*[35] stated that the relative rates of reaction and of purging determine the spectral response. A three-dimensional stacked plot with information about the spectral ranges and the absorbances of the released gases as a function of the time, and hence through the heating rate the temperature, at which they are released can also be obtained from the TG-FTIR results (see **Figure 2.4**).

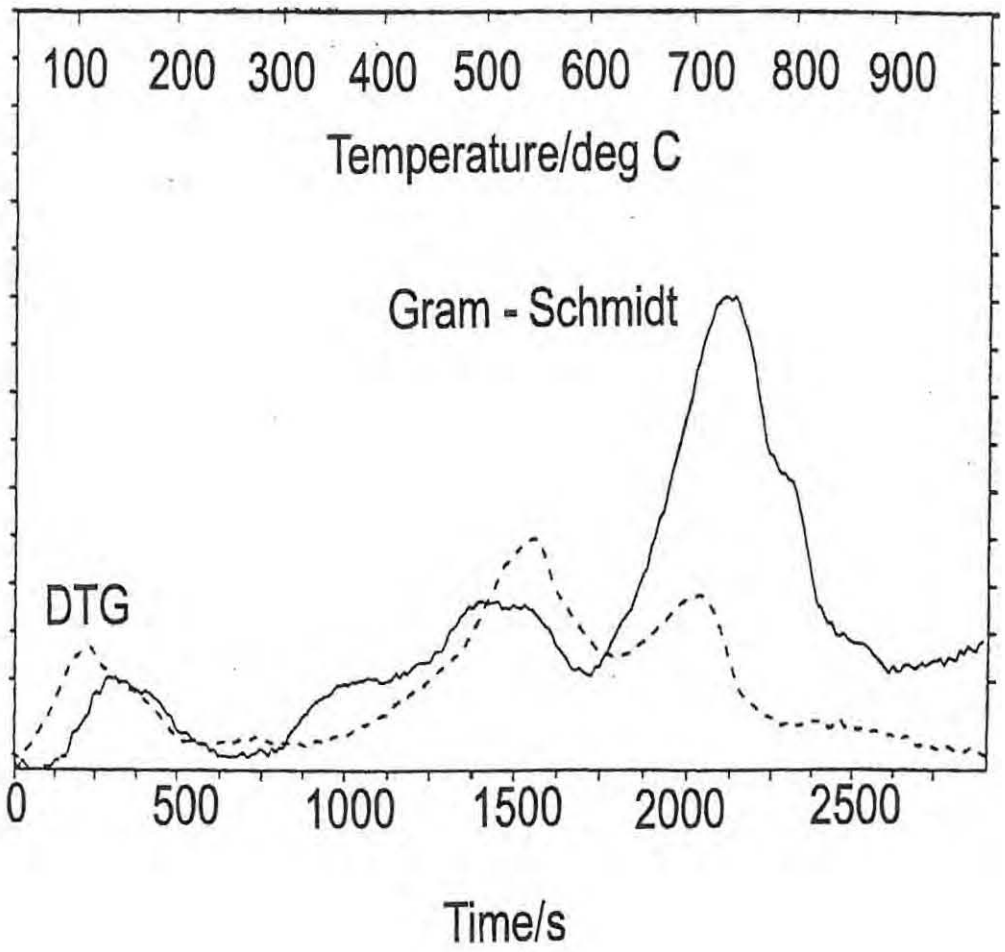

Figure 2.3 A typical Gram-Schmidt plot of total IR absorption over a set wavelength window against time, compared with a DTG curve (dashed line), showing the evolution of HCl, CO_2 and SO_2 from brick clay as three main peaks [33].

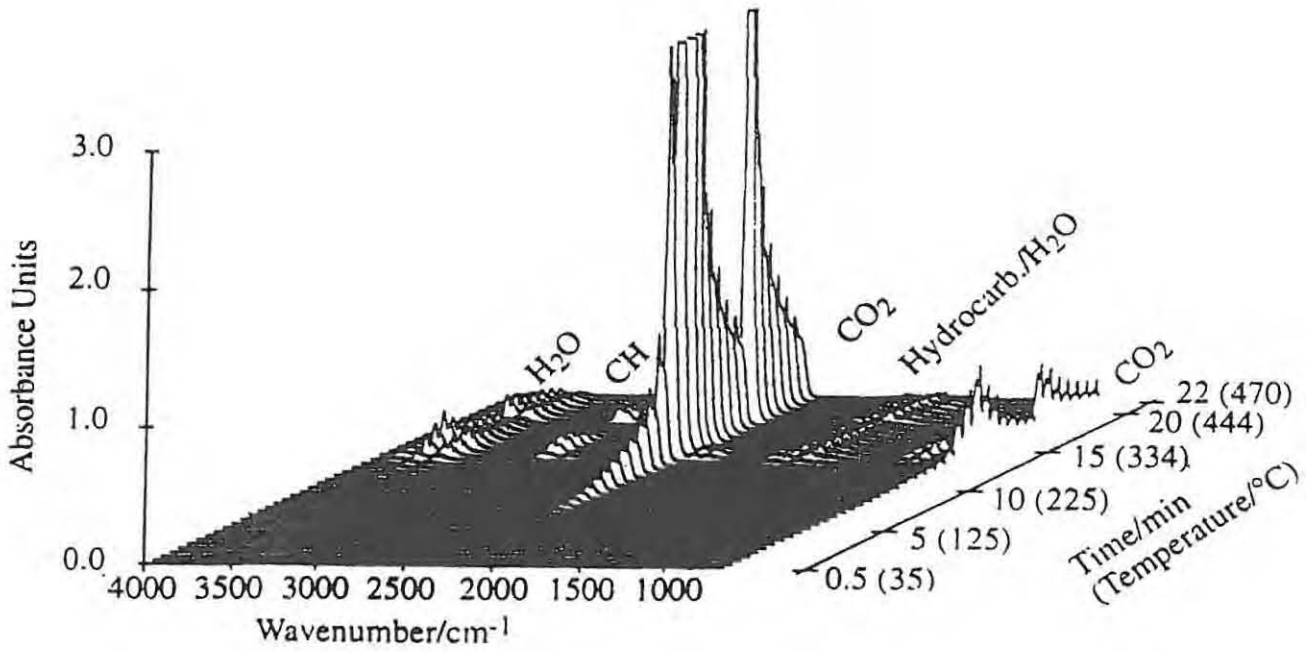

Figure 2.4 Stacked plot for the degradation of polystyrene, showing IR absorbance against temperature and time. The peaks correspond to the release of H_2O (3600-3400 and 1650-1600 cm^{-1}), CO_2 (2360-2340 and 750 cm^{-1}) and aromatic hydrocarbons (CH) (3040 and 1600-1580 cm^{-1}). The temperature and the time are related through the heating programme [34].

2.1.6 Thermomicroscopy (or Hot-Stage Microscopy, HSM)

This technique involves microscopic examination of the outward appearance of the sample during a heating programme and can provide evidence of processes such as sintering, decrepitation and creeping and foaming of melts that are only really detectable by direct observation [36]. Controlled temperature stages for microscopes are readily available and can cover wide temperature ranges [32]. These instruments are equipped with standard photographic equipment, or video cameras which can record the observations as the events are taking place.

2.2. Applications of thermal analysis in the study of pharmaceuticals

2.2.1 General

Thermal analysis has many applications within the pharmaceutical discipline. These applications include morphological studies, melting behaviour, determination of purity, stability in the solid state and drug-excipient interactions [37, 38]. Some examples of pharmaceutically important information derived from the various thermal analysis techniques [37] are given below:

Table 2.1 Applications of thermal analysis in the study of pharmaceuticals [37].

Processes	**DSC**	**HSM**	**TG**	**DTA**
Melting points	a	a	na	a
Polymorphic transitions	a	a	a	a
	a	a	a	a
Glass transition	a	na	na	a
Purity determination	a	pa	na	pa
Drug-excipient interaction	a	pa	pa	pa
Decomposition	a	na	a	a
Desolvation	a	a	na	a

key: a-applicable, na- not applicable, pa- potential application.

2.2.2 Purity determination

Use of pure active and inactive ingredients for the preparation of pharmaceutical products is essential because undesirable impurities could have serious consequences. The DSC method of purity determination is based on the principle that the presence of impurities (solute) in an organic compound (solvent) depresses the melting point and that the degree of impurity for dilute systems is described by the van't Hoff equation [39]. The theory only holds true if the following conditions are fulfilled: a binary eutectic system is formed, the components are miscible in the liquid state, thermodynamic equilibrium is achieved and no decomposition occurs on melting. Even though there are these limitations, analysis of DSC measurements can yield all the information required to determine the purity, the melting point and the heat of fusion of a substance without the need for a pure sample of the substance being tested.

2.2.3 Processing of solid pharmaceuticals

Thermal analysis techniques can be used to provide information and understanding of how key production parameters and the manufacturing environment may affect the morphology and physical properties of a drug [37]. Temperatures of thermal events such as the glass transition, melting, boiling, sublimation, decomposition and isomerisation are obviously important. When hydrates or solvates or volatile compounds are involved in the formulation, the loss of water or volatile compounds can be followed. A manufacturer needs to ascertain how factors such as concentration, stir-rate and reaction temperature affect the crystal habit and the morphology of the material; how pressure, temperature and relative humidity affect crystallinity during particle-size reduction, and how purity and crystallinity affect the stability of the final product. Many drugs under development do not reach the market, because their instability can produce degradants with unpredictable side-effects. Thermal analysis can also be used for identification purposes by simple "fingerprint"-type of comparison of TG and /or DSC curves for the sample with those for known reference samples. DSC can also be used to monitor the behaviour of, or identify, polymers used in packaging material. For example, the glass transition of amorphous cellulose derivatives can be used to identify the film coatings of biodegradable drugs [40].

2.2.4 Drug-excipient interactions

For drug/excipient mixtures, any interaction between the drug and the excipient, such as miscibility in the melt, could lead to eutectic formation, effectively decreasing the purity of the drug. Comparison of the DSC curves of the individual compounds with those of mixtures can reveal changes that could be due to interaction in the solid state, such as complex formation or other chemical reactions [40].

2.2.5 Polymorphism

The study of polymorphism of drug substances is of great importance. Many drugs exists in different crystalline modifications, as well in the amorphous state. These forms all melt to give the same liquid phase, but properties such as melting and sublimation temperatures, stability and solubility are different. In dosage forms, these differences usually lead to differences in dissolution and bioavailability [40]. DSC can be used to detect: a) solid-solid transitions before melting, b) melting of the crystalline form and recrystallisation to a second form from the melt which has a higher melting point, and c) cases where each crystalline form melts without any transition to the other form.

2.2.6 Atmospheric conditions

Thermal analysis can also be used to study the effects of atmospheric conditions, such as the presence of oxygen and / or water on the stability of drugs, many of which are very susceptible to oxidation and/or hydrolysis.[41].

Chapter 3

3. DRUG STABILITY TESTING

3.1 Introduction

The stability of a drug [45] can be affected by factors such as the presence of impurities or additives, and the container and environment used for storage. Included under environment would be the effects of temperature and the presence of oxygen and water or other solvents. Impurities or additives may cause discolouration of tablets and, in certain containers, transfer of drug among a set of normally equivalent tablets may occur after several months and result in decreased uniformity of the contents. Alam and Parrot [42] found a close correspondence between the changes occurring in the dissolution rate of hydrochlorothiazide tablets at elevated temperatures and those occurring after prolonged storage at room temperature.

Before marketing of a product, packaging tests and shelf-life determinations are essential to the manufacturer, as well as the determination of photostability, so that the storage conditions can be specified. Exposure of a drug to light might produce undesirable side-effects such as photosensitivity effects, or may bring about loss of therapeutic activity.

3.2 Accelerated testing

The effects of storage for long periods at ambient temperatures can be simulated by short periods of treatment at elevated temperatures, provided that extrapolation of results is not done over a temperature range that includes phase transitions. In long-term stability tests, samples can be stored for specified times under specified conditions and analysed at regular intervals. Any changes in the product can then be recognized from sample to sample. A more rapid procedure is to investigate the kinetics of the decomposition reactions. Such studies may be made under a range of different isothermal conditions, as in conventional homogeneous kinetic experiments, or under programmed temperature conditions using TG or DSC results obtained at a series of different heating rates. Many methods of extracting kinetic information from non-isothermal measurements have been proposed [32]. If the kinetic measurements have been made reliably and a valid kinetic analysis

was used, the results should allow limited predictions about decomposition behaviour to be made. Interpolation of kinetic measurements within the range of experimental parameters used is always more reliable than extrapolation outside the range. Extrapolation has to be done with caution because of the generally low melting points and the existence of several polymorphic forms of drugs, so a single degradation mechanism may not apply.

3.3 Drug-excipient interactions

The morphology of an excipient may also play an important role in the stability of the final product [43]. The chemical stability of the drug is usually compared with the stability of mixtures of the drug with each excipient. Chemical instability is defined as a chemical interaction that causes a detrimental change to the material and can lead to a loss of potency. This interaction may also result in the formation of potentially harmful degradation products. Degradation can be environmentally initiated (e.g. photodegradation, atmospheric oxidation, hydrolysis) [43], or be initiated from within the drug formulation by autocatalysis and/or interactions with other excipients [44], or impurities associated with the excipients.

3.4 Solid dosage forms

Most of this study is concerned with the solid-state stability of FR. Drug stability in the solid state is important because solid dosage forms are more common than other forms and the first clinical trials are usually carried out on solid dosage forms [45]. When a solid drug is placed in a vacuum and exposed to temperatures at which it decomposes at a measurable rate, the following reaction types may occur:

i) Solid → solid + solid
ii) Solid → solid + liquid
iii) Solid → liquid + liquid
iv) Solid → solid + gas
v) Solid → liquid + gas
vi) Solid → gas + gas

Some of these reaction schemes are theoretically possible but not very likely. Reactions of types iv) and v) have been the most investigated reaction schemes in pharmaceutical science.

3.5 Effects of moisture

Moisture adsorption plays an important role in the physical and chemical stability of solid dosage forms, excipients and polymers for sustained-release formulations [46]. Many drugs are known to undergo hydrolysis or oxidation in the presence of moisture, so it is important to study the rate of moisture uptake and the equilibrium moisture content (EMC) of solid dosage forms and excipients to obtain information useful for choosing excipients such as tablet-disintegrating agents, direct compression carriers and binders, and for deciding on the humidity control required during storage [46]. Moisture determination is thus part of shelf-life determination.

The moisture absorbed by drugs and excipients influences the flow, compression characteristics and the hardness of granules and tablets [46]. A typical example of a drug whose stability can be affected by moisture is aspirin [47]. Even though most of the water is driven off after wet granulation, there is still sufficient residual moisture to induce excessive decomposition on subsequent storage. Dry granulation methods thus have to be used (i.e. slugging, roller compaction). Measurements of moisture transmission through polymer films may be useful for characterization of the dissolution and the transport of drugs from their dosage forms [46]. Edgar and Swan [48] listed four major factors that affect the rate of moisture absorbed by drug substances: a) the water vapour pressure gradient between the atmosphere and the adsorbed moisture layer on the drug substance, b) the temperature, c) the surface area of solid drug exposed to the water vapour, d) a reaction constant characteristic of the solid [48].

Mikulinskii and Rubinshstein [49] studied the kinetics of moisture uptake by $MgSO_4$ and concluded that the process of moisture uptake is dependent on two steps: a) surface adsorption, occurring at a rate proportional to the difference between the partial pressures of the water vapour in the atmosphere and that of the saturated salt solution, and b) water diffusion into the crystal, at a rate dependent on the product of the diffusion coefficient and water concentration gradient. The thickness of the layer of the drug substance also influences the water uptake [50].

Studies on moisture uptake by pharmaceutical powders at various relative humidities were done by Czetsch-Lindenwald [51] and three classes of hygroscopicity were identified: a) softening substances, b) substances retaining moisture, and c) antistatica (disturbance by moisture in the environment surrounding the solid material causes the particles to be loosely bound). Carstensen *et al.*[52] emphasised the importance of performing moisture-stress tests of tablets, because when gelatin softens it becomes more oxygen-permeable and therefore the stability of the drug will decrease. Admirat and Grenier [53] defined the hygroscopicity of a substance in terms of the critical relative humidity (CRH). This is the humidity in equilibrium with a saturated solution of the substance. They gave a practical example of the definition of hygroscopicity where, if the CRH of drug A was 30 % and drug A was stored below or at 30 % RH (relative humidity), no moisture adsorption would take place. However, if drug A was stored at over 30 % RH, moisture would be adsorbed and the drug A would be said to be hygroscopic [53].

In a solid dosage form, moisture may be bound or unbound. Unbound moisture is available to participate in hydrolysis reactions, while bound moisture is similar to water of crystallization and is not readily available for hydrolysis. The available moisture may form an adsorbed layer or a rubbery phase in which hydrolysis can occur in a dissolved state.

3.6 Effects of temperature

The effect of temperature on the stability of solid dosage forms can be complicated when: a) humidity is not simultaneously controlled, b) one of the ingredients, either the drug or an excipient, has a low melting point, c) one of the ingredients has loosely bound water, and alterations in temperature change the degree of binding of the water to the excipient, d) one of the ingredients of the dosage form is present as a hydrate or solvate and is capable of giving up this bound solvent to an unbound state as a result of temperature changes [54].

Temperature is known to affect the solubility of a drug in a solvent layer and temperature changes may also alter the availability of solvent. If degradation in solution is rapid, the amount of degradation will increase if the amount of solvent available increases with increasing temperature, that is if "bound" solvent in the form of a solvate is released, but degradation may decrease if the

higher temperature actually helps drive off the loosely bound water in the tablet, thus decreasing the amount of solvent present. Excipients may affect the stability of drugs by: a) acting as surface catalysts, b) altering the pH of the moisture layer, and c) undergoing direct chemical reaction with the drug [54].

Chapter 4

4. CYCLODEXTRINS AND DRUG/CYCLODEXTRIN MIXTURES

4.1 Cyclodextrins (CDs)

Natural cyclodextrins are produced from starch by the action of cyclodextrin glycosyltransferase (CGTase), an enzyme produced by several organisms, *Bacillus macerans* being the most common, to form a mixture of cyclic and acyclic dextrins. The three major cyclodextrins are crystalline homogeneous, non-hygroscopic substances, with torus-like macrocycles built up from glucopyranose units. Structurally these units consist of 6,7 or 8 (i.e. alpha, beta, and gamma respectively) D-glucopyranosyl units connected by alpha-(1,4) glucosidic linkages. The molecular structure of naturally-occurring gamma-cyclodextrin [55] is shown in **Figure 4.1**.

The 3-D molecular configuration of these very stable, non-reducing cyclic oligosaccharides takes the form of a toroid with the upper (larger) and lower openings of the toroid presenting secondary and primary hydroxyl groups, respectively, to the solvent environment (see **Figure 4.2**). The exterior of the toroid is hydrophilic as a result of the electron-rich environment provided, whereas the interior is intensely hydrophobic [56].

The cyclodextrins are reasonably soluble in water, with beta-cyclodextrin being the least soluble (as can be seen from **Table 4.1**). Szejtli [57] reported that the solubility of beta-cyclodextrin increases sharply with temperature and this allows easy crystallization on cooling (see **Figure 4.3**).

Pagington [58], and Brewester *et al.* [59] have reviewed some of the properties of cyclodextrins which limit their application. These are as follows:

i) The cyclodextrins are fairly stable in alkaline media, but are susceptible to acid hydrolysis,

ii) They are hygroscopic, with beta-cyclodextrin being the least hygroscopic and the most stable in air. Storage may require containers to be sealed under dry conditions.

iii) They can be expensive, although recent advances in enzyme technology and in large-scale production techniques have lowered their prices.

iv) Toxicity has been a problem, for example the use of beta-cyclodextrin in parenteral dosage administration. Toxicity tests have shown, however, that orally-administered beta-cyclodextrin is harmless, without any embryotoxicity or teratogenic effects,

v) The low aqueous solubility of the most widely used cyclodextrin, beta-cyclodextrin is a major limitation in its use.

vi) In damp conditions, cyclodextrins are subject to bacterial attack. Thymol or phenol can be used to prevent bacterial growth and product degradation.

It was not until the late 1970's that researchers started modifying cyclodextrins with the intention of solving the problems of toxicity and aqueous solubility. Pitha [60] looked at the enhanced solubilizing effect achieved by modifying each of the natural cyclodextrins with alkyl groups. Since that time, cyclodextrins have been modified with many different groups.

Table 4.1 Physical properties of some of the naturally-occurring cyclodextrins [55, 61]

	Alpha (α)	**Beta (β)**	**Gamma (γ)**
molar mass (g mol^{-1})	972	1135	1297
glucose monomers	6	7	8
internal cavity diameter (Å)	4.7-5.3	6.0-6.5	7.5-8.30
height of toroid (Å)	7.9 ± 0.1	7.9 ± 0.1	7.9 ± 0.1
outer diameter (Å)	14.6 ± 0.4	15.4 ± 0.4	17.5 ± 0.4
approx. volume of cavity (10^6 pm^3)	174	262	427
water solubility (g/100 ml:25 ^{0}C)	14.2	1.85	23.2
melting range (^{0}C)	255-260	255-265	240-245
water of crystallization (mass %)	10.2	13.2-14.5	8.1-17.7
water molecules in the cavity	6	11	17

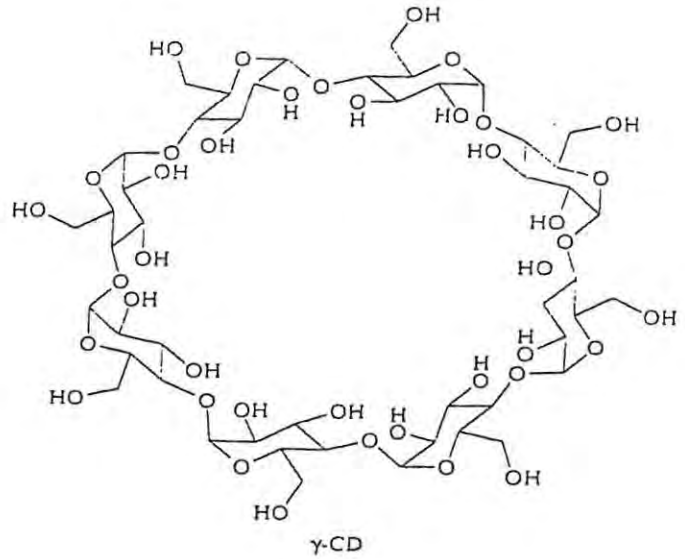

Figure 4.1 The molecular structure of naturally-occurring gamma-cyclodextrin [55]

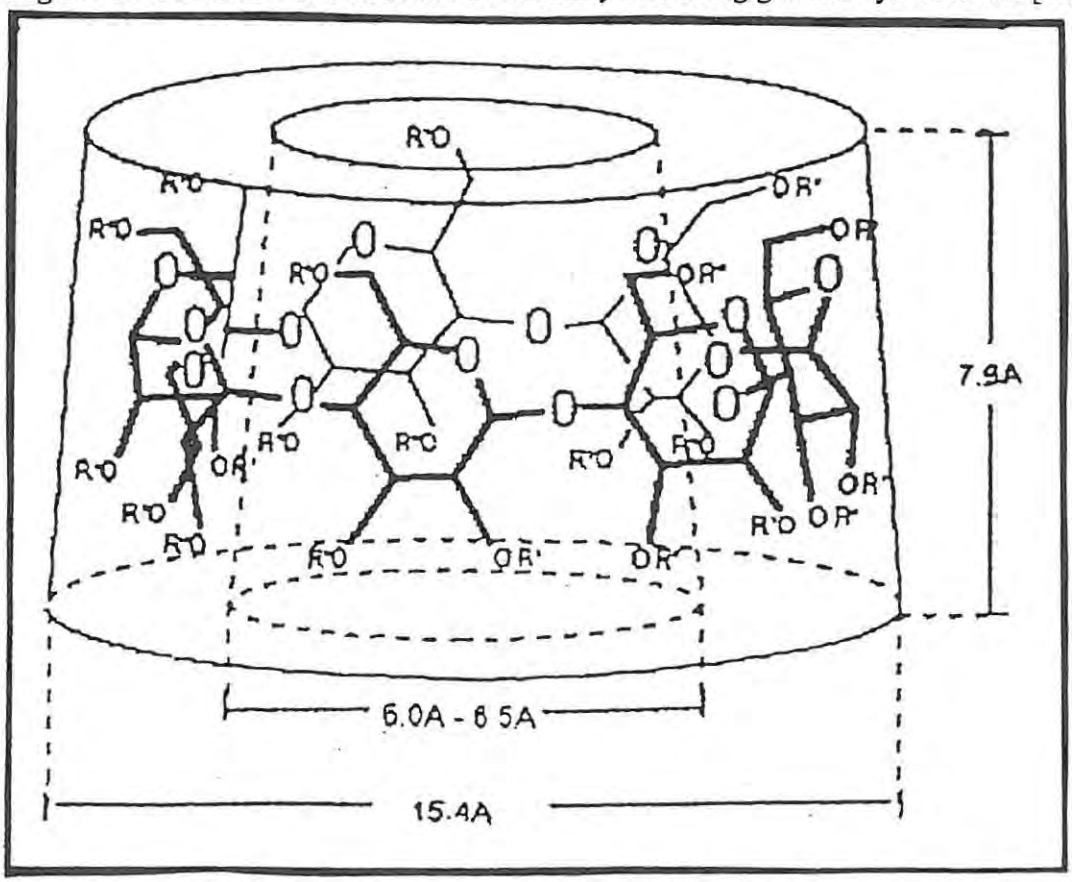

Figure 4.2. Illustration of the lower and upper openings of the toroid of a general structure of cyclodextrins where R can be H in case of natural CDs or a substituent in case of modified CDs [61].

4.2 Inclusion complexes

The cyclodextrins have different cavity sizes, so that inclusion complexes can be formed between the cyclodextrins and "guest" molecules if the size of the guest molecule does not exceed that of the internal cavity of the cyclodextrin (i.e."host" molecule) [61].

Frank [62] defined an inclusion compound as a unique form of chemical complex in which one molecule is enclosed within another molecule or structure of molecules. The combination of the "guest" with "host" is characterized by the absence of ordinary chemical bonding. Coetzee [63] reported that inclusion or complex formation was dependent on the stereochemistry and polarity of the molecules involved. The close fit of the components involved in complex formation produces a combination of significant strength due to complete distribution of forces that are present between the interacting compounds [62].

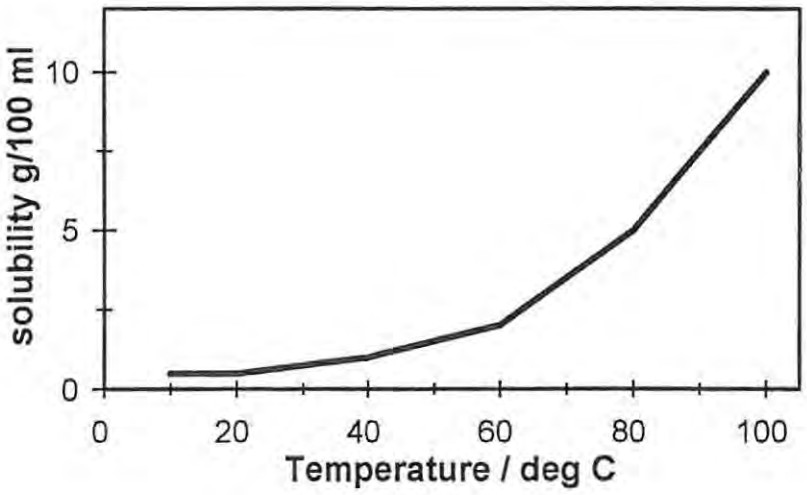

Figure 4.3 Solubility of beta-cyclodextrin in water (Szejtli) [57].

Cramer *et al.* [64] investigated the inclusion compounds formed between azo-dyes and α-cyclodextrin and identified six steps leading to complex formation:

a) the approach of the guest molecule to the cyclodextrin molecule,

b) the loss of water from the interior of the cyclodextrin cavity,

c) breaking down of the water structure around the portion of the cavity where the guest molecule is to be included and the transportation of some of these water molecules into solution,
d) interaction of the guest molecule substituents with the groups on the rim of the cyclodextrin,
e) possible formation of hydrogen bonding between the guest molecule and the cyclodextrin,
f) reconstruction of the water structure around the exposed parts, if any, of the guest molecule after inclusion has taken place.

Inclusion complex formation thus proceeds by an energetically favoured interaction of a relatively non-polar guest molecule with an imperfectly solvated hydrophobic cavity. Cyclodextrins are stabilized by various intermolecular interactions which include hydrophobic interactions, hydrogen-bonding between the guest and host, and Van der Waals forces (both permanent induced dipole-dipole interactions and London dispersion forces) [65]. **Figure 4.4** gives an illustration of the equilibrium binding of a drug (guest) and a cylodextrin (host) to form a complex.

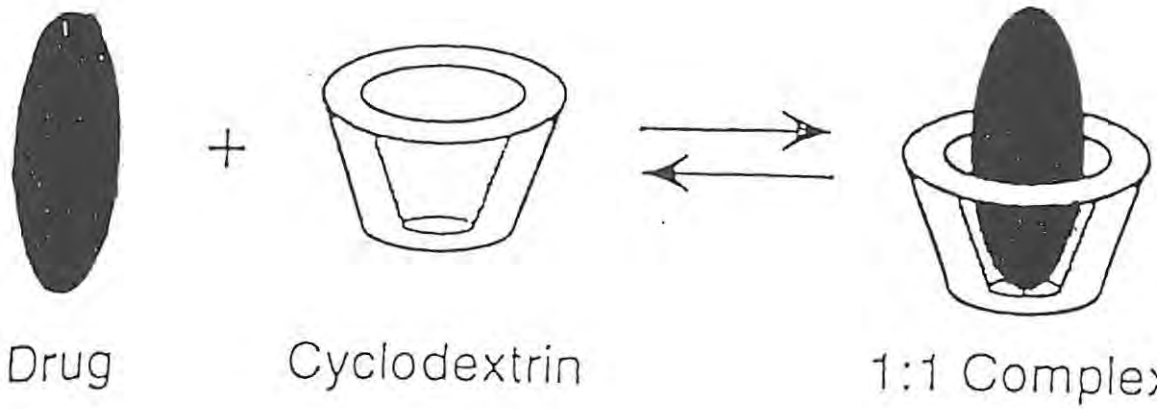

Figure 4.4 Illustration of the equilibrium binding of a drug and a cyclodextrin in inclusion complex formation [66].

Hedges [67] mentioned that complexes are easily formed and the most commonly used methods for preparation of complexes are coprecipitation, mixing as slurries or pastes (called kneading) as well as dry mixing (also known as physical mixing). Cyclodextrins are known to contain water molecules within their cavities and this has been noted to influence complex formation because water is often the medium for dissolution of the cyclodextrin and the guest, as well as being the driving force for the hydrophobic interaction of the guest with the cavity of the cyclodextrin [67]. Les Bas *et al.*[68] explain how water can assist in the formation of a complex. Water molecules in the cavity of the cyclodextrin molecules can form a bridge between the hydroxyl groups of adjacent cyclodextrin molecules to form a cage that assists in trapping the guest inside the cavity and thus forming a complex.

4.3 Some industrial uses of cyclodextrins

Cyclodextrins have many industrial uses. For example, in the dyeing of fabrics [67] the use of cyclodextrins [69] enhances the solubility of the dye in water and, hence, more dye goes into the fabric, thus decreasing the amount of dye wasted in the effluent. CDs can also increase the efficiency of biodegradation of hydrocarbons [70] by increasing their solubility and decreasing their toxicity, thus resulting in an increase in microbial and plant growth.

CDs can also be used to control the viscosity of water-based paints during their manufacturing [68]. Thickeners are complexed with cyclodextrins in order to decrease the viscosity thus making mixing easy. The desired viscosity can then be restored by addition of other paint components that will displace the thickener from the cyclodextrin cavity. CDs can also remove undesirable components selectively from mixtures, for example cholesterol from animal fats [71] and polyphenolic compounds, which cause enzymatic browning, from fruit and vegetable juices [72]. CDs also can be used in masking or eliminating the irritating or toxic effects of insecticides [73], and generally in decreasing volatility, e.g .in the prevention of odour in skin tanning preparations [74].

4.4 Drug / cyclodextrin mixtures

Because cyclodextrins are able to form inclusion complexes [75] with suitably-sized molecules, the inclusion of drug molecules has come to be particularly important. This inclusion process can occur in the solid state, as well as from solution. These inclusion complexes can have physical, chemical and biological properties that are dramatically different from those of either the parent drug or the cyclodextrin. The solubility and dissolution rate of the drug may be increased, while the volatility may be decreased. Release rates of the drug may be altered and local irritation effects may be modified. A major desirable effect of inclusion is a possible increase in the thermal and or photostability of the drug.

Access of the drug molecule to the cavity of a particular cyclodextrin is determined mainly by the molecular geometry of the guest molecule. Inclusion complexes usually form quite rapidly (equilibrium may be attained in minutes), because even the most lipophilic compounds are solvated by water to some extent. These discrete hydrated molecular particles are better able to get past the hydrophilic hydroxyl groups at the entrance to the cyclodextrin cavity.

The water molecules involved in hydrating the potential guest molecule can interact with the hydroxyl groups on the rims of the cyclodextrin toroid, or they may simply shield the hydrophobic drug molecule from being repelled by the hydroxyl groups. Once past the rim of hydroxyls, the hydrating molecules of water are driven from the hydrophobic cavity leaving the naked drug molecule to find its most stable position in the cavity. In such a situation, inclusion results in some protection against hydrolysis of the drug molecule. For extremely insoluble substances, true equilibrium may not be achieved for hours, or even days, because molecular segregation due to hydration occurs extremely slowly.

For enhancement of the photostability of a drug by cyclodextrins, the photosensitive moiety of the guest molecule normally has to be located inside the cyclodextrin cavity. Complexation of furosemide with cyclodextrins has been studied by Özdemir and Ordu [29]. They reported an improvement of the dissolution properties of furosemide by complexation with beta-cyclodextrin (BCD).

4.5 Cyclodextrins as excipients

Excipients are compounds that are used in drug formulation and tableting (i.e. making of the tablet pellets). Starch products are widely used in tableting for both their disintegration and binding properties [38]. Cyclodextrins thus form a special class of excipients and the possibility always exists that drug molecules can be included within the cavities of CD molecules.

Formulation of a stable, effective dosage form requires careful selection of excipients for compatibility [76]. The administration, consistent release and bioavailability of the drug and the protection of the active moiety from the environment must be ensured. Fassihi and Persicaner, [77] reported that excipients are often assumed to be inert, but chemical and physical interactions between drugs and excipients are common .

Most excipients have appreciably high water contents. Moisture may exert either beneficial or adverse effects on the drug. Connors, Amidon and Stella [54] reported that starch with a fairly high moisture content, compared with lactose and micro-crystalline cellulose, caused minimal degradation of the drug molecule. Excipients can also affect the stability of a drug by: (1) acting as surface catalysts; (2) altering the pH of the moisture layer; and (3) undergoing direct chemical reaction with the drug.

Interactions may be desirable or undesirable. Desirable interactions are those that stabilize the drug against thermal or photodegradation, and/or improve the solubility of an active ingredient. Undesirable interactions are also known as incompatibility and these interactions are those that lead to changes in one or more of the components which then bring about loss of activity, or complete deactivation of a preparation, or even production of toxic degradants.

Thermal analysis (**Chapter 2**) can be used to study interactions between the drug and excipients and whether or not the drug is actually being stabilized by the presence of the excipients.

4.6 Drug delivery

For pharmaceutical use, the behaviour of the drug / cyclodextrin complex in the gastrointestinal tract is important, because the guest (the drug) has to be absorbed. The dissolution and dissociation of an inclusion complex on contact with water (i.e. gastrointestinal fluid) is represented [78] by the following equilibria:

solid inclusion complex ⇔dissolved inclusion complex ⇔free cyclodextrin + free active ingredient

The generally hydrophobic, active ingredient is thus presented in a molecular state to the lipoid mucosa of the gastrointestinal tract and it is therefore easily absorbed. Absorption would result in a displacement of the previous equilibrium with the appearance of new free molecules of the active ingredient. The drug absorption process from a solid complex is illustrated in **Figure 4.5** [79].

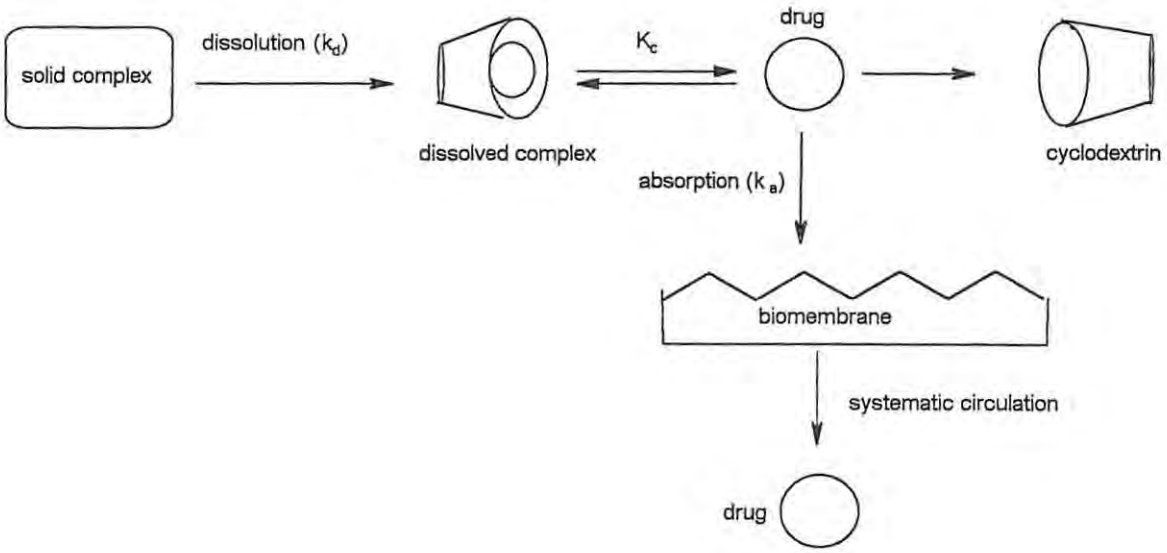

Figure 4.5 Schematic representation showing how the drug is absorbed from the drug-cyclodextrin complex (solid complex) through biological membranes [79].

4.7 Limitations of furosemide and the objectives of this study

Furosemide is known to exhibit poor bioavailability and high bioinequivalence due to its low aqueous solubility and is also known to be highly light and heat sensitive (as explained in **Chapter 1**). Cyclodextrins have been used with great success to increase the solubility of drugs and also to increase their stability to light and heat. Thus the objective of this study was the evaluation of the extent of interaction between FR and CD's through examination of *kneaded* and *physical* mixtures of FR and gamma and beta-cyclodextrin. The thermal and photostabilities of mixtures FR with cyclodextrins were also compared with the behaviour of pure furosemide under the same conditions.

Chapter 5

5. EXPERIMENTAL

5.1 Materials

5.1.1 Furosemide

Furosemide (Tradename: Lasix®) (also known as frusemide)

Empirical formula:	$(SO_2NH_2).(Cl).C_6H_2.(COOH).NHCH_2.C_4H_3O$					
Molar mass: 330.8 g mol^{-1} (molecular fragments)	80	35.5	74	45	29	67
% composition	24.2	10.7	22.4	13.6	8.8	20.3

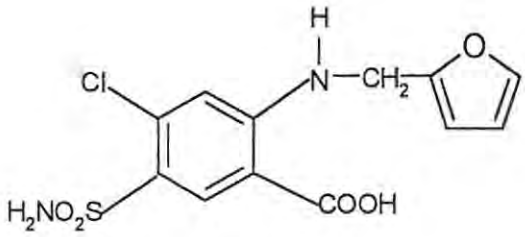

Figure 5.1 Furosemide (FR)

Melting range 216-222 ^{0}C [19].

5.1.2 Spectroscopic characterization of the furosemide sample

A sample of FR was characterized by UV-visible, NMR, IR and mass spectroscopy.

UV-visible spectroscopy: Samples of furosemide (FR) were dissolved in 0.5 M NaOH solution in which it is very soluble. The solution was then examined in the wavelength region of 90-400 nm. Maxima were obtained at 330.9 nm, 272.0 nm and 229.3 nm. From the analytical profile of furosemide, the UV the spectrum of FR in 0.1 N NaOH was reported to exhibit several maxima wavelength values ranging from 226 nm to 336 nm [3].

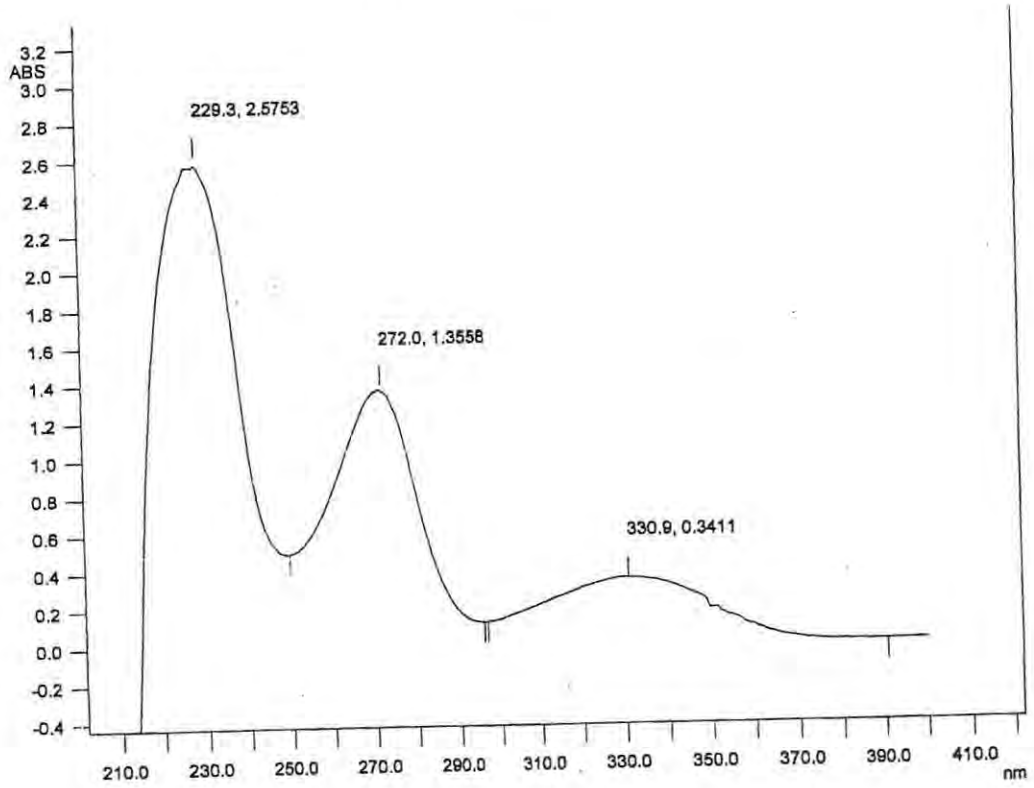

Figure 5.2 UV-visible spectrum of furosemide in 0.5 M NaOH solution.

Mass spectroscopy: 1.055 mg of furosemide was dissolved in 10 ml of methanol to make a homogeneous solution. The solution was then injected into the mass spectrometer. A base peak was observed at 330 g mol^{-1} which is the molar mass of furosemide. The peaks observed in the MS spectra represent the molecular fragments of furosemide. The fragment appearing at 81 g mol^{-1} is possibly $-CH_2.C_4H_3O$; and the one at 96 g mol^{-1} could be $HNCH_2.C_4H_3O$.

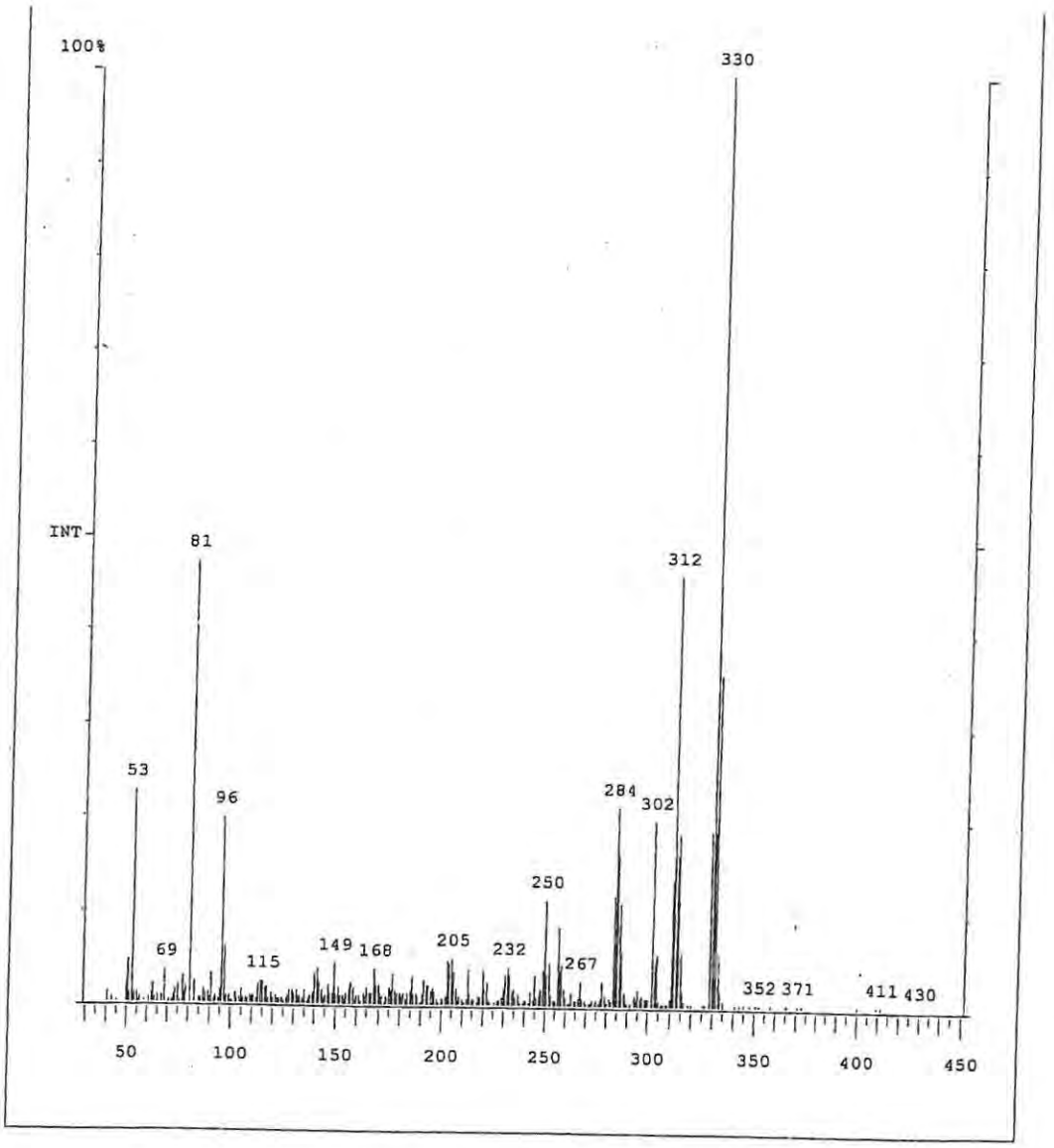

Figure 5. 3 Mass spectrum of furosemide in methanol solution

Nuclear magnetic resonance spectroscopy (NMR): Furosemide was dissolved in DMSO-d_6. Chemical shifts of the protons were consistent with literature values. All the peaks of FR proton spectrum are reported [3] to appear as sharp singlets with the following chemical shifts: -CH_2 at 4.5 δ (ppm), H_3 and H_4 of the furan ring at 6.41δ (ppm), H_2 of furan ring at δ (ppm), H_3 of phenyl group at 7.32 δ (ppm) and H_6 of phenyl group at 8.42 δ (ppm).

Infrared spectroscopy (IR):- Furosemide was mixed with Nujol to form a mull and the sample was examined in the region 14000-700 cm^{-1} in transmittance mode. The functional groups present were confirmed by the absorption bands at the wavenumbers shown in **Table 5.1.**

Table 5.1 Infrared absorption bands of furosemide

Vibrations	****Literature [3] values /cm^{-1}**	**Experimental values /cm^{-1}**
N-H (R_2NH)	3350-3400	3500 - 3100
C=O (COOH)	1671	1668.0
N-H (NH_2)	1596	1455.6
S=O (symmetric S=O)	na (not applicable)	1141.3
S=O (SO_2)	1322	1321.4
C-Cl	582	581.7

**** the FR was run using a KBr-disc**

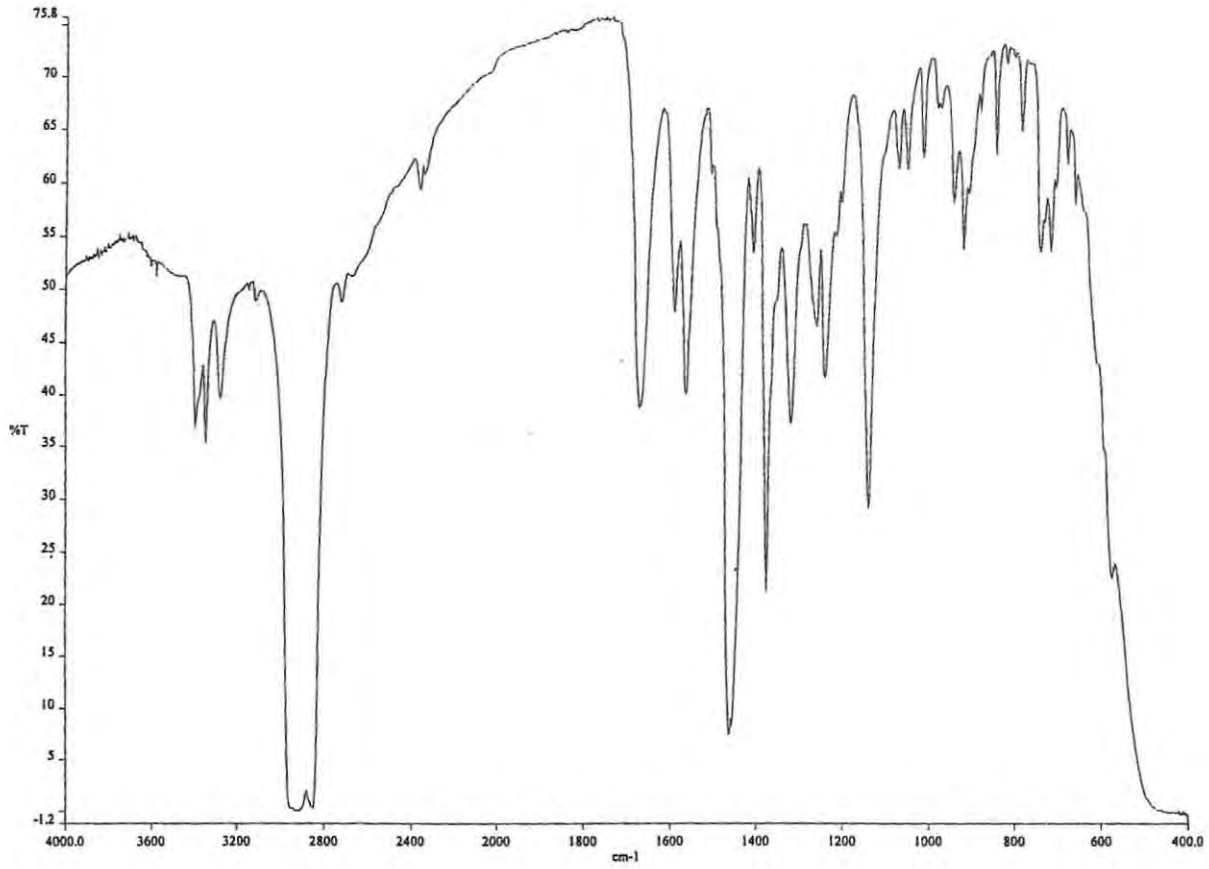

Figure 5.4 IR spectrum of furosemide in a Nujol mull

5.1.3 Cyclodextrins (CDs)

Details of the cyclodextrins used in this study are given in **Table 5.2.** The water contents were given by the suppliers.

Table 5.2 The properties of the cyclodextrins used in this study [55].

Cyclodextrin	**Abbreviation**	**Molar mass/ g mol^{-1}**	**Total water content % by mass**	**Cavity diameter/nm**
Beta-	BCD	1135	14.9	0.8
Gamma-	GCD	1295	11.2	1.0

The water contents of the cyclodextrins were determined using the Karl Fischer method. Approximately 100 mg of the samples was weighed accurately, dissolved in methanol (~ 40 ml) and then titrated with Hydranal composite (i.e. Karl Fischer reagent). 1 ml of reagent corresponds to approximately 5 ml of H_2O. The percentages obtained (**Table 5.3**) indicate the total amounts of water in each of the cyclodextrins, i.e. inside and outside the cavity.

Thermogravimetric results for samples of beta-cyclodextrin and gamma-cyclodextrin, heated in nitrogen at 10 ^{0}C min^{-1} from 50 to 250 ^{0}C, are shown in **Figure 5.6** and **Figure 5.7**, respectively. **Table 5.3** shows the initial mass losses for both BCD and GCD.

Table 5.3 Water contents (mass percentages) of the cyclodextrins determined by Karl Fischer titration and by thermogravimetry (TG)

Cyclodextrin	Karl Fischer (%)	Water molecules per CD molecule	TG (%)	Water molecules per CD molecule
BCD	16 ± 4	12	12.0 (52-120 °C)	9
GCD	12 ± 3	9	8.0 (38-126 °C)	6

Calculations of the number of water molecules present in the cyclodextrins according to the results obtained from the TG (in mass percentage):

BCD.xH$_2$O where x is the number of water molecules present in BCD

therefore 18 x/ (1135 + 18 x) = 12 /100, (as seen in **Table 5.3**)

x = 9, so BCD has **9** water molecules giving BCD.**9**H$_2$O.

GCD. xH$_2$O, 18x/(1297 + 18x) = 8/100, x = 6 so GCD has **6** water molecules making GCD.**6**H$_2$O.

Calculations of the number of water molecules present in the cyclodextrins according to the results obtained from the Karl Fischer titrations:

BCD.xH$_2$O where x is the number of water molecules present in BCD

therefore 18 x/(1135 + 18 x) = 16/100, x = 12, so BCD has **12** water molecules giving BCD.**12**H$_2$O.

GCD.xH$_2$O, 18 x / (1297 + 18x) = 12/100, x = 10, so GCD has **10** water molecules making GCD.**10**H$_2$O

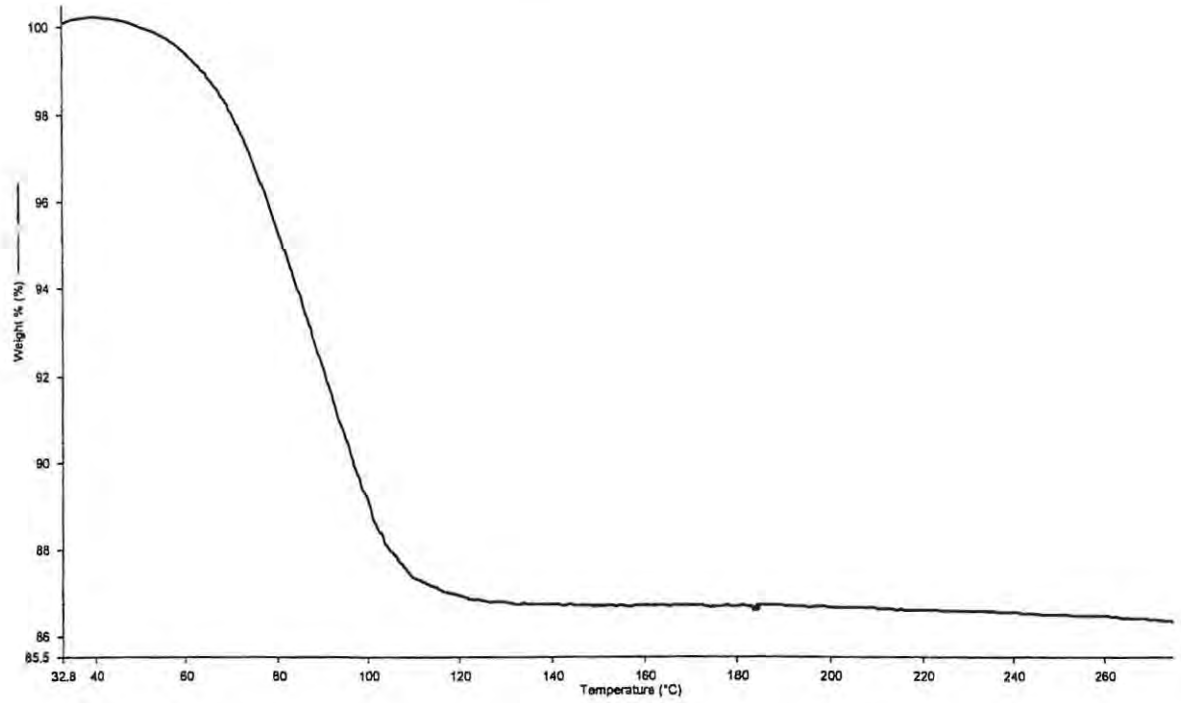

Figure 5.6 TG curve of BCD heated at 10 ^{0}C min^{-1} in nitrogen.

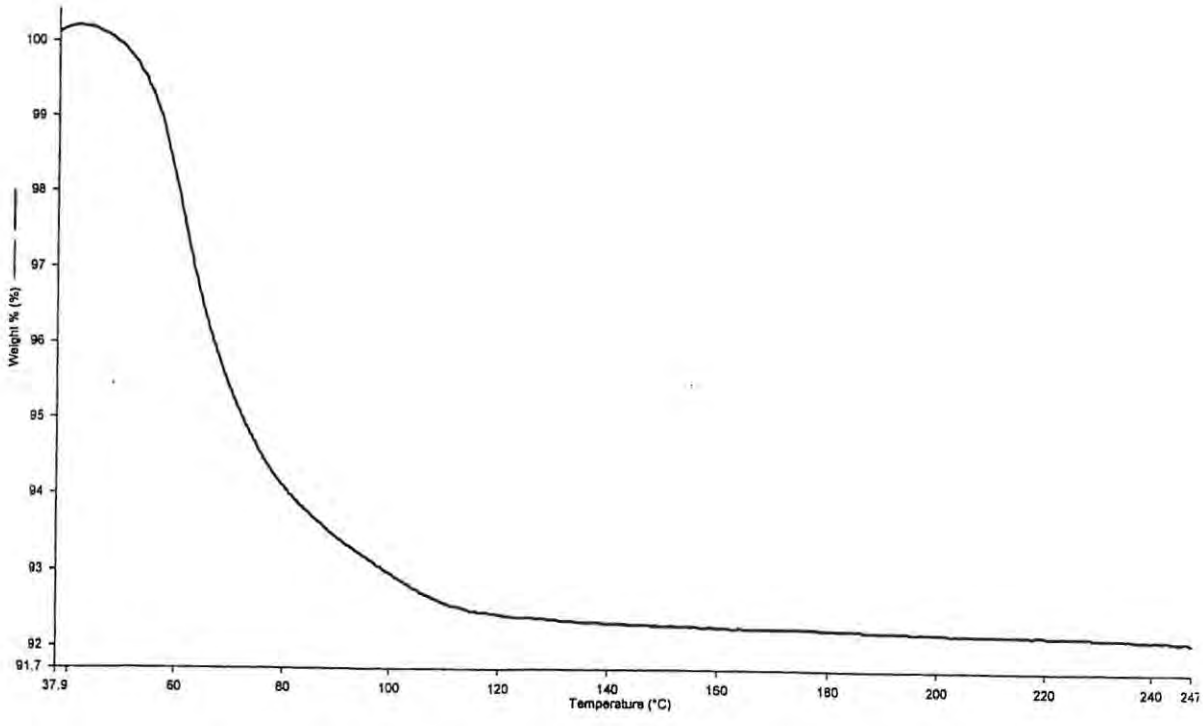

Figure 5.7 TG of GCD heated at 10 ^{0}C min $^{-1}$ in nitrogen.

The lower percentages of water obtained from TG measurements suggest that not all of the water is driven off during heating under these conditions.

5.2 Preparation of drug/cyclodextrin mixtures

FR/CD mixtures in the mole ratios 1:1, 1:2, 1:3, were prepared as *physical* mixtures by simple mixing of the weighed amounts with a spatula without grinding, or as *kneaded* mixtures by using small amounts of a solvent (in this case ethanol), during the mixing to give a paste, followed by drying in air at room temperature.

5.3 Equipment

5.3.1 Thermal analysis (TA)

Thermogravimetry (TG) and differential scanning calorimetry (DSC) were carried out using Perkin-Elmer Series 7 instruments with Pyris software. Unless otherwise specified, the atmosphere was flowing nitrogen and the heating rate was10 ^{0}C min^{-1}. The DSC samples were placed in Al pans with lids, but without crimping. The TG samples were placed in open Pt pans.

The DSC temperature was calibrated using pure indium metal which has a melting point of 156.4 ^{0}C and zinc which melts at 419.5 ^{0}C. The enthalpy calibration was based on the enthalpy of melting of indium at 28.7 ± 0.1 J g^{-1}. The TG temperature was calibrated using magnetic standards of known Curie points, namely nickel at 354 ^{0}C and perkalloy at 596 ^{0}C.

5.3.2 Thermogravimetry coupled with Fourier transform infrared spectroscopy (TG-FTIR)

Because TG measures sample mass as a function of temperature, but gives no information on the chemical basis of the mass change process, combination with FTIR spectroscopy allows for the real-time collection of the spectra of gases evolved during the sample heating and, hence, correlation with the observed mass losses. In this study, the Perkin- Elmer Series 7- TG was linked to a Perkin-Elmer spectrum 2000 FTIR spectrometer. The PC controlling these instruments was equipped with TR-IR software for the System 2000 and 1700-X for the interface. The temperatures of the interface and the cell were set to 200 ^{0}C to prevent condensation of the

evolved gases. The purge gas used was nitrogen and the scan range was 4000-400 cm^{-1}. Samples were weighed and run using the normal TG procedure and IR spectra were recorded simultaneously.

5.3.3 X-ray powder diffraction (XRD)

X-ray powder diffraction is an effective method of distinguishing solid phases having different crystal structures. Powdered samples were spread evenly on the surface of the sample container and then exposed to Cu-Kα, X-rays at goniometer angles from 5 ° to 55 °, with a voltage of 40 kV and a current of 20 mA, at a speed of 2 ° per minute. The powder pattern for pure FR is shown in **Figure 5.6**, and is similar to that reported by Özdemir and Ordu [29].

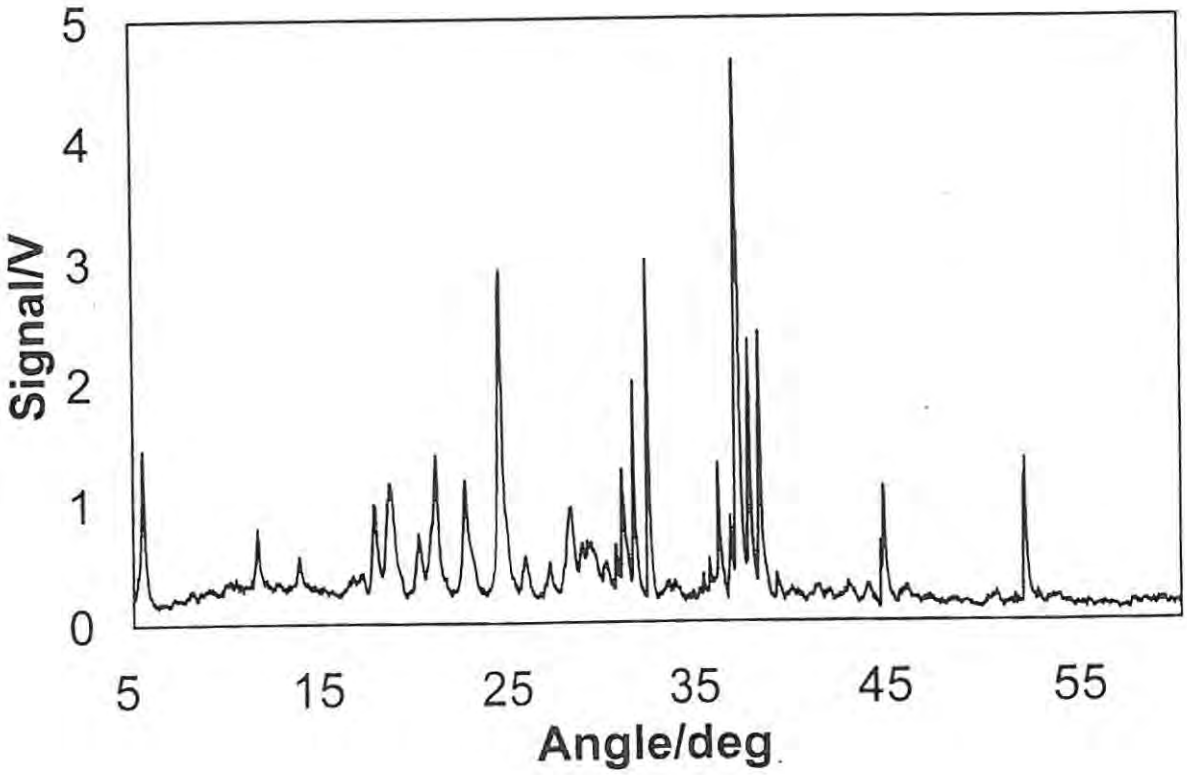

Figure 5.6 X-ray powder diffraction pattern of pure furosemide (FR)

5.4 Photostability testing

An Atlas SUNTEST CPS+ (Alta Material Testing Technology B. V, Germany), fitted with a xenon lamp and solar ID65 filter was used for irradiation of the samples. The samples (i.e. FR and FR/CD mixtures) were irradiated at a dose rate of 550 W h m^{-2} for set time periods, with the temperature of the instrument kept at 40 ^{0}C. The samples (10 mg) were covered in plastic wrap and placed in 30 ml clear glass beakers. The samples were spread evenly in the beaker so as to try to expose the maximum number of particles to the irradiation. Six samples at a time were placed alongside each other for the duration of the irradiation. The ICH recommended conditions are exposure for 10 to 12 hours at 200-250 watts h m^{-2}. So an exposure of about 5 hours at 550 watts h m^{-2} would be approximately 44 hours at 200-250 watts h m^{-2}. After such an exposure, the samples appeared to be unaffected, so even longer exposures were used.

Dark control samples, covered with aluminium foil, were included in the irradiation process to determine whether any thermal decomposition occurred under these conditions.

5.5 High performance liquid chromatography (HPLC) analysis

An HPLC method [84] was used to determine the amount of drug remaining after irradiation. The mobile phase was prepared by measuring volumes of methanol, water and acetic acid accurately in the ratio 60:39:1, to give a total volume of 250 ml. Samples were prepared as follows: 10 mg of furosemide was weighed, dissolved in 2 ml HPLC water and made up to 50 ml using Higher Grade HPLC methanol to give a solution of concentration 0.8 mg ml^{-1} which was then diluted to 0.08 mg ml^{-1} for use in the analysis.

A 30 cm, 4.6 mm i.d, C_{18} 10 µm bondapak column was used. The detector wavelength used was 254 nm and the flow rate was 1 ml min^{-1}, with a pressure of 1990 to 2208 psi for the injections. 20 µl of the sample was injected and the data were recorded at a chart speed of 30 cm h^{-1} with the sensitivity of the detector being 0.1 AUFS.

Chapter 6

6. RESULTS OF THE THERMAL STABILITY STUDIES

6.1 Furosemide (FR)

A typical DSC curve for furosemide heated at 10 ^{0}C min^{-1} in N_2 (**Figure 6.1**, curve B) shows a small endotherm (about 2 J g^{-1}) with onset at about 138 ^{0}C, followed by an endotherm at about 222 ^{0}C (melting) which is immediately swamped by a large exotherm (-107 J g^{-1}) (decomposition). ΔH values are very dependent upon the baseline choice. Other estimates of ΔH for the exotherm were -94 and -100 J g^{-1} .

The TG curve for FR at 10 ^{0}C min^{-1} in N_2 (**Figure 6.1** , curve A) shows a two-step mass loss, with the first mass loss having an onset at about 208 ^{0}C, which then accelerates until about 218 ^{0}C. The second step follows immediately, from about 218 ^{0}C to 247 ^{0}C. The mass loss for the first step was about 2 % and the temperature range corresponds closely with the melting endotherm followed by exothermic decomposition seen in the DSC curve.

The mass loss for the second step is acceleratory and is far from complete at 280 ^{0}C (10 %). The temperature range is extended to 650 ^{0}C in **Figure 6.4.** Decomposition is still incomplete (about 30 % mass loss) at this high temperature and the rate of mass loss is approximately constant at about 1 % per minute.

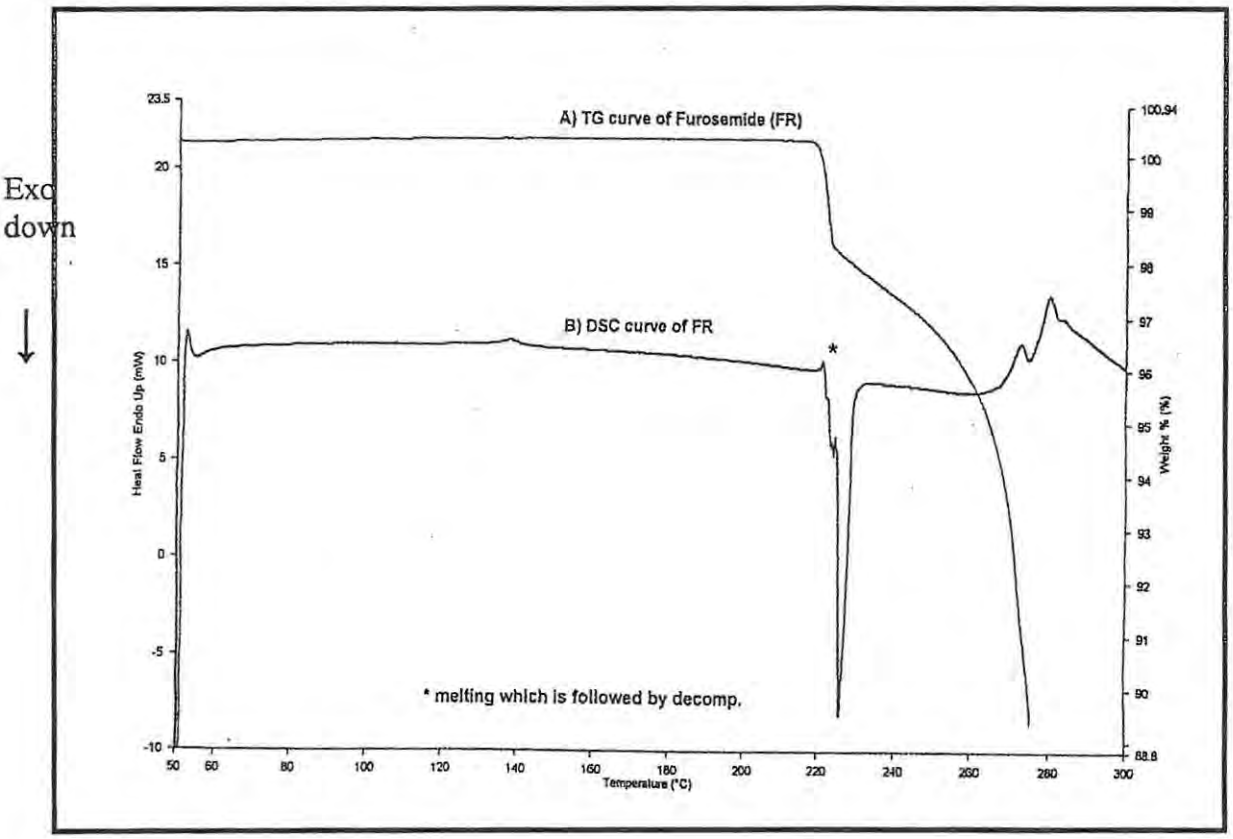

Figure 6.1 TG (curve A) and DSC (curve B) results for FR heated at 10 ^{0}C min^{-1} in nitrogen, showing the melting of FR accompanied by rapid exothermic decomposition.

To test for reversibility of the small endotherm with onset of about 138 ^{0}C, a sample of furosemide was weighed and then heated in the DSC from 50 -180 ^{0}C at 10 ^{0}C min^{-1}. The sample was cooled and then heated again from 50-180 ^{0}C at 10 ^{0}C min^{-1} (**Figure 6.2**). After heating, the sample retained its white colour and there was no mass loss. The endotherm was clearly visible in the repeated scan, indicating that the process is readily reversible.

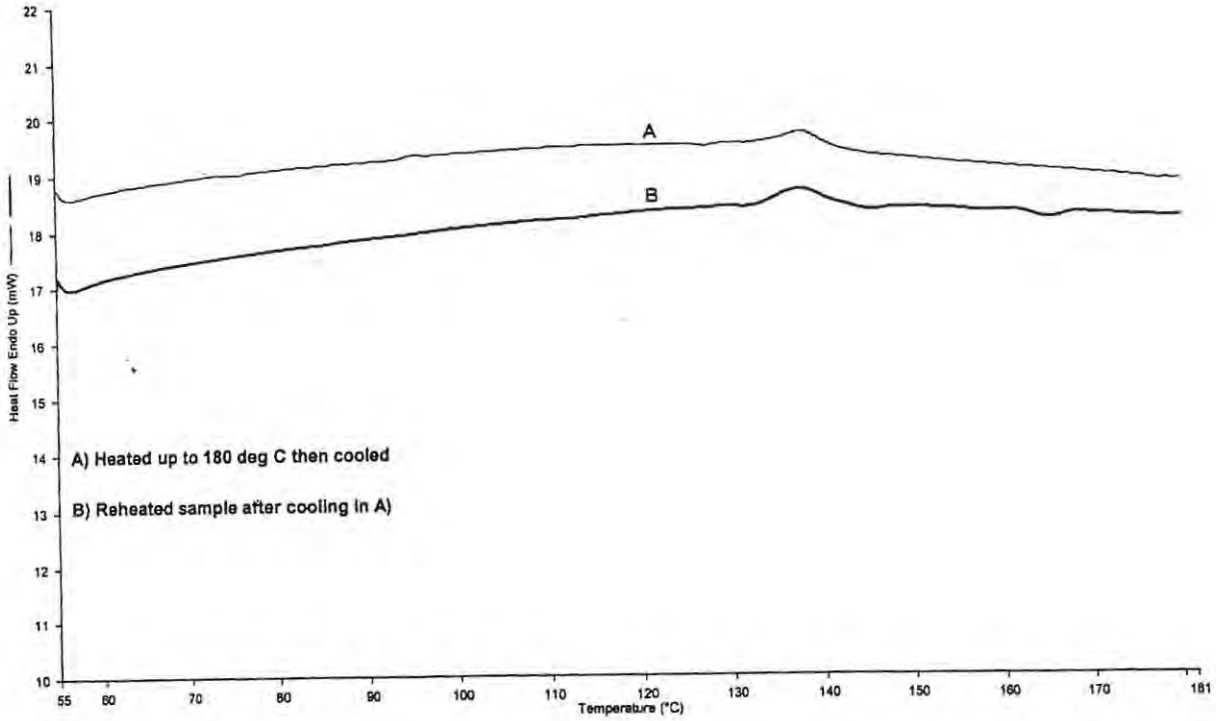

Figure 6.2 DSC curves for furosemide showing the reversibility of the small endotherm with the onset at about 138 ^{0}C, after initial heating to 180 ^{0}C, followed by cooling and reheating the sample.

TG-FTIR was used to determine the gaseous decomposition products formed on heating FR. From the molecular structure of FR, CO_2 and SO_2 were considered to be possible gaseous products so the appropriate spectral regions [34], namely 2100-2600 cm^{-1} for CO_2 and 1150-135 cm $^{-1}$ for SO_2, were selected for examination. Other possibilities for gaseous decomposition products of FR are HCl and NH_3. No convincing evidence for these gases was found in the region of 3059-2650 cm^{-1} for HCl and 986-931 cm^{-1} for NH_3. A stacked plot of FTIR spectra obtained during a TG run (**Figure 6.3**) on FR from 0.00 to 60.0 minutes (50 to 650 ^{0}C at 10 ^{0}C min^{-1}) is shown in **Figure 6.4(a)**. The changes in absorbance in the regions characteristic of CO_2 and SO_2 are evident.

The Gram-Schmidt curves (i.e. total IR absorption against time curves) of CO_2 and SO_2 (see **Figure 6.4(b)**) showed that both these gases were initially released simultaneously for up to 30 minutes (350 ^{0}C). The evolution of SO_2 then decreased slowly while the evolution of CO_2 increased and was still being evolved at 650 ^{0}C. At this temperature (650 ^{0}C), the overall mass-loss of the drug is seen to be about 71 % but is still incomplete.

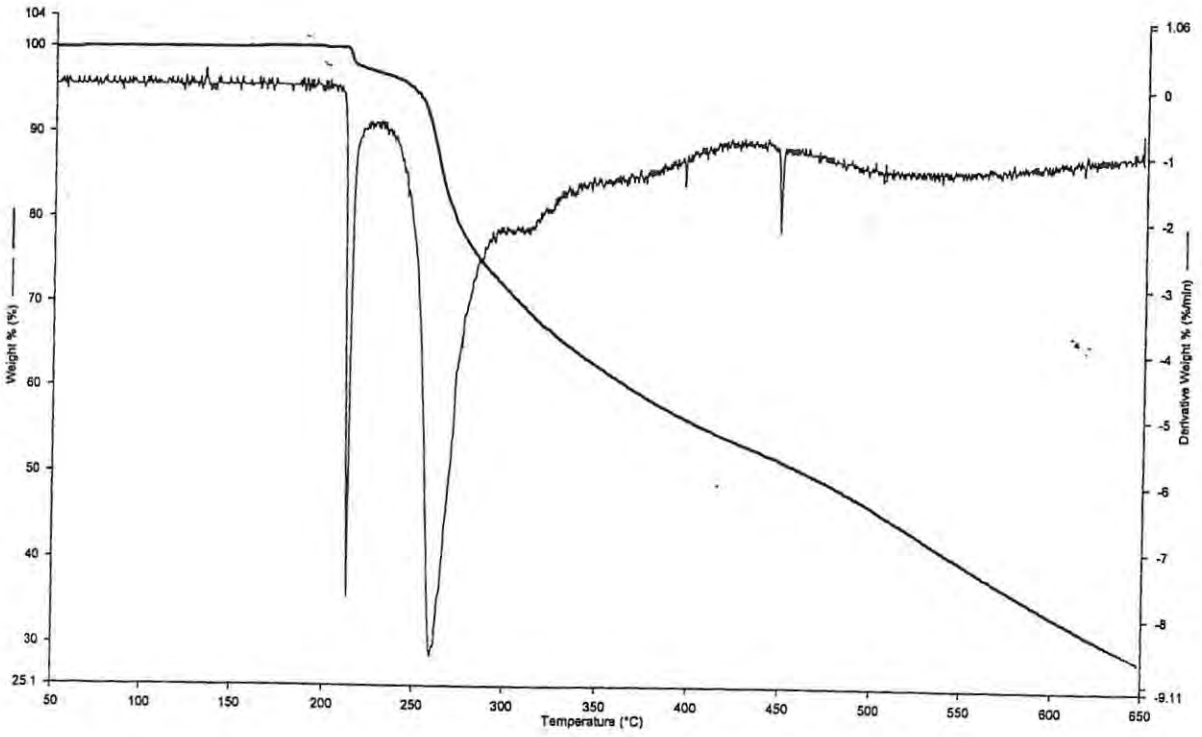

Figure 6.3 TG and DTG curves for furosemide heated at 10 ^{0}C min^{-1} in nitrogen. The FTIR results shown in **Figure 6.4** were obtained during this experiment.

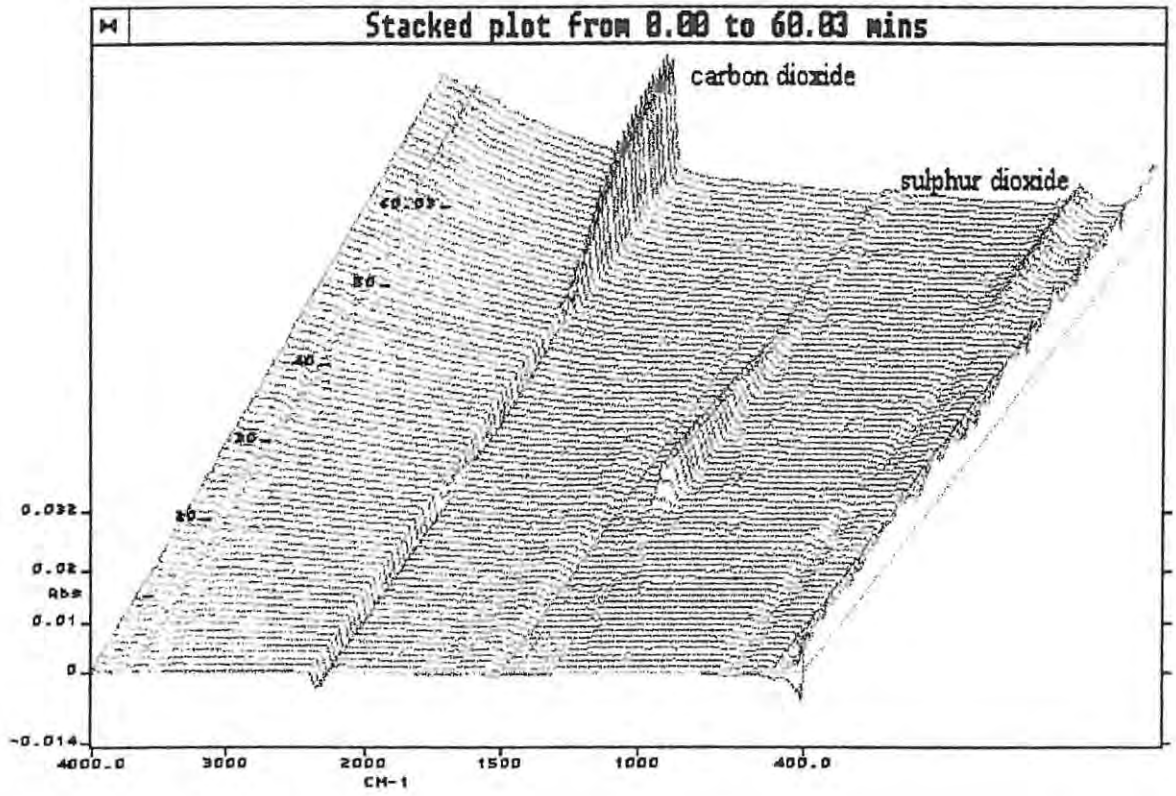

Figure 6.4(a) Stacked plot of FTIR spectra for furosemide from 0.00 to 60.00 minutes heated from 50 to 650 ^{0}C at 10 ^{0}C min^{-1} showing the release of CO_2 and SO_2.

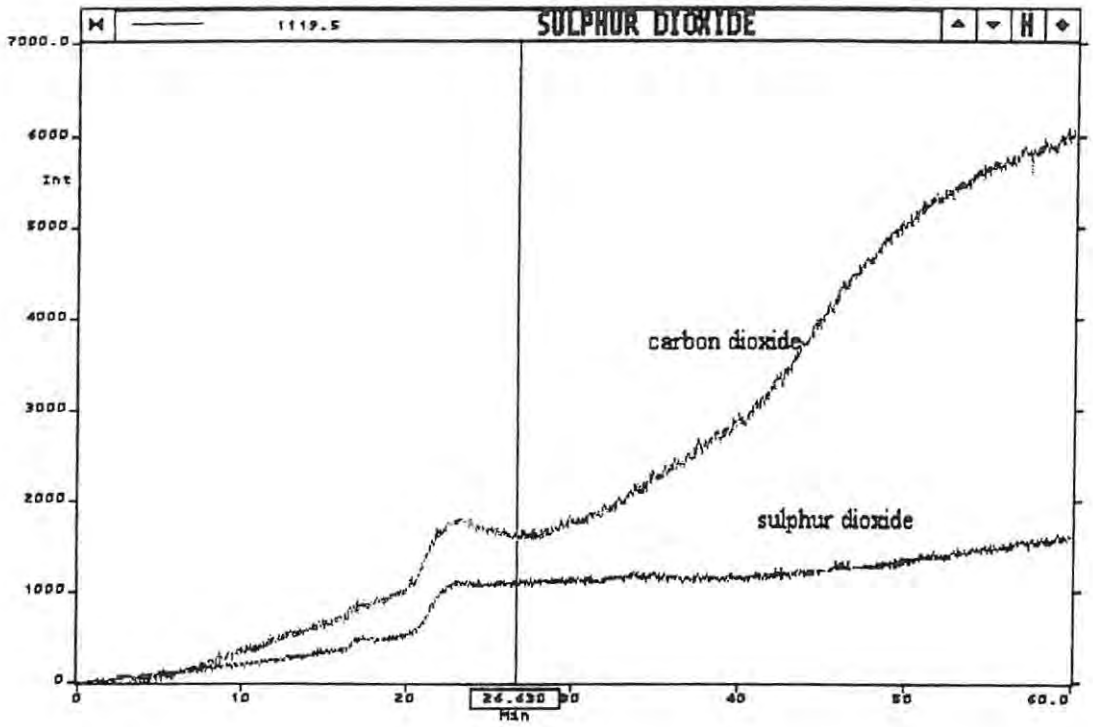

Figure 6.4(b) Gram-Schmidt curves of the IR absorption of gases evolved on heating furosemide from 50 to 650 ^{0}C at 10 ^{0}C min^{-1} in nitrogen.

6.2 Cyclodextrins (CDs)

6.2.1 Beta-cyclodextrin (BCD)

BCD, on heating at 10 ^{0}C min^{-1} in air is reported [55] to lose water (about 14 %) up to 100 ^{0}C. There is an endotherm at about 220 ^{0}C associated with a reversible transition. Thermal decomposition (or oxidation in air) starts at 250 ^{0}C. An endotherm (melting) occurs near 300 ^{0}C. Ignition occurs at above 300 ^{0}C in air.

The DSC curve of beta-cyclodextrin (BCD) heated from 50-350 ^{0}C at 10 ^{0}C min^{-1} in nitrogen, (**Figure 6.5**, curve B) showed a large endotherm 60-120 ^{0}C (ΔH = 223 J g^{-1}). There is a small exotherm (transition) at about 220 ^{0}C and degradation (overlapping endo-and exothermic events) occurs above 300 ^{0}C.

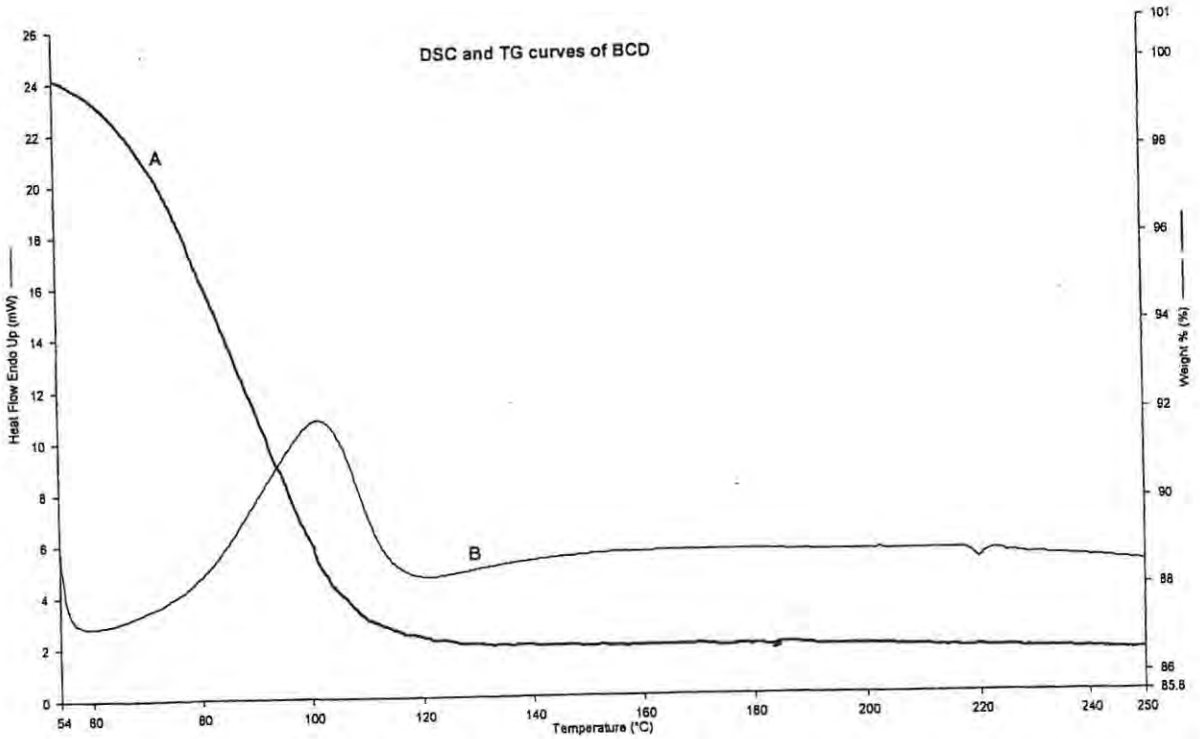

Figure 6.5 DSC (curve B) and TG (curve A) results for beta-cyclodextrin (BCD) heated at 10 ^{0}C min^{-1} in nitrogen.

The TG curve (**Figure 6.5**, curve A) shows a gradual mass loss in a single stage between 52 and 120 ^{0}C. The overall mass-loss is 12 %. The temperature range corresponds with the endotherm observed in the DSC curve for BCD. This process is attributed to removal of water from the cyclodextrin.

6.2.2 Gamma-cyclodextrin (GCD)

The DSC curve (**Figure 6.6**, curve B) for gamma-cyclodextrin (GCD) heated from 50 to 280 ^{0}C at 10 ^{0}C min^{-1} in nitrogen, showed a broad endotherm from 50 to 100 ^{0}C ($\Delta H = 62$ J g^{-1}). The TG curve (**Figure 6.6**, curve A) shows a mass loss of about 8 % between 38 and 115 ^{0}C. Again this is attributed to removal of water from the cyclodextrin.

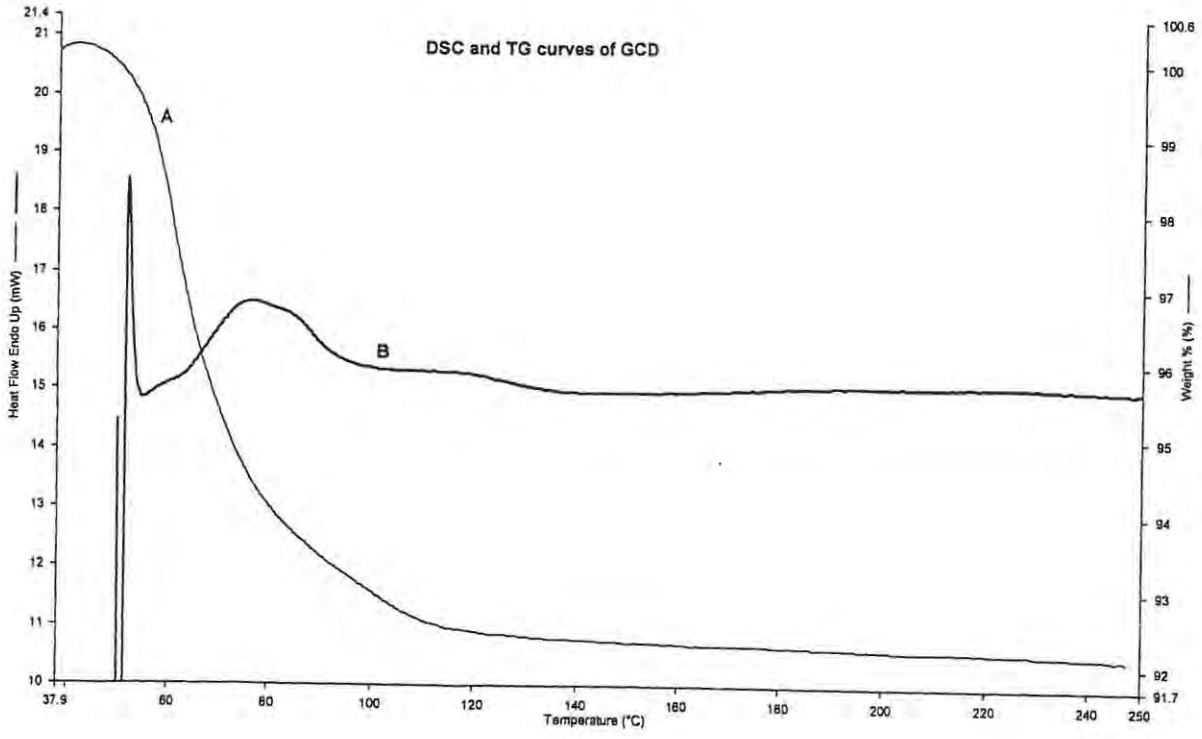

Figure 6.6 DSC (curve B) and TG (curve A) results for GCD heated at 10 ^{0}C min^{-1} in nitrogen.

6.2.3 Comparison of the thermal behaviour of BCD and GCD

The thermal behaviour of the cyclodextrins used is summarized in **Table 6.1**

Table 6.1 Thermal behaviour of the cyclodextrins used

Cyclodextrins	**Molar mass/g mol^{-1}**	**TG mass loss %**	**Moles H_2O**	**Dehydration: ΔH/ J g^{-1}**	**kJ (mol CD)$^{-1}$**	**Temp range / ^{0}C**
BCD	1135	12	9	223	253	50 - 120
GCD	1295	8	6	62	80	40 - 100

From the temperature ranges, mass losses and enthalpy values in **Table 6.1**, it can be seen that water is much less strongly bound in GCD than in BCD. The enthalpies of dehydration, per mole of water removed, are 13.8 kJ for GCD and 33.3 kJ for BCD. Bilal *et al.* [81] studied the thermal decomposition of the BCD-water complex. The BCD used contained 14 % H_2O by mass. They determined (using solution calorimetry) that to remove one mole of H_2O from one mole of BCD required ΔH = 10.50 kJ per mol of anhydrous BCD.

$$BCD.nH_2O\ (s) \rightarrow BCD.\ (n\text{-}1)\ H_2O\ (s) + H_2O\ (l)$$

The ΔH value obtained from DSC was 385 J (g BCD)$^{-1}$ or 50.2 kJ (mol H_2O)$^{-1}$.

$$BCD.\ n\ H_2O\ (s) \rightarrow BCD.\ (n\text{-}1)\ H2O\ (s) + H_2O\ (g)$$

The difference 50.2-10.5 kJ is 39.7 kJ is close to the enthalpy of vaporization of water at 100 ^{0}C = 40.6 kJ mol^{-1}. No definite hydrate of BCD exists and the maximum water content depends upon the temperature and the water-vapour pressure. At 29 ± 1 ^{0}C the number of water molecules per BCD is 10 to 12 [83].

6.3 FR/ cyclodextrin mixtures

6.3.1 Mixtures of FR and BCD

DSC curves (**Figure 6.7**) of FR/BCD *physical* mixtures, with various molar ratios, heated from 50 to 250 ^{0}C at 10 ^{0}C min^{-1} in nitrogen, showed the dehydration endotherm from BCD at 55 to 110 ^{0}C. The FR transition at 138 ^{0}C is visible, as are some of the other features of the FR trace between 220 and 230 ^{0}C. These events obscure the small exotherm seen in the BCD curve at about 220 ^{0}C. Attempts were made to use any changes in the enthalpy values as a measure of the extent of any complexation (see **Table 6.2**). The DSC curves for the kneaded FR/BCD mixtures are shown in **Figure 6.8**.

Table 6.2 DSC results for mixtures of furosemide (FR) and BCD heated at 10 ^{0}C min^{-1} in nitrogen.

FR/BCD ratio	**FR melting (216-223 ^{0}C) ΔH /J (g FR)$^{-1}$**	**small endo (138 ^{0}C) ΔH/J (g FR)$^{-1}$**	**BCD dehydration (60-100 ^{0}C) ΔH/ J (g BCD)$^{-1}$**	**Expected ΔH for BCD contribution**
BCD only	0	0	223	-
FR only	14.6	2	0	-
physical mixtures				
1:1 FR/BCD	14.4	1.3	171	173
1:2 FR/BCD	3.9	0.6	146	195
1:3 FR/BCD	5.4	Virtually eliminated	172	203
1:4 FR/BCD	0.5	3.1	176	208
2:1 FR/BCD	7	2.4	112	141
3:1 FR/BCD	11.3	1.2	105	119
kneaded mixtures				
1:1 FR/BCD	30	1	169	173
1:2 FR/BCD	7.1	2.2	190	195
1:3 FR/BCD	1.8	Virtually eliminated	195	203
1:4 FR/BCD	2.5	Virtually eliminated	190	208
2:1 FR/BCD	1.5	2	103	141
3:1 FR/BCD	15.1	2.7	113	119

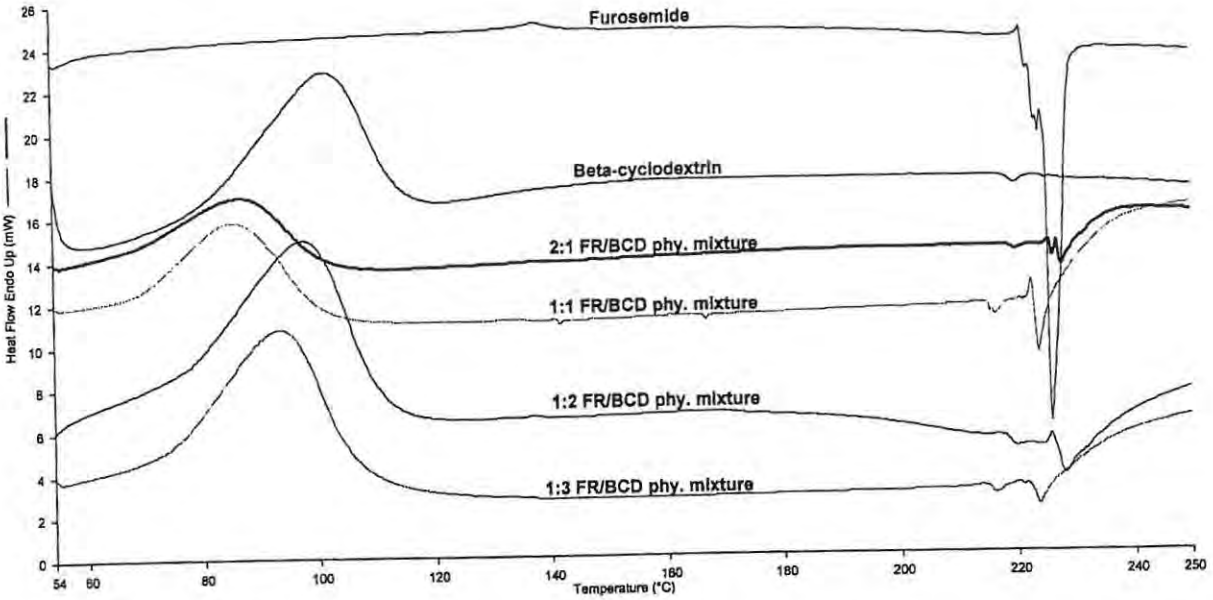

Figure 6.7 DSC curves for *physical* mixtures of FR/BCD heated at 10 ^{0}C min^{-1} in nitrogen

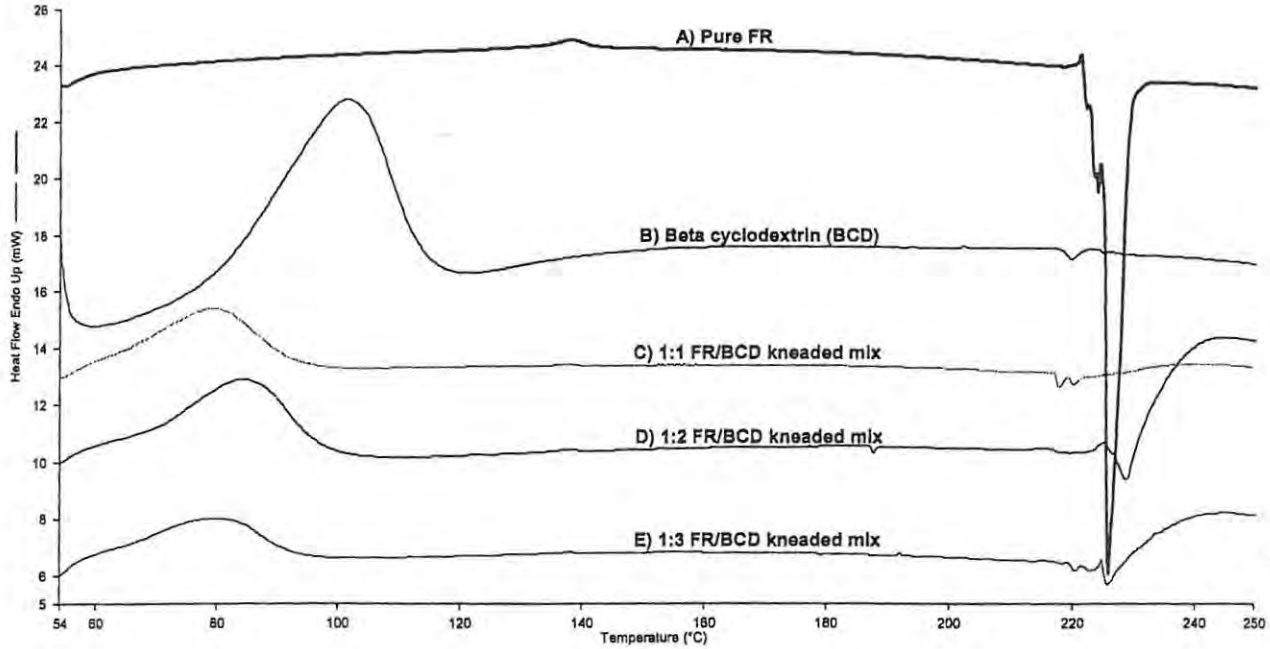

Figure 6.8 DSC curves of FR/BCD *kneaded* mixtures, heated at 10 ^{0}C min^{-1} in nitrogen.

DSC results for the physical and kneaded mixtures are not very different. The dehydration endotherm of BCD is not greatly affected by mixing, which suggests that water is not displaced from the BCD cavity during mixing and hence inclusion of significant amounts of the drug is not likely. The complex melting/ decomposition process of FR is, however, altered by the presence of BCD. It is of interest that the small endotherm shown by BCD at about 220 ^{0}C is very close to the melting of FR and this may enhance an interaction other than inclusion. Because the DSC results indicated little, if any, interaction between FR and BCD, TG curves were only recorded for the kneaded mixtures (see **Table 6.3** and **Figure 6.9**).

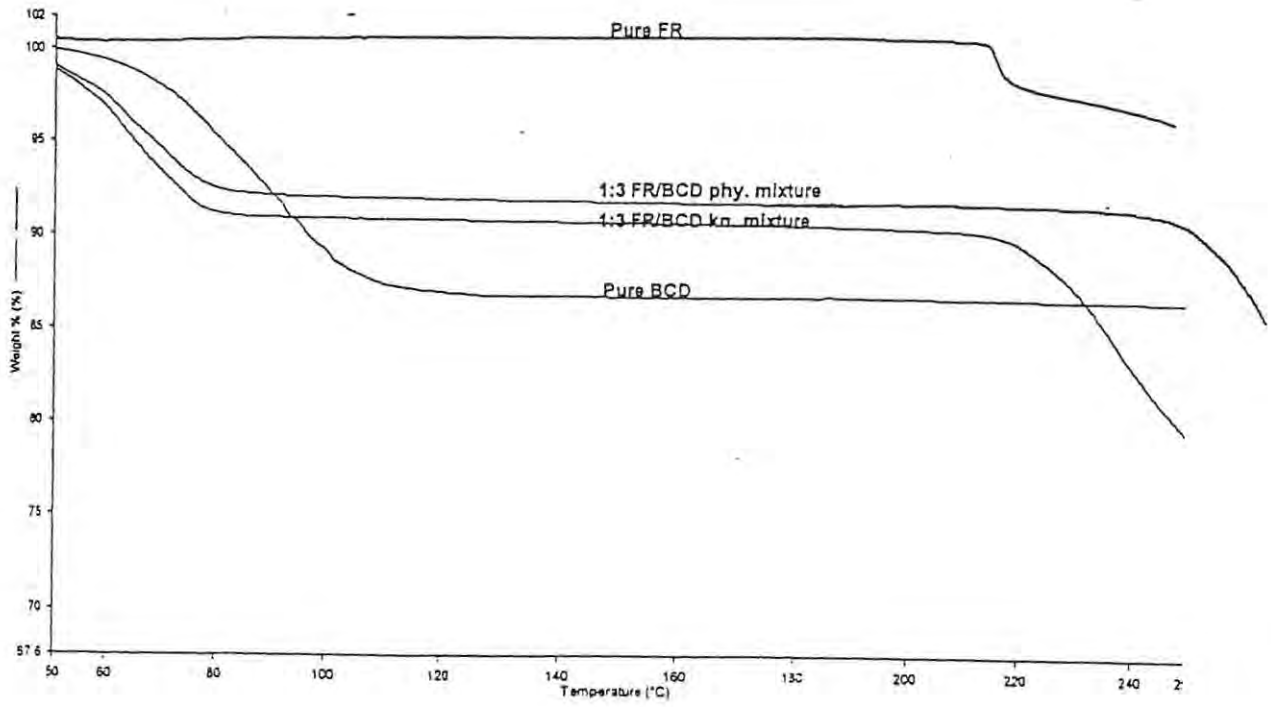

Figure 6.9 TG curves of 1:3 FR/BCD *physical* and *kneaded* mixtures heated at 10 ^{0}C min^{-1} in nitrogen

Table 6.3 TG results for the *kneaded* mixtures of FR and BCD heated at 10 ^{0}C min^{-1} in nitrogen.

FR/BCD molar ratios	**1st mass loss % (30 - 90) ^{0}C**	**expected values for BCD % (30-90) ^{0}C**	**2nd mass loss % (209 - 280) ^{0}C**
BCD only	12	12	0
FR only	0	0	~14.0
1:1 FR/BCD	11.5	9.3	20.2
1:2 FR/BCD	10.0	10.5	24.4
1:3 FR/BCD	9.0	10.9	20.8
1:4 FR/BCD	6.5	11.2	22.0
2:1 FR/BCD	5.3	7.6	12.6
3:1 FR/BCD	13.1	6.4	21.1

The first mass loss is due to the dehydration taking place in BCD. The second mass loss is due to the degradation of furosemide which is accompanied by melting, as shown by the temperature range where this occurs and comparison with the DSC results.

6.3.2 Mixtures of FR and GCD

Figure 6.10 shows the DSC curves of *physical* mixtures of FR and GCD heated at 10 ^{0}C min^{-1} in nitrogen. An endotherm in the range 50-100 ^{0}C, corresponding to the dehydration of GCD, the weak FR transition around 138 ^{0}C and the FR exotherm around 220 ^{0}C were visible. The last two curves at the extremes of the mixing ratios are of greatest interest. In the 1:3 FR/GCD mixture, the melting/decomposition of FR appears to be suppressed. The dehydration endotherm of GCD is still clearly evident. For the 2:1 FR/GCD mixture, in spite of the increase proportion of FR, the melting/decomposition is very much suppressed and the dehydration endotherm of GCD has virtually disappeared.

The DSC curves for *kneaded* mixtures of FR/GCD, shown in **Figure 6.11**, support and strengthen the above observations. Kneading has increased the interaction between FR and GCD, as shown by the DSC results for the physical and kneaded mixtures of FR/GCD which are summarized in **Table 6.4. Figure 6.12** shows the TG curves of FR/GCD mixtures.

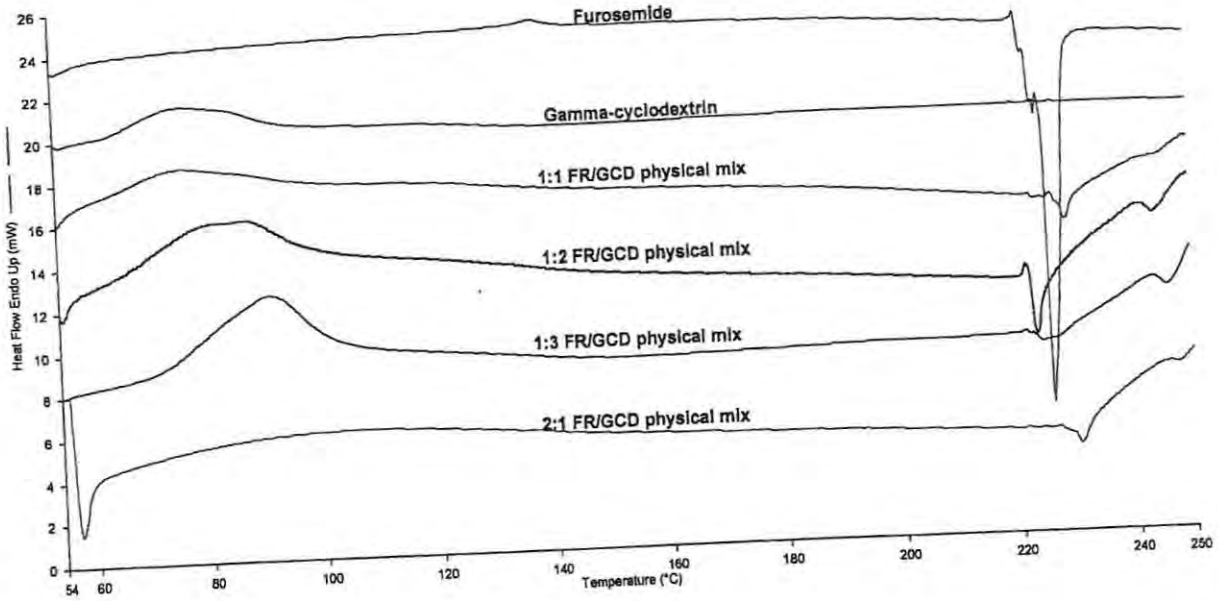

Figure 6.10 DSC curves for *physical* mixtures of FR/GCD heated at 10 ^{0}C min^{-1} in nitrogen.

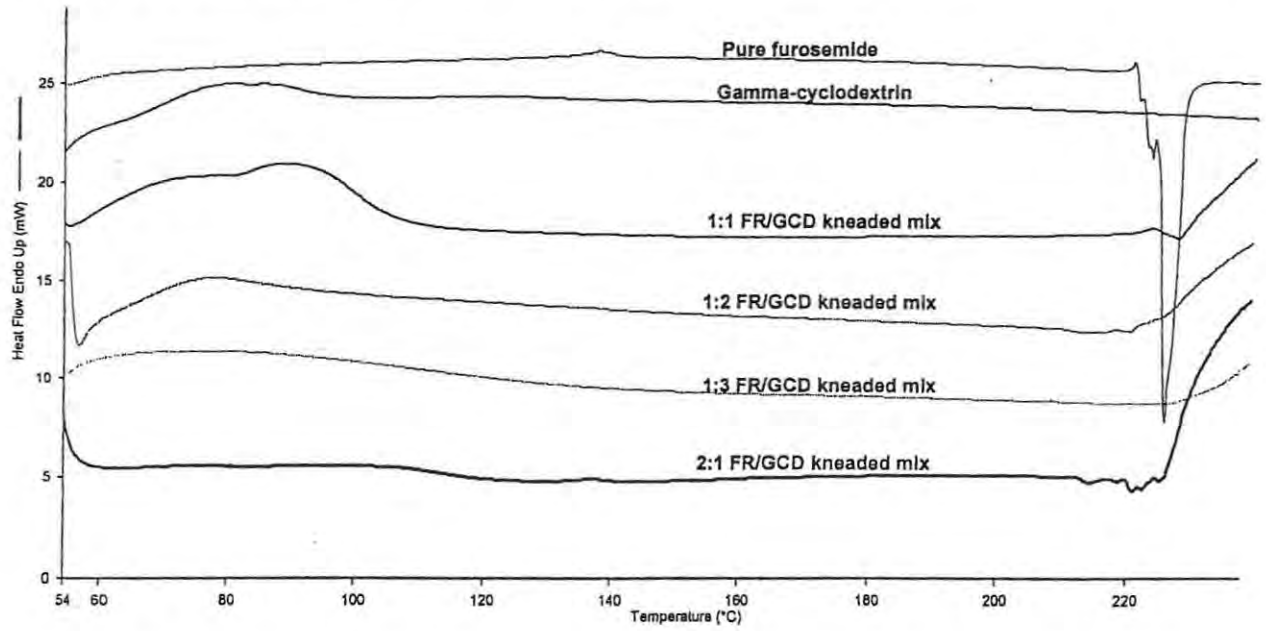

Figure 6.11 DSC curves for *kneaded* mixtures of FR/GCD heated at 10 ^{0}C min^{-1} in nitrogen.

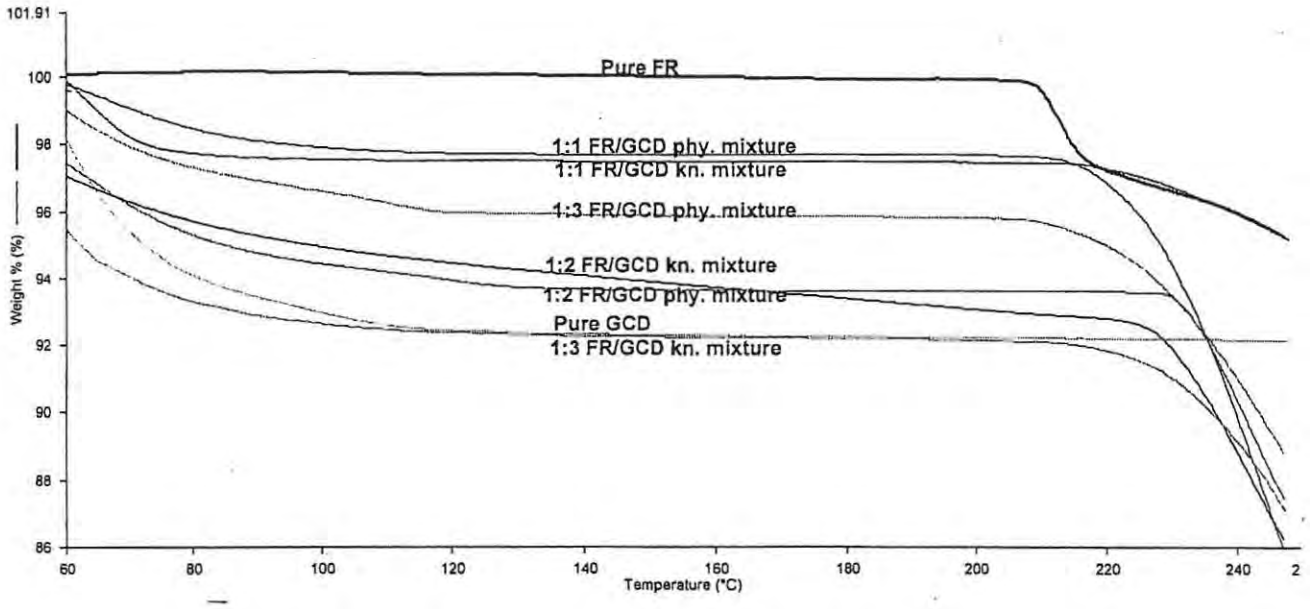

Figure 6.12 TG curves of the *physical* and *kneaded* mixtures of FR and GCD heated at 10 ^{0}C min^{-1} in nitrogen.

Table 6.4 DSC results for mixtures of FR and GCD heated at 10 ^{0}C min^{-1} in nitrogen

FR/GCD molar ratio	**GCD dehydration (60-100 ^{0}C) of ΔH/J(g GCD)$^{-1}$**	**Expected ΔH dehydration for GCD**	**FR melting range in FR/GCD mixture**
GCD only	62	-	0
FR only	0	-	216-226
physical mixtures			
1:1 FR/GCD	56	49.4	220-223
1:2 FR/GCD	58	55	220-223
1:3 FR/GCD	62	57.2	219-223
2:1 FR/GCD	virtually eliminated	41	223-226
kneaded mixtures			
1:1 FR/GCD	(30 + 53) = 88	49.5	222-225
1:2 FR/GCD	52	55	223-227
1:3 FR/GCD	virtually eliminated	57.2	237-255
2:1 FR/GCD	virtually eliminated	41	217-219

6.3.3 Comparison of the results for mixing of FR with BCD and GCD

The DSC results described above suggest that the interaction between FR and GCD is greater than between FR and BCD. One of the pointers to this interaction is the change in ΔH for dehydration of the CD component of the mixture which could be an indication of replacement of water in the CD cavity by FR. These changes in ΔH values for mixtures of FR with BCD and GCD are summarized in **Table 6.5.**

Table 6.5 Effect of mixing on the dehydration enthalpies (J (g CD)$^{-1}$) of the cyclodextrins

FR/CD ratio	BCD ΔH dehydration	GCD ΔH dehydration
Pure	0	0
BCD	223	0
GCD	0	62
1:1	169	30 + 53 = 88
1:2	190	52
1:3	195	virtually eliminated

6.3.4 The effect of the kneading solvent on FR and on the cyclodextrins

Because of the quite marked effects found for kneaded mixtures of FR and GCD in particular, the possible effects of the kneading process, carried out separately on the drug and on the cyclodextrins, were examined. Samples of the cyclodextrins were mixed in ethanol and treated in the same way as the kneaded samples were prepared, except that no FR was present. A sample of FR treated in ethanol was also dried in an oven for one hour at 30 ^{0}C. These samples were then heated in the DSC under the same conditions as for the mixtures, i.e. at 10 ^{0}C min^{-1} with nitrogen as a purge at 20 ml min^{-1}. Results are given in **Table 6.6.**

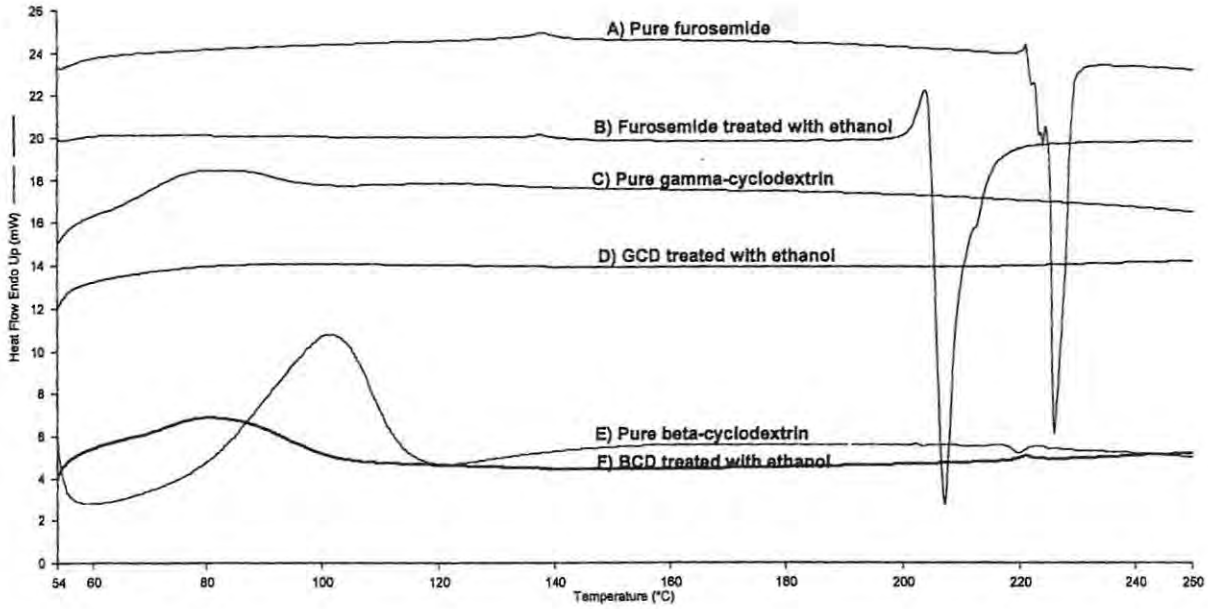

Figure 6.13 DSC curves for FR, GCD and BCD showing the effect of treatment with the kneading solvent (ethanol) heated at 10 ^{0}C min^{-1} in nitrogen.

Table 6.6 DSC results for the solvent-treated cyclodextrins and furosemide

Cyclodextrins	**ΔH dehydration (after ethanol treatment) (J g^{-1})**	**T range (^{0}C)**	**ΔH dehydration (untreated) (J g^{-1})**	**T range (^{0}C) J g^{-1}**
BCD	112	56-105	223	65-112
GCD	74	58-131	62	60-95
FR	**ΔH melting (after ethanol treatment) (J g^{-1})**	**T range (^{0}C)**	**ΔH melt (untreated)(J g^{-1})**	**T range (^{0}C) J g^{-1}**
FR small endo	1	137-138	2	137-138
FR melting endo	16	201-205	14.4	216-226

From the results obtained, it appears that the kneading solvent may replace some of the water from the cavity of the cyclodextrins. The melting temperature of the drug treated with the solvent is lowered. The effect of the solvent, and hence of the kneading process, could be to increase the complexity of the competition between the guest molecule (in this case furosemide) and water and ethanol for space in the cyclodextrin cavity.

6.3.5 Effect of ageing of mixtures

Because the 1:3 FR/GCD kneaded mixture showed the most pronounced changes from the physical mixture, it was chosen for studying any effects of ageing. A DSC run on the 1:3 FR/GCD kneaded mixture was done a month after it had been prepared. The sample was kept in a cupboard in a capped sample vial wrapped with aluminum foil to prevent exposure to sunlight. The results (**Figure 6.14**) showed two overlapping endotherms instead of one dehydration endotherm for the cyclodextrin. The first endotherm appeared at about (59-73) ^{0}C and the second at (74-97) ^{0}C. The overall ΔH value was about 152 J g^{-1}. The features of FR were not visible in either curve. These results suggest that the mixture may have adsorbed additional water from the atmosphere.

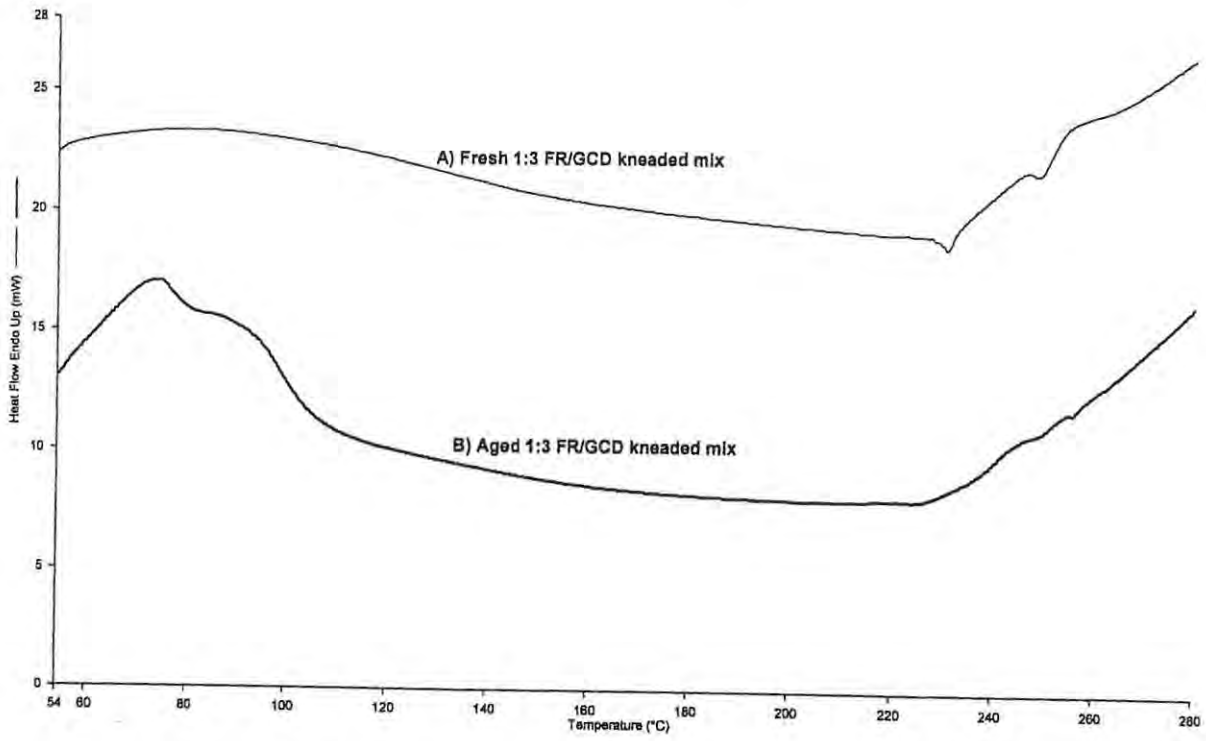

Figure 6.14 DSC curves of 1:3 FR/GCD *kneaded* mixtures A) fresh sample B) aged (1 month) sample heated at 10 ^{0}C min^{-1} in nitrogen.

6.4 Infrared spectroscopy of FR /cyclodextrin mixtures

6.4.1 FR/BCD mixtures

Thermal analysis results suggest that there may be some inclusion of FR in the BCD cavity. Some changes were observed in the IR spectra of the kneaded mixtures, where the N-H stretching band at 3274-3336 cm^{-1} decreased in intensity and the major characteristic of FR, the carbonyl stretch (C=O) at about 1668.0 cm^{-1}, was observed at 1660.9 cm^{-1} and was weak and broad. The other characteristic vibrations of furosemide were still observed, but most of them were weak, with the C-Cl stretch showing at 572.2 cm^{-1} instead of 581.7 cm^{-1}, (see **Table 6.7**). Interactions between guests and cyclodextrins in the solid state are known to cause shifts in the IR absorptions spectra. Inclusion of drug in the cyclodextrin cavity can lead to changes in bond strengths and hence shifts and / or changes in intensity in absorption bands [82].

Table 6.7 Infrared absorption maxima for FR/BCD mixtures

Samples	ν(C=O)/cm^{-1}	ν(CN-H)/cm^{-1}	ν(SO_2N-H)/cm^{-1}	ν(S=O)/cm^{-1}	ν(C-Cl)/ cm^{-1}
Furosemide	1668	3348.9	1321.4	1141.3	581.7
1:1FR/BCD phy.	1660	3692.9	1458	1321	575.2
1:1 FR/BCD kn.	no change	no change	no change	no change	no change
1:2 FR/BCD phy.	no change	weak band	no change	no change	no change
1:2 FR/BCD kn.	decrease in band intensity	weak band	weak band	no change	no change
1:3 FR/BCD phy.	broad and intense band	weak band	weak band	no change	575.2
1:3 FR/BCD kn.	weak and less intense	disappeared	disappeared	weak	575.2

6.4.2 FR/GCD mixtures

Water absorption bands were seen in the region (3600-3300) cm^{-1} for all the cyclodextrins. The spectrum of the 1:3 FR/GCD kneaded mixture shows some noticeable changes in the characteristic band for FR. The N-H stretching band in the region of 3500 cm^{-1} had disappeared and the NH_2 band had decreased in intensity. The C=O vibration band from the COOH group had also decreased in intensity. This could be due to hydrogen bonding taking place inside or outside the cavity with the strength of the C=O thus decreasing the leading to the decrease in the intensity of the absorption band. The C-Cl band had virtually disappeared. Results are summarized in **Table 6.8.**

Table 6.8 Infrared absorption maxima for FR/GCD mixtures

Samples	**ν(C=O)/cm^{-1}**	**ν(CN-H)/cm^{-1}**	**ν(SO_2N-H)/cm^{-1}**	**ν(S=O)/cm^{-1}**	**ν(C-Cl)/cm^{-1}**
Furosemide	1668	3348.9	1321.4	1141.3	581.7
1:1FR/GCD phy.	1668	3285-3338	1560-1595	1316	579
1:1 FR/GCD kn.	no change	no change	no change	no change	no change
1:2 FR/GCD phy.	decrease in intensity	weak band	no change	no change	no change
1:2 FR/GCD kn.	decrease in band intensity	weak band	no change	no change	no change
1:3 FR/GCD phy.	broad and less intense	disappeared	decrease in intensity	no change	decrease in intensity
1:3 FR/GCD kn.	disappeared	disappeared	disappeared	disappeared	decrease in intensity

Thermal analysis results for the 1:3 FR/GCD mixture (kneaded) suggested that some inclusion could be occurring. The IR spectra of these mixtures showed some noticeable differences from the rest of the mixtures. Firstly, the N-H stretching band in the region of 3500 cm^{-1} had disappeared. Secondly, the characteristic carbonyl band from COOH had also decreased in size relative to all the other mixtures. Thirdly, the NH_2 absorption band, which is also characteristic of furosemide, had also decreased significantly. Finally, the C-Cl band is very weak or absent. In the furosemide spectrum it appeared at 581 cm^{-1} [20], but in all the spectra of the mixtures it appeared around 571 cm^{-1}. A shift in the C-Cl vibration is indicative of an interaction taking place between the cyclodextrin and FR which is most probably due to hydrogen-bonding.

6.5 X-ray powder diffraction patterns of mixtures of FR with the CDs

6.5.1 FR/BCD mixtures

The XRD powder patterns of pure FR and pure BCD are shown in **Figure 6.15 (a)** and **(b)**. These patterns indicate crystalline compounds. The maximum diffraction intensity of FR occurs at 2θ = 35 ° and of BCD at 2θ = 15 °. The diffraction pattern of a 1:3 FR/BCD physical mixture (**Figure 6.15 (c)**) is mainly a superimposition of the patterns of the individual components. The pattern of the 1:3 FR/BCD kneaded mixture (**Figure 6.15 (d)**) is very different with some crystallinity and a diffraction maxima at 2θ = 45 °.

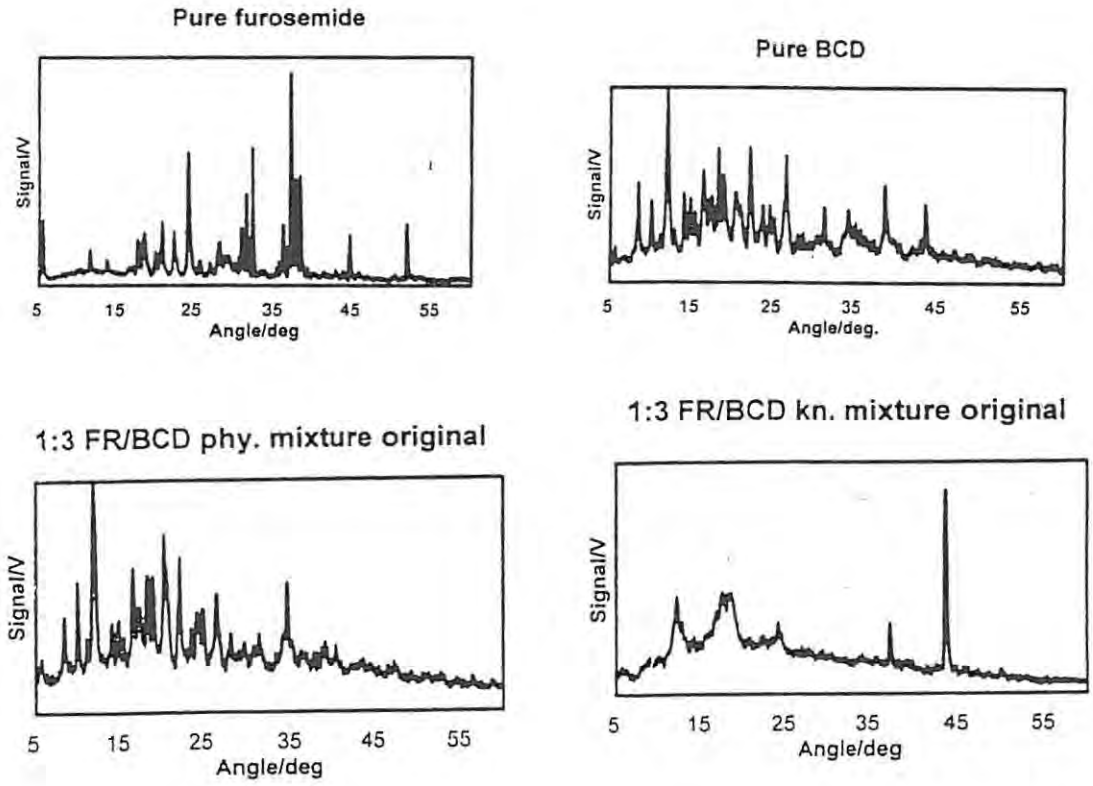

Figure 6.15 X-ray powder diffraction patterns of **a)** furosemide (FR) **b)** beta-cyclodextrin (BCD) **c)** 1:3 FR/BCD *physical* mixture and **d)** 1:3 FR/BCD *kneaded* mixture.

These results support the formation of an inclusion compound under the kneading conditions.

6.5.2 FR/GCD mixtures

The XRD powder patterns of pure FR and pure GCD are shown in **Figure 6.16 (a)** and **(b)**. These patterns indicate crystalline compounds. The maximum diffraction intensity of FR occurs at 2θ = 35 ° and of GCD at 2θ = 45 °. The diffraction pattern of a 1:3 FR/GCD physical mixture (**Figure 6.16 (c)**) shows not simply a superimposition of patterns of the components, but absence of the major lines of FR. This trend is carried further in the pattern of the 1:3 FR/GCD kneaded mixture (**Figure 6.16 (d)**) where a strong low angle (2θ =7 °) peak has developed.

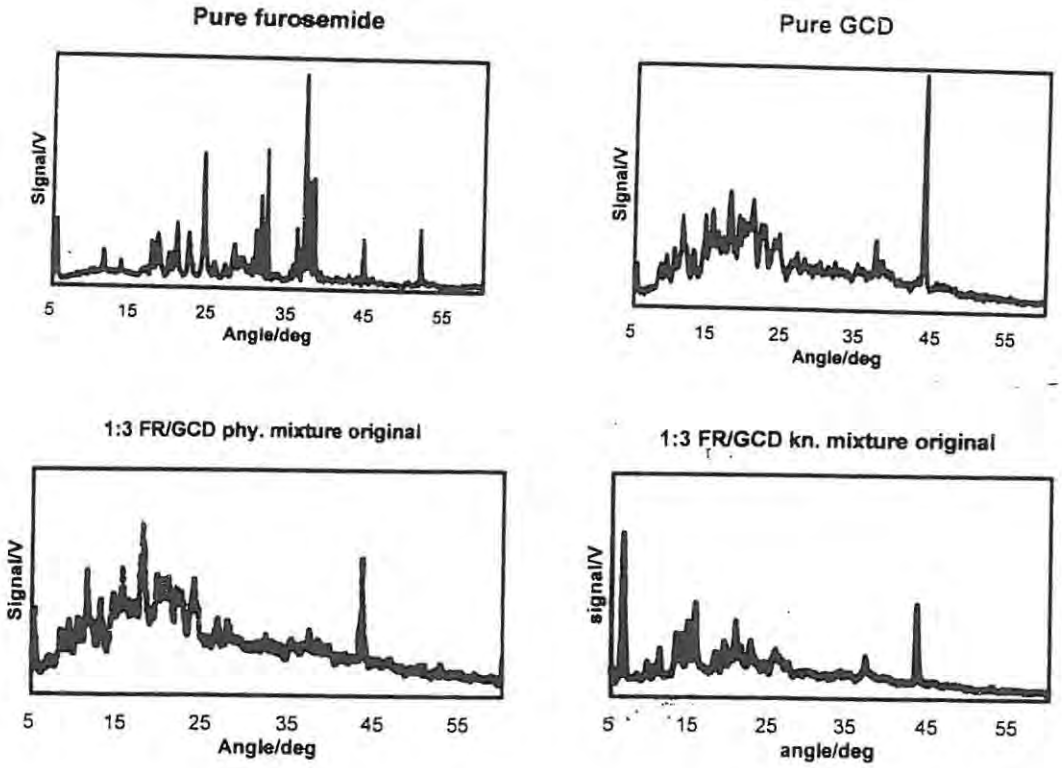

Figure 6.16 X-ray powder diffraction patterns of **a)** furosemide (FR), **b)** gamma-cyclodextrin (GCD), **c)** 1:3 FR/GCD *physical* mixture and **d)**1:3 FR/GCD *kneaded* mixture.

There results support the occurrence of significant interaction between FR and GCD even without kneading.

Chapter 7

7. RESULTS OF THE PHOTOSTABILITY STUDIES

7.1 Irradiation and HPLC analysis

Powder samples of the pure drug and of mixtures of the drug with cyclodextrins were irradiated at a dose rate of 550 W h m^{-2}, under the conditions described in detail in **Section 5.4.** After irradiation, samples were analysed using HPLC as described in **Section 5.5**. The results of analyses after various times of irradiation up to 24 hours are given in **Table 7.1**, and illustrated in **Figure 7.1.**

Table 7.1 HPLC analysis of 10 mg samples of furosemide after being irradiated for various times at 550 W h/m^2. (h_0 is the peak height for the pure drug.)

Exposure time/hrs of FR	**Peak height/h_0**	**% Drug remaining**
0	16.2/16.2	100
8	15.6/16.2	96.3
12	15.3/16.2	94.4
16	16.7/18.8	88.8
24	9.2/12.3	74.8

The colour of the sample changes from white to cream during the exposure period.

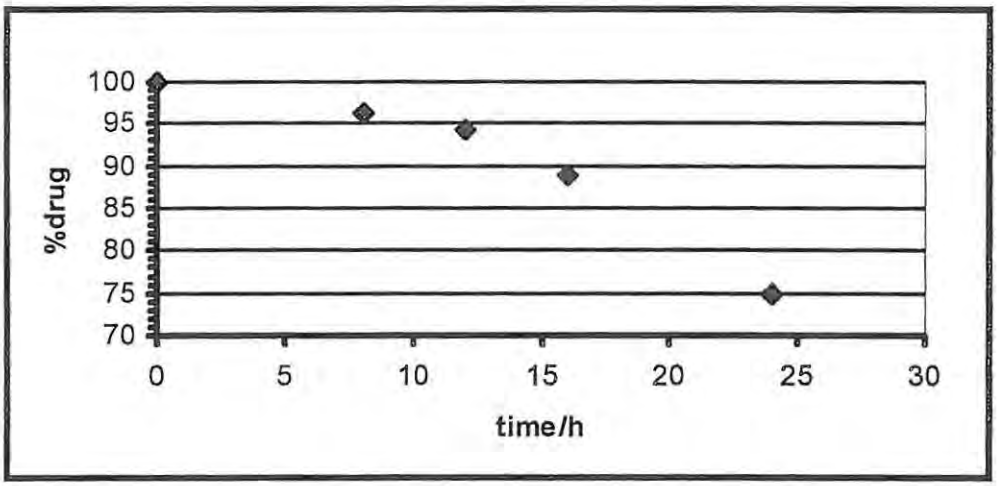

Figure 7.1 Photodegradation of FR after various times of irradiation at 550 W h m^{-2}.

From **Table 7.1** it can be seen that the changes in furosemide after up to 12 hours of exposure under the experimental light conditions small. The colour of the powder changed from white to cream. To increase the extent of degradation, the time of irradiation of the sample was increased to 16 hours and mixtures of furosemide and the cyclodextrins were also irradiated. The exposure recommended for accelerated photostability testing by the ICH corresponds to the minimum irradiance level of 1.2 million lux hours (21.8 hours SUNTEST exposure at 250 W h m^{-2}) referred to the visible wavelength range from approximately 400 nm to 800 nm, using a photometric unit with the spectral sensitivity of the human eye.

Physical and kneaded mixtures of FR and BCD and of FR and GCD, that had been prepared as described in **Section 6.3**, were irradiated under similar conditions to those used for the irradiation of pure FR. Dark control samples were also included in the SUNTEST cabinet. All samples were analysed using the HPLC method used for pure FR and described in **Section 5.5.** The results for the mixtures are shown in **Tables 7.2 and 7.3** and **Figures 7.2 and 7.3**.

Table 7.2 Results of 16 hours irradiation of FR and of FR/BCD mixtures at 550 W h m^{-2}

Sample	HPLC peak height/cm	% FR remaining
FR (0 h)	18.8	100
FR (16 h)	16.7	89.0
1:1 FR/BCD physical	11.9	63.3
1:1 FR/BCD kneaded	10.7	57.0
1:2 FR/BCD physical	13.4	71.3
1:2 FR/BCD kneaded	10	53.2
1:3 FR/BCD physical	11.2	59.6
1:3 FR/BCD kneaded	14.8	78.7
Dark control (8 h)	16.0/16.2	98.8
Dark control (12 h)	16.0/16.2	98.8
Dark control (16 h)	16.1/16.2	98.7

These results are illustrated in **Figure 7.2.** There is a general destabilizing effect due to the presence of BCD but no consistent trend with composition or with pretreatment of the mixture. The colour of all irradiated samples had changed from white to cream, while the dark control samples remained white.

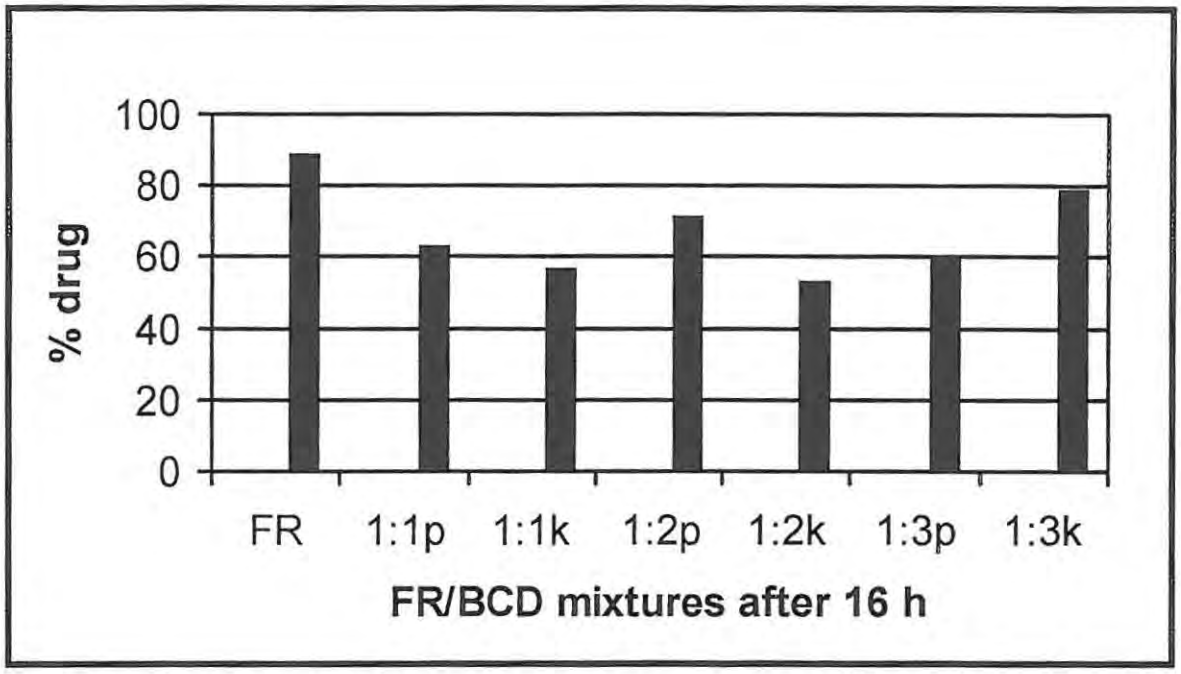

Figure 7.2 Photodegradation of FR and FR/BCD mixtures after irradiation for 16 h at 550 W h m^{-2}. The molar ratios of the mixtures are shown and p = *physical* mixture and k = *kneaded* mixture.

Table 7.3 Results of 16 hours irradiation of FR and FR/GCD mixtures at 550 W h m^{-2}

Sample	HPLC peak height/cm	% FR remaining
FR (0 h)	16.6	0
FR (16 h)	14.9	10.5
1:1 FR/GCD physical	12.3	25.9
1:1 FR/GCD kneaded	11.9	28.1
1:2 FR/GCD physical	12.5	24.1
1:2 FR/GCD kneaded	10.1	39.7
1:3 FR/GCD physical	10.9	34.3
1:3 FR/GCD kneaded	7.2	57.8
Dark control (8 h)	16.0/16.2	98.8
Dark control (12 h)	16.0/16.2	98.8
Dark control (16 h)	16.1/16.2	98.7

The photodegradation of FR/GCD mixtures is illustrated in **Figure 7.3.** The destabilizing effect due to the presence of the cyclodextrin is again considerable. The kneaded mixtures are more susceptible to photodegradation than the physical mixtures and the greater the proportion of GCD, the more extensive the degradation. It is of interest that the 1:3 FR/GCD kneaded mixture showed improved thermal stability (see **Section 6.3.2**) but the same mixture shows decreased photostability. This is discussed further in **Section 7.4.** The colour changes from white to cream on irradiation were similar to those for the FR/BCD mixtures except for the irradiated 1:3 FR/GCD mixture where the colour decreased to yellow (physical) and orange (kneaded).

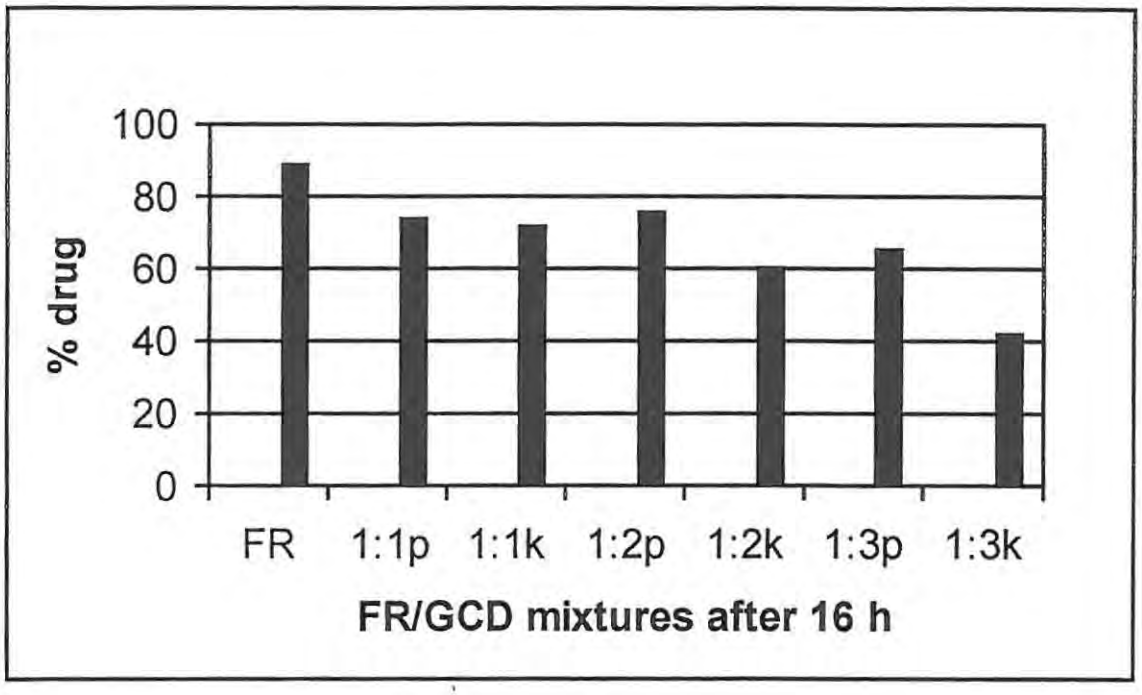

Figure 7.3 Photodegradation of FR and FR/GCD mixtures after irradiation for 16 h at 550 W h m^{-2}. The molar ratios of the mixtures are shown and p = *physical* mixture and k = *kneaded* mixture.

To check on the reliability of the HPLC analyses the percentage of FR recovered from the mixtures, with the irradiation steps omitted, are given in **Table 7.4.** These results show that the recovery is virtually complete, particularly in relation to the very much larger changes produced by irradiation.

Table 7.4 The extent of recovery of FR from FR/CD mixtures for comparison with analyses of the irradiated mixtures (see **Tables 7.2 and 7.3**)

Samples	**Peak height/cm**	**% FR recovered**
FR standard	17.6	100
1:1 FR/BCD phy.	17.4	98.9
1:1 FR/BCD kn.	17.2	97.7
1:2 FR/BCD phy.	16.9	96
1:2 FR/BCD kn.	17.3	98.3
1:3 FR/BCD phy.	17.2	97.7
1:3 FR/BCD kn.	17.2	97.7
1:1 FR/GCD phy.	17	96.6
1:1 FR/GCD kn.	17.3	98.3
1:2 FR/GCD phy.	17.5	99.4
1:2 FR/GCD kn.	17.2	98.7
1:3 FR/GCD phy.	17.6	100
1:3 FR/GCD kn.	17.1	97.2

7.2 Thermal behaviour of irradiated FR

7.2.1 DSC and TG

Samples of FR were irradiated for 16 hours as described in **Section 5.3.2.** DSC and TG were used to compare the behaviour of the irradiated samples with that of the original sample.

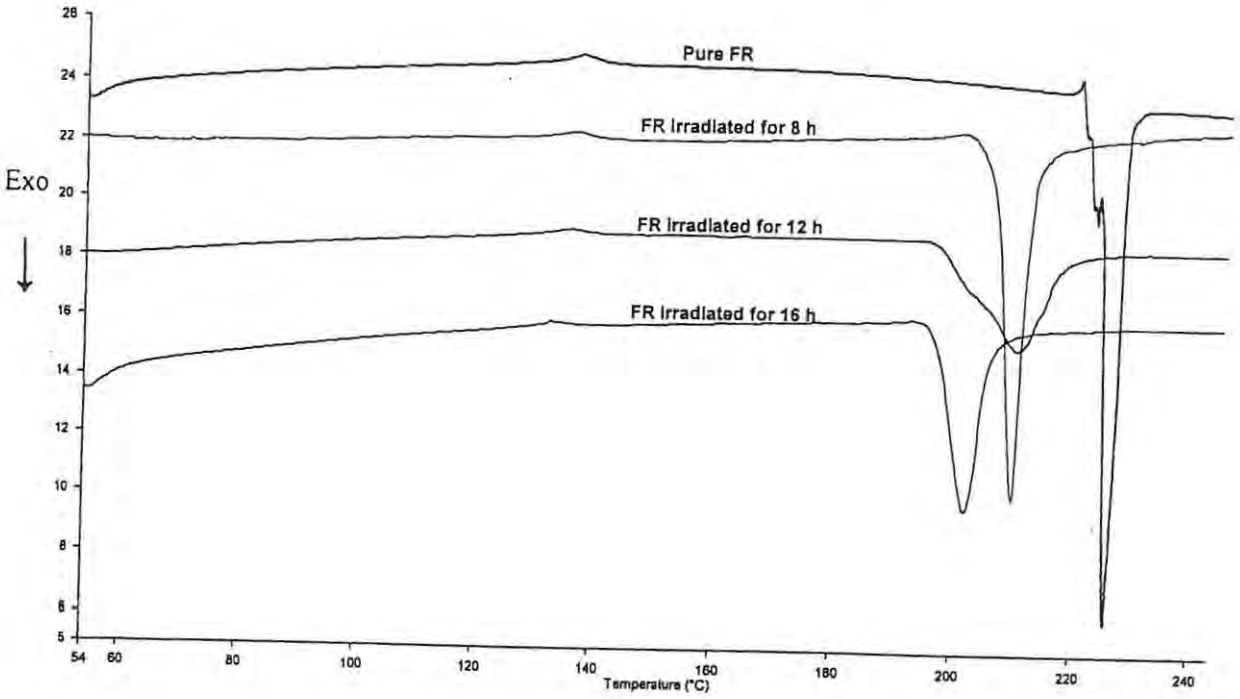

Figure 7.4 DSC curves for pure FR and samples of FR irradiated for various times heated at 10 $^{0}C\ min^{-1}$ in nitrogen. (**Note**: baselines are arbitrarily shifted vertically for ease of comparison).

From the DSC curves shown in **Figure 7.4**, it can be seen that the characteristic features of the curve for pure FR, namely the small endotherm at about 138 ^{0}C and the melting at 222 ^{0}C followed immediately by exothermic decomposition, are affected by irradiation and that the effects increase with radiation dose. The small endotherm remains visible (ΔH about 2 $J\ g^{-1}$) but onset shifts slightly to lower temperatures with radiation dose.

After 8 h irradiation, the melting endotherm is absent, the exotherm has broadened slightly and the onset has shifted to lower temperature (207 ^{0}C). After 12 h irradiation the broadening has increased and the onset temperature is lower (200 ^{0}C). After 16 h irradiation, HPLC results (**Table 7.2**) indicate about 11 % (by mass) degradation of FR and the exotherm has sharpened somewhat (onset 196 ^{0}C). The ΔH values of the exotherms were not significantly changed (see **Table 7.5**). The DSC curves of samples used as dark controls showed no changes from that of the original FR.

Table 7.5 Effects of irradiation dose at 550 W h m^{-2} on the thermal behaviour of FR.

Dose / h	**Onset T of exotherm / ^{0}C**	**ΔH /J g^{-1}**
0	224	-107
8	207	-95
12	200	-90
16	196	-96

The TG curves for FR and samples of FR irradiated for various times (corresponding to the DSC curves shown in **Figure 7.4**) are shown in **Figure 7.5**. The onset temperature of the mass loss associated with exothermic decomposition at above 220 ^{0}C decreases slightly with radiation dose, but the extent of the initial step (about 2 %) is not significantly altered.

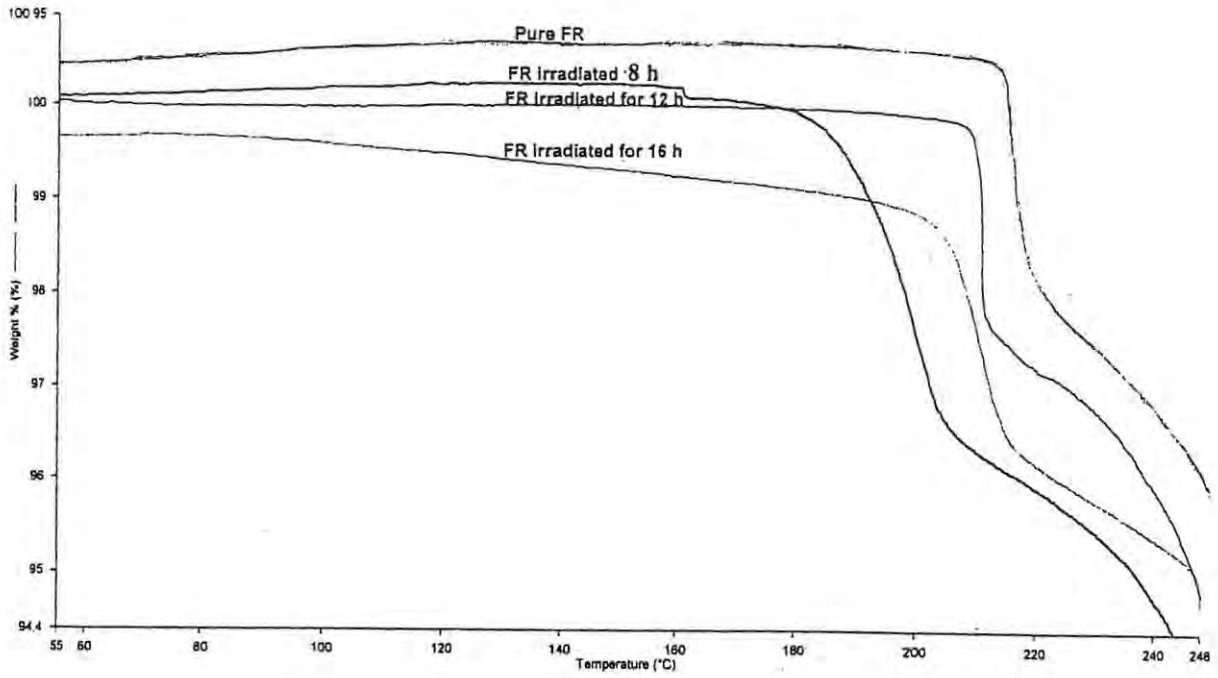

Figure 7.5 TG curves of pure FR and FR samples irradiated for various time, heated at 10 ^{0}C min^{-1} in nitrogen.

A major conclusion from these results is that the photodegradants formed in the solid drug result in a product that has decreased thermal stability. The onset temperature of exothermic decomposition is decreased by about 30 ^{0}C after 16 h irradiation under the conditions described. This effect could be an autocatalytic affect of the photodegradants on the solid-state decomposition of FR, or it could be that the degradants lower the melting temperature of FR and hence the onset of decomposition of the molten FR.

7.2.2 TG-FTIR

The TG and the DTG curves of the samples of the original and irradiated FR, heated at 10 ^{0}C in nitrogen, are shown in **Figure 7.6.** Differences are relatively slight.

TG-FTIR was used to determine the gaseous decomposition products formed on heating samples of FR that had been irradiated for 16 hours at 550 W h m^{-2}. Because the only gaseous products that were observed on heating unirradiated FR were CO_2 and SO_2 in the spectral regions of 2600-2100 cm^{-1} (CO_2) and 1350-1150 cm^{-1} (SO_2), the same regions were selected for the irradiated drug (16 h), with the possibility of also observing the release of HCl and /or NH_3 in the spectral regions of 3059-2650 cm^{-1} and 931-986 cm^{-1}. **Figure 7.7 (a)** shows the stacked plot of FTIR spectra obtained during the TG run . The Gram-Schmidt curves (i.e. the total IR absorption against time curves) of FR irradiated for 16 h (see **Figure 7.7 (b)** showed the evolution of CO_2 and SO_2 . The TG-FTIR results for irradiated FR (16 h) gave no indication of the release of HCl and /or NH_3.

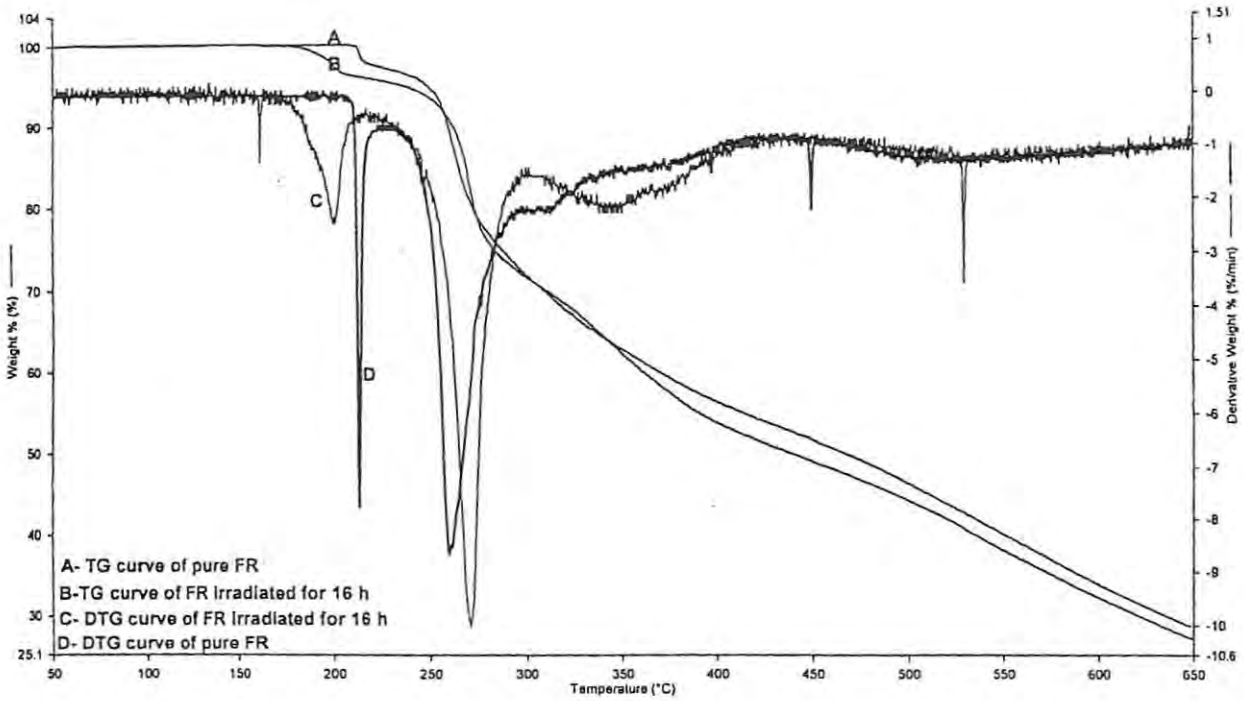

Figure 7.6 Comparison of the TG and DTG curves of samples of pure FR with those of FR irradiated for 16 h at 550 W h m^{-2} heated at 10 ^{0}C min^{-1} in nitrogen.

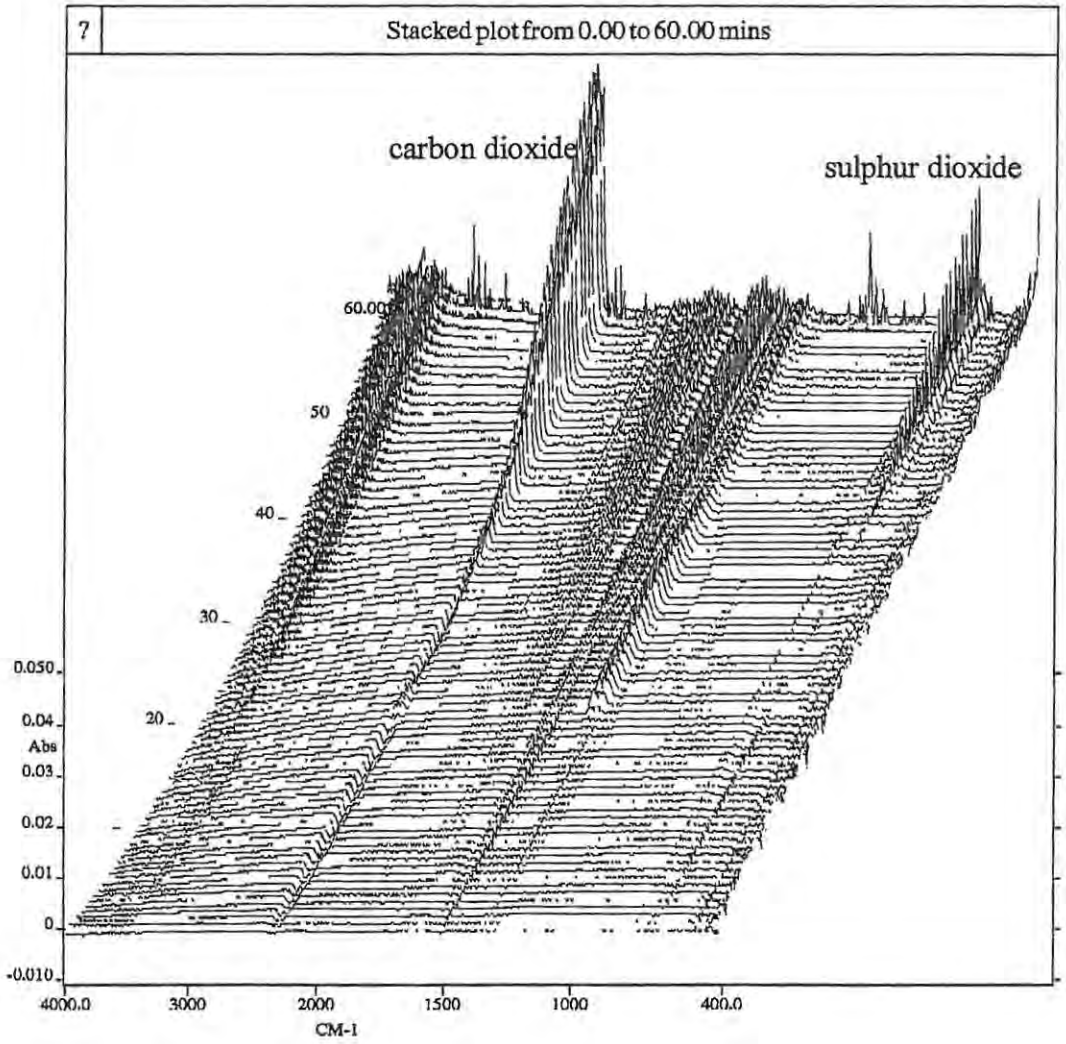

Figure 7.7(a) Stacked plot of FTIR spectra for FR irradiated for 16 h 550 W h m^{-2} heated at 10 ^{0}C min^{-1} in nitrogen from 0.00 to 60.00 minutes showing the release of CO_2 and SO_2.

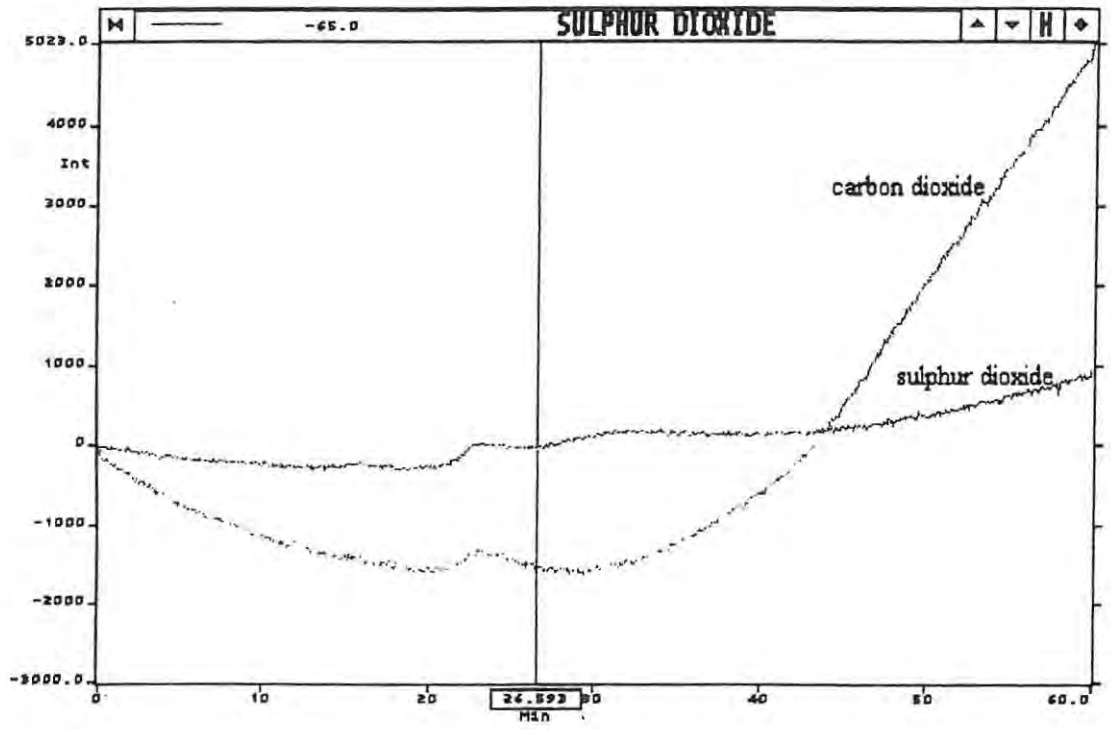

Figure 7.7 (b) Gram-Schmidt curves of the IR absorption of gases evolved on heating FR irradiated for 16 h at 550 W h m^{-2} heated at 10 ^{0}C min^{-1} in nitrogen.

7.3 XRD powder pattern of irradiated FR

XRD powder patterns were recorded for samples of the original FR and that which had been irradiated for 16 hours. The results are shown in **Figure 7.8**.

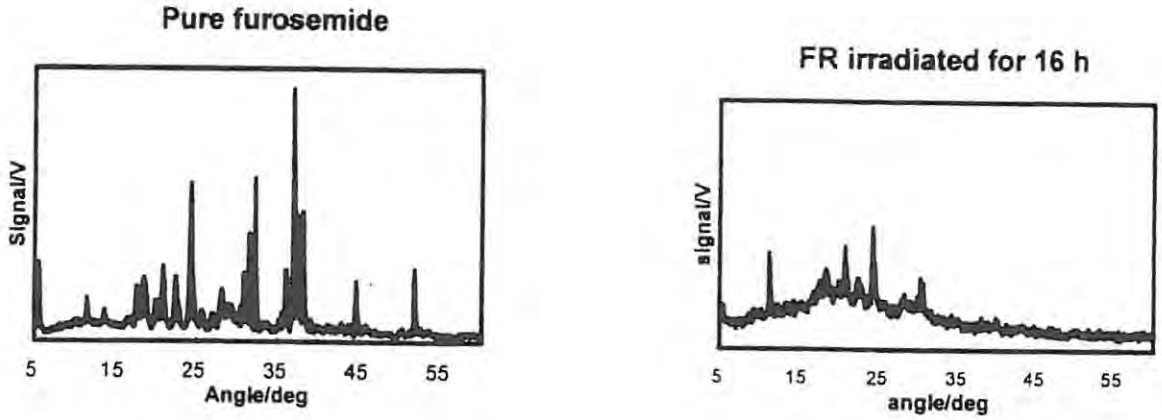

Figure 7.8 XRD powder patterns of pure FR and of FR irradiated for 16 h at 550W h m^{-2}.

The XRD powder patterns of the irradiated (16 h) and original FR are considerably different. The intense peak observed around $2\theta = 35°$ in pure FR is not present in the pattern of the irradiated FR (16 hours). The approximately 11 % of photodegradants formed is thus sufficient to disrupt the FR crystal structure.

7.4 Thermal behaviour of irradiated FR/CD mixtures

7.4.1 FR/BCD mixtures

The thermal behaviour of both physical and kneaded mixtures of FR/BCD after irradiation for 16 h at 550 W h m^{-2} was examined. The DSC curves for the physical mixtures are illustrated in

Figure 7.9 and for the kneaded mixtures in **Figure 7.10.** A comparison of some of the quantitative aspects of these curves is given in **Table 7.6.**

The DSC curves (**Figure 7.9**) of the irradiated physical mixtures of FR/BCD show some indication of the melting /decomposition of the pure FR except at a high BCD proportion (1:3 FR/BCD) where neither the BCD dehydration nor the FR features appear.

Irradiation of the kneaded mixtures results in the FR features being undetectable, although they are visible in the original kneaded mixtures. The changes are, again, greatest in the 1:3 FR/BCD mixtures.

7.4.2 FR/GCD mixtures

The thermal behaviour of both physical and kneaded FR/GCD mixtures, after irradiation for 16 h at 550 W h m^{-2}, was examined. The DSC curves for the physical mixtures are illustrated in **Figure 7.11** and for the kneaded mixtures in **Figure 7.12.** These DSC results are compared with those for the unirradiated mixtures in **Table 7.7**.

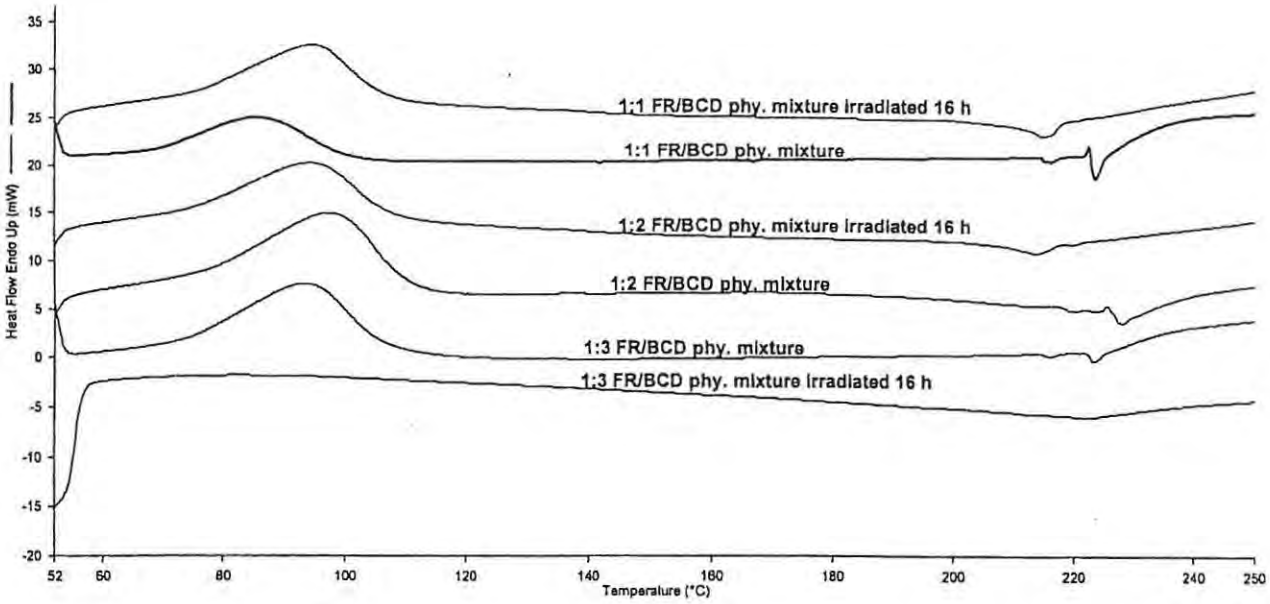

Figure 7.9 DSC curves of FR/BCD *physical* mixtures irradiated for 16 h compared with unirradiated *physical* mixtures heated at 10 ^{0}C min^{-1} in nitrogen.

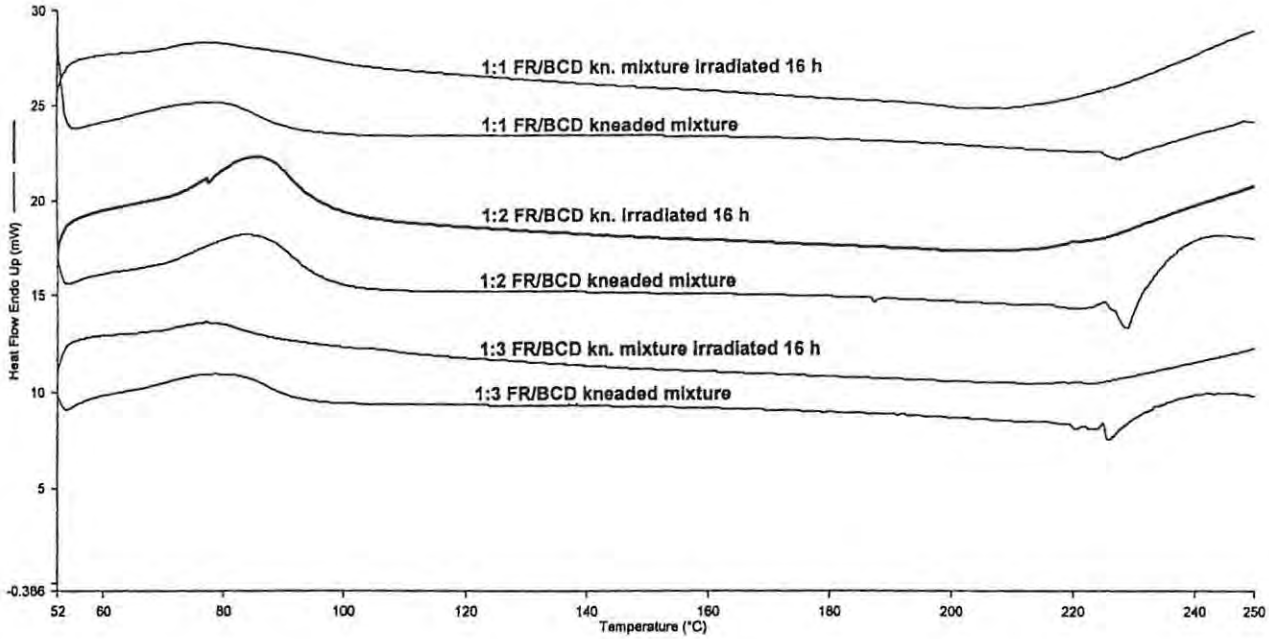

Figure 7.10 DSC curves of FR/BCD *kneaded* mixtures irradiated for 16 h compared with unirradiated *kneaded* mixtures heated at 10 ^{0}C min^{-1} in nitrogen.

Table 7.6 Comparison of the thermal behaviour of irradiated samples of FR/BCD mixtures with those of the original samples

Samples	**Expected ΔH dehydration for of the BCD proportion in the mixtures / J (g BCD)$^{-1}$**	**ΔH of dehydration of BCD in the original mixtures / J (g BCD)$^{-1}$**	**FR melting range in the original FR/BCD mixture / ^{0}C**	**ΔH of dehydration of BCD in the irradiated (16 h) FR/BCD mixtures / J (g BCD)$^{-1}$**	**FR melting range in the irradiated (16 h) FR/BCD mixture / ^{0}C**
FR standard	-	-	216-226	0	216-226
FR irradiated	-	-	-	0	220 ^{0}C
1:1 FR/BCD phy.	173	171	216 -223	172	212-218 ^{0}C
1:1 FR/BCD kn.	173	169	220-223	(32 + 23) = 55	not visible
1:2 FR/BCD phy.	195	146	220-223	162	209-218 ^{0}C
1:2 FR/BCD kn.	195	190	220-224	77	not visible
1:3 FR/BCD phy.	203	172	219-223	Not visible	not visible
1:3 FR/BCD kn.	203	195	213-225	(67 + 17) = 84	not visible

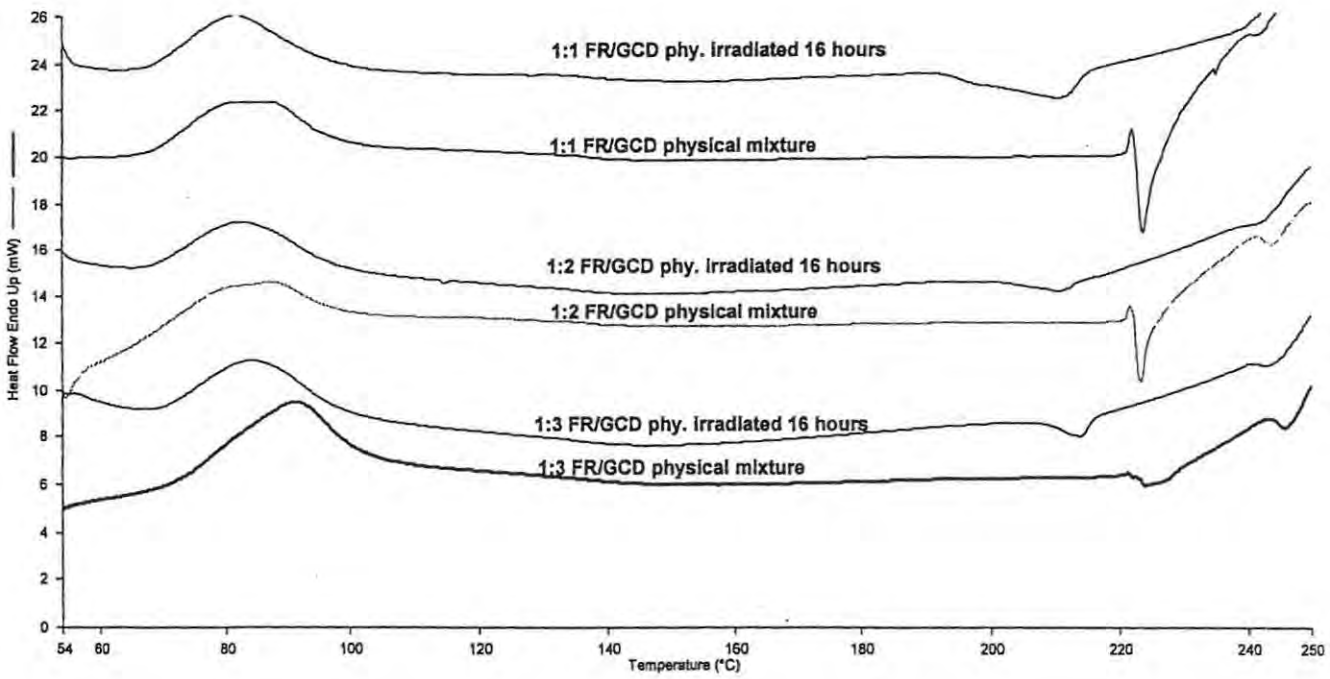

Figure 7.11 DSC curves of FR/GCD *physical* mixtures irradiated for 16 h compared with unirradiated *physical* mixtures heated at 10 ^{0}C min^{-1} in nitrogen.

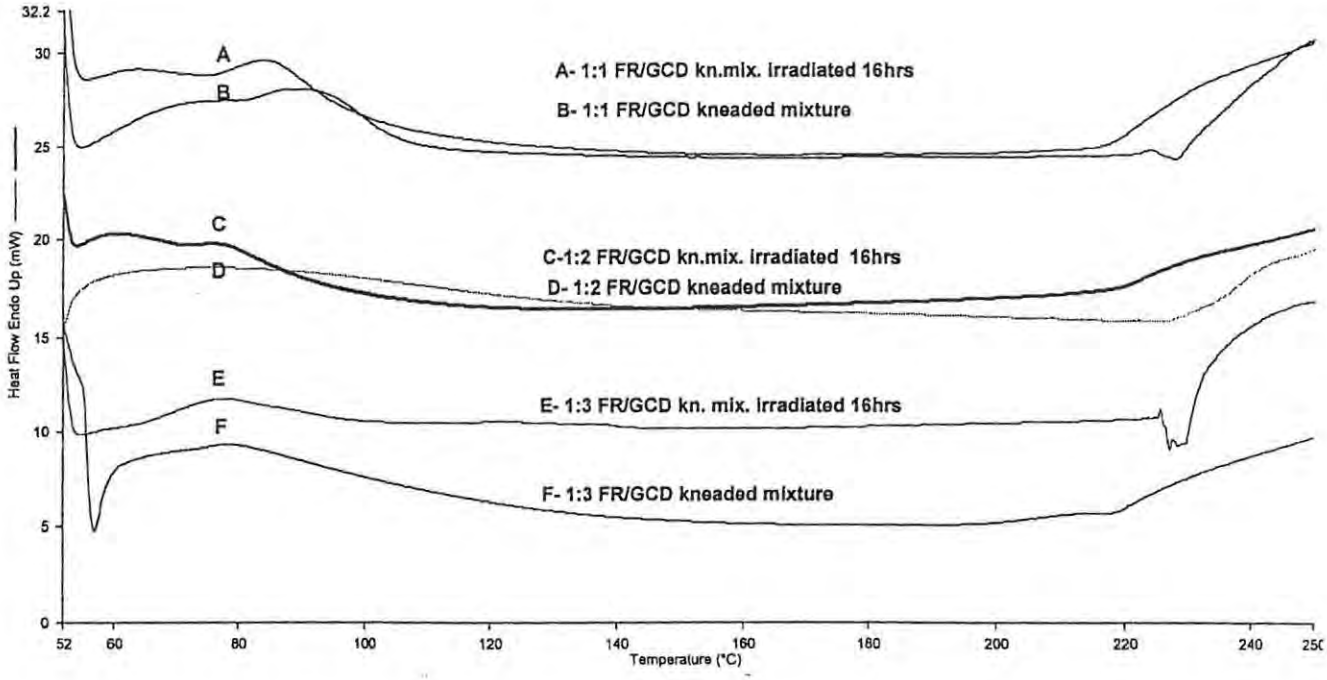

Figure 7.12 DSC curves of FR/GCD *kneaded* mixtures irradiated for 16 h compared with unirradiated *kneaded* mixtures heated at 10 ^{0}C min^{-1} in nitrogen.

Table 7.7 Comparison of the thermal behaviour of irradiated samples of FR/GCD mixtures with those of the original samples

Samples	**Expected ΔH dehydration of GCD proportion in the mixtures / J (g GCD)$^{-1}$**	**ΔH of dehydration of GCD in the original mixtures / J (g GCD)$^{-1}$**	**FR melting range in the original FR/GCD mixture / ^{0}C**	**ΔH of dehydration of GCD in the irradiated (16 h) FR/GCD mixtures / J (g GCD)$^{-1}$**	**FR melting range in the irradiated (16 h) FR/GCD mixture / ^{0}C**
FR standard	-	-	216-226	0	216-226
FR irradiated	-	-	-	0	220 ^{0}C
1:1 FR/GCD phy.	49	56	220 -226	52	220 ^{0}C
1:1 FR/GCD kn.	49	(30 + 53) = 88	223-225	(6 + 13) = 19	not visible
1:2 FR/GCD phy.	55	58	220-223	76	220 ^{0}C
1:2 FR/GCD kn.	55	52	223-227	(17 + 13) = 30	not visible
1:3 FR/GCD phy.	41	62	219-223	73	220
1:3 FR/GCD kn.	41	virtually eliminated	237-255	68	not visible

The DSC curves for the irradiated FR/GCD physical mixtures (**Figure 7.11**) show indications of the thermal behaviour of irradiated pure FR (see **Section 7.1**) with the melting/decomposition feature broadened and shifted to a lower temperature. The above features were not observed in the DSC curves for the irradiated, kneaded mixtures (**Figure 7.12**).

7.4.3 Discussion

Physical mixing of FR with either BCD or GCD does not offer complete protection against changes in thermal behaviour resulting from irradiation. Some of the FR in the mixture is affected by irradiation in a similar manner to pure FR. The kneading process does change the properties of the mixture.

Irradiation of both the FR/BCD and FR/GCD mixtures can results in changes of the dehydration behaviour of the cyclodextrin component. This could be due to the heating effects of irradiation. Generally mixing with cyclodextrins appears to enhance the thermal stability of FR. This is most evident for kneaded mixtures with GCD in high molar proportions. As is shown in **Section 6.3**, however, this mixing results in decreased photostability of FR.

7.5 X-ray powder diffraction patterns of irradiated FR/CD mixtures

The X-ray powder diffraction patterns of irradiated FR/CD mixtures are compared with the patterns of the original mixtures in **Figure 7.13**.

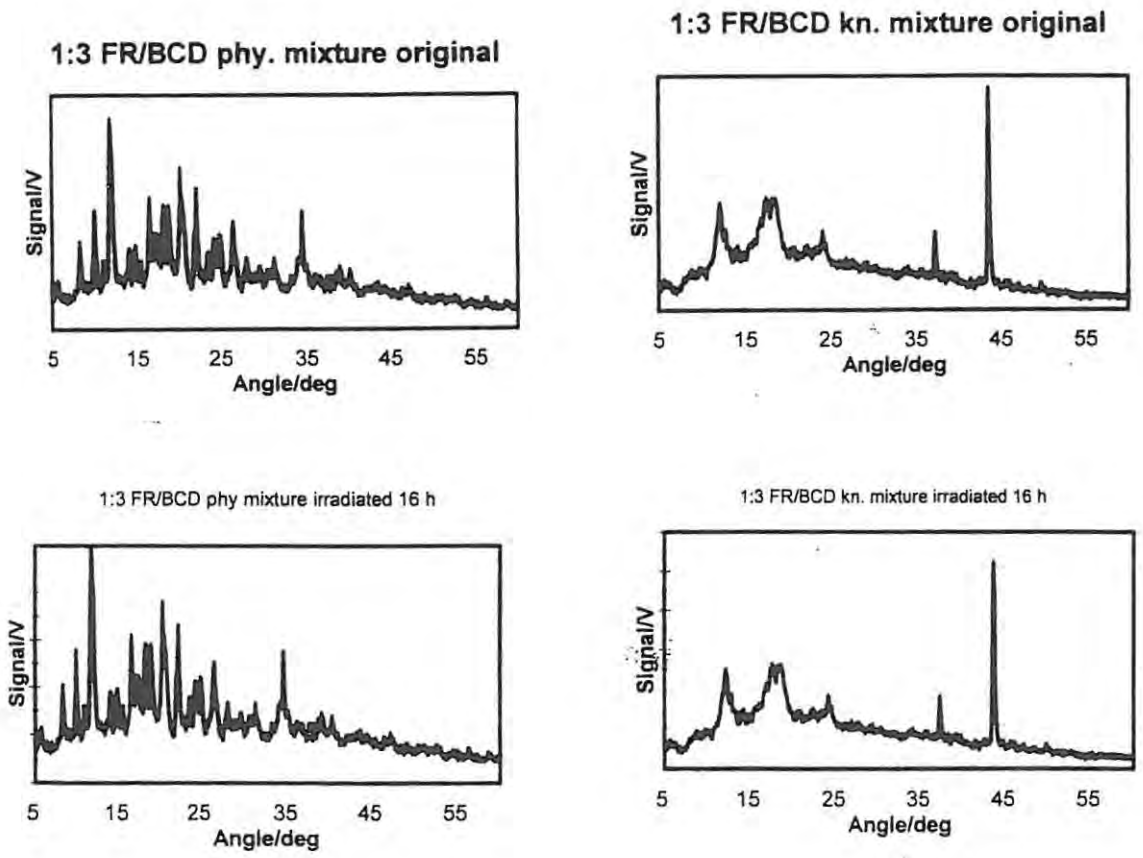

Figure 7.13 XRD patterns of **a)** the original 1:3 FR/BCD *physical* mixture, **b)** the original 1:3 FR/BCD *kneaded* mixture, **c)** a 1:3 FR/BCD *physical* mixture irradiated for 16 h and **d)** a 1:3 FR/BCD *kneaded* mixture irradiated for 16 h all at 550 W h m^{-2}.

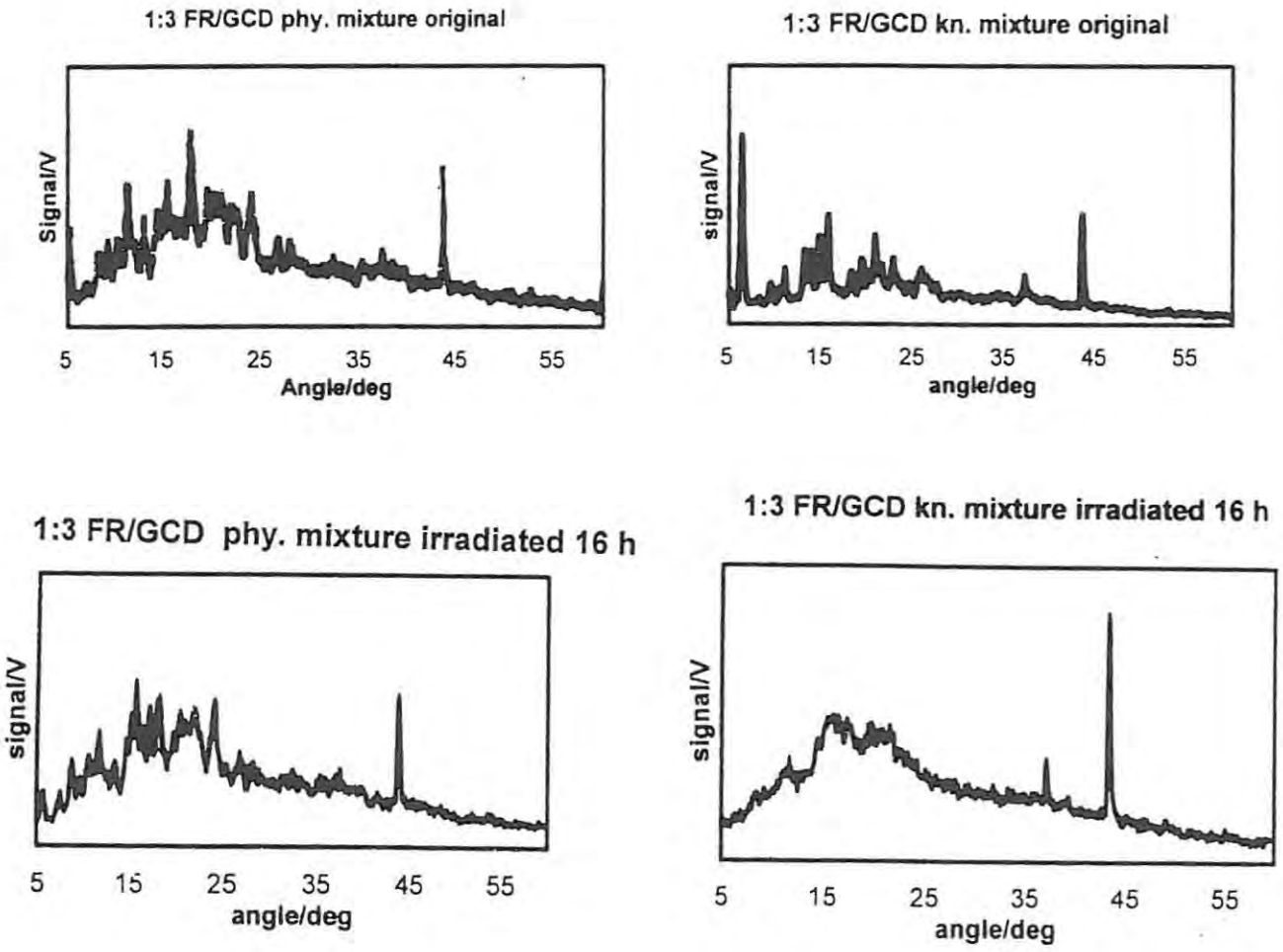

Figure 7.14 XRD patterns of **a**) the original 1:3 FR/GCD *physical* mixture, **b**) the original 1:3 FR/GCD *kneaded* mixture, **c**) a 1:3 FR/GCD *physical* mixture irradiated for 16 h and **d**) a 1:3 FR/GCD *kneaded* mixture irradiated for 16 h all at 550 W h m^{-2}.

There are large differences between the XRD powder patterns of the physical and the kneaded mixtures of FR/BCD (**Figure 7.13**). Against this, the changes caused by irradiation (16 h) of the kneaded mixture are not easy to identify. There are definite changes in the pattern of the irradiated physical mixture and these appear to be related to the changes produced by irradiating pure FR.

7.6 Infrared spectroscopic studies

The infrared spectrum of pure and irradiated FR and of the original and irradiated FR/cyclodextrin mixtures were recorded as described in **Section 6.5**. The main features are summarized in **Table 7.8**.

Table 7.8 IR absorption maxima for pure and irradiated (for 16 h at 550 W h m^{-2}) samples of FR and FR/CD mixtures

Samples	**ν(C=O)/cm^{-1}**	**ν(CN-H)/cm^{-1}**	**$\nu(SO_2N$-H)/cm^{-1}**	**ν (S=O)/cm^{-1}**	**ν(C-Cl)/cm^{-1}**
FR pure	1668	3348.6	1321.4	1141.3	581.7
FR (16 h)	1667	3338.2	1319.5	1136.5	576.8
1:3 FR/BCD phy original	broad & less intense	weak band	weak band	weak band	575
1:3 FR/BCD phy. 16 h	broad & less intense	weak bands	1323	broad & less intense	573
1:3 FR/BCD kn. original	weak band	disappeared	disappeared	weak band	575
1:3 FR/BCD kn. 16 h	1656 broad & less intense	disappeared	disappeared	disappeared	577
1:3 FR/GCD phy original	broad & less intense	disappeared	decreased in intensity	no change	decrease in intensity
1:3 FR/GCD phy. 16 h	1657 broad & less intense	disappeared	1371	1146 broad	disappeared
1:3 FR/GCD kn. original	disappeared	disappeared	disappeared	disappeared	decreased in intensity
1:3 FR/GCD kn. 16 h	1652 broad & less intense	disappeared	1367	1151 broad & less intense	573

From the results in **Table 7.8** it can be seen that the main absorption maxima of FR are shifted after irradiation for 16 h. The spectra of the irradiated 1:3 FR/CD mixtures also some indicate changes compared with the unirradiated samples. The carbonyl stretch C=O in the1:3 FR/BCD kneaded mixture irradiated for 16 h appears around 1656 cm^{-1} and the S=O band had disappeared, even though it was visible in the unirradiated mixture. In the irradiated 1:3 FR/GCD physical mixture, the carbonyl stretch C=O appears around 1657 cm^{-1} and the C-Cl stretch has disappeared even though it is visible for the original sample. For the irradiated 1:3 FR/GCD kneaded mixture the C=O band appears around 1652 cm^{-1} and the NH_2 band appears around 1367 cm^{-1} and the S=O band is at 1151 cm^{-1}, even though these bands were not visible in the spectrum of the original sample. These results indicate that irradiation causes changes in the drug and in the drug/cyclodextrin mixtures.

7.6 UV/visible spectra of pure FR and irradiated FR

The spectra shown in **Figure 7.15** were recorded for solutions of pure and irradiated FR with methanol and water in 50/50 v/v. The concentration used was 5 mg l^{-1} for all the samples. There was no significant difference between the spectra of these samples.

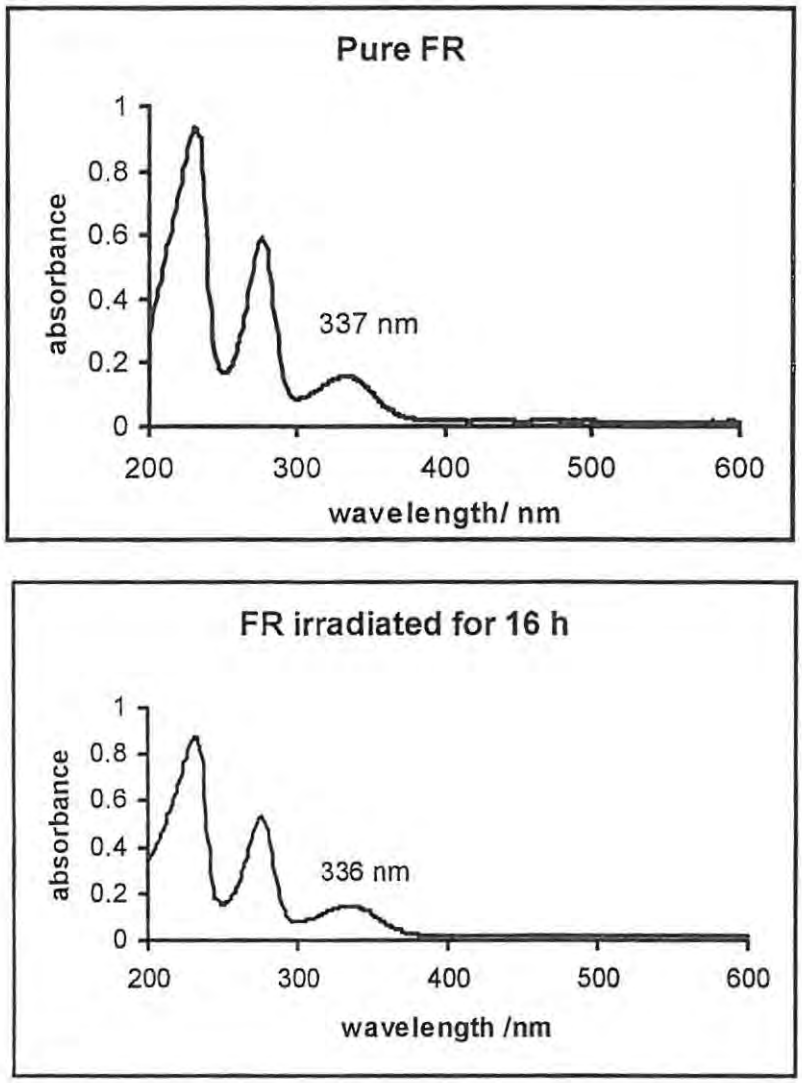

Figure 7.15 UV/visible spectra of pure FR and FR irradiated for 16 hours

Chapter 8

8. CONCLUSIONS

8.1 Furosemide forms

Several different solvent-dependent, crystalline forms of FR have been reported [20]. Fortunately most of the detailed studies have been based on the readily available, commercial form, Form I, and the sample used in this study was identified as this form from its X-ray powder diffraction pattern (see **Figure 5.8**) and its IR spectrum (see **Figure 5.5**).

8.2 Thermal behaviour of FR

Furosemide undergoes an endothermic transition (about 2 J g^{-1}) at about 138 ^{0}C. The transition was found to be readily reversible on cooling. Melting occurs at about 222 to 226 ^{0}C and is immediately followed by exothermic decomposition (about -107 J g^{-1}). Decomposition occurs in at least two overlapping stages (this can be observed from the TG curve of FR in **Figure 6.1**). TG-FTIR results showed that decomposition is still incomplete on heating at 10 ^{0}C min^{-1} to 650 ^{0}C and that major gaseous products evolved above 250 ^{0}C are SO_2 and CO_2.

The DSC and TG observations are in agreement with those reported by Doherty and York [19] (**Figure 1**), Beyers *et al.* [18] (**Figure 1 and 2**), Matsuda *et al.* [80] (**Figure 3 (a)**), and Matsuda and Tastumi [20] (**Figure 4 (a)**). Doherty and York suggested [19] that the small endotherm at about 138 ^{0}C was due to a solid-solid transition from Form I to Form II. Özdemir and Ordu [29] misidentified the endo/exothermic direction in their DSC traces (**Figure 3**), but otherwise the features are similar.

8.3 Photostability of FR

Furosemide has been reported [83] to degrade (both in the solid state in aqueous solution) with accompanying discolouration on exposure to light . De Villiers *et al.* [83] exposed samples of FR,

Forms I and II, to sunlight, in the presence and in the absence of oxygen. The initial stages of degradation were acceleratory and the extent of degradation of Form II was generally greater than for Form I under the same conditions. They measured the extent of degradation of FR in terms of the amount of the degradation product, 4-chloro-5-sulphamoylanthranilic acid (CSA), formed. In this study, only samples of Form I were irradiated. The atmosphere was air and the source of illumination was the Suntest cabinet (550 W h m^{-2}). De Villiers *et al.* [83] described the acceleratory parts of their degradation curves by the power law with n = 2, i.e. :

$$\alpha^{1/2} = kt + C$$

where α is the extent of degradation, k is the rate coefficient, t is the time and C is a constant. In this study, the extent of degradation was determined from the amount of FR remaining. A plot of $\alpha^{1/2}$ against time is shown in **Figure 8.1.** From linear regression ($R^2 = 0.9942$), the value of k is 0.0206 ± 0.0009 h^{-1} which is not too different from the k values for sunlight reported by De Villiers *et al.* [83] (Form I in oxygen: 0.0148 h^{-1}).

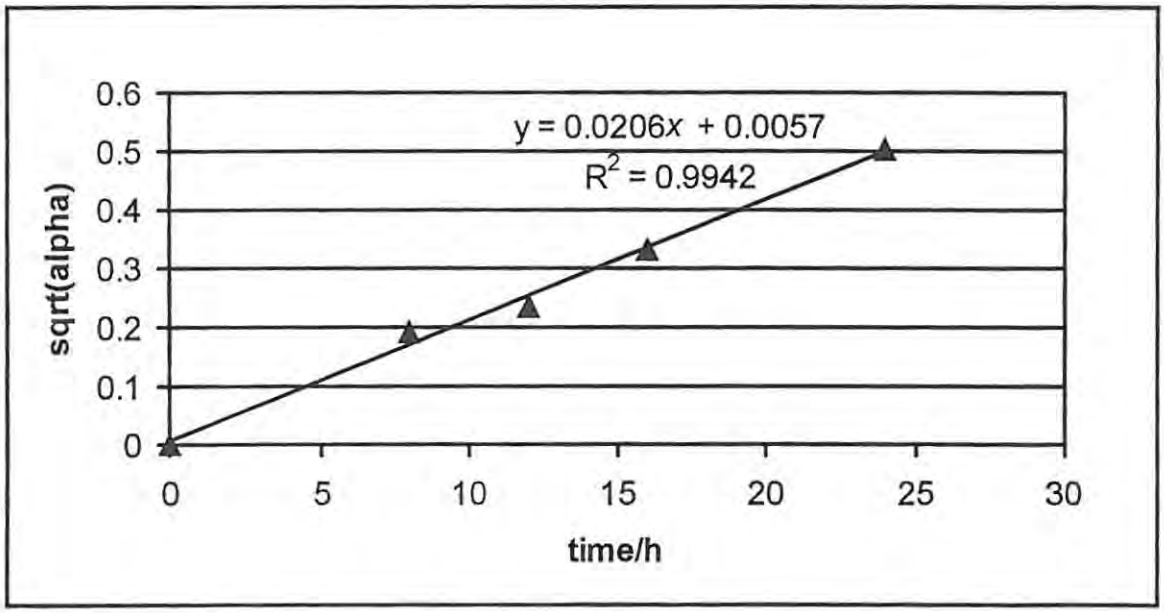

Figure 8.1 Application of the power law with n = 2 to the extent of photodegradation of FR with time of irradiation at 550 W h m^{-2}. The original data are shown in **Table 7.1**

8.4 Thermal behaviour of irradiated FR

DSC and TG curves for samples of FR that had been irradiated for 16 h (at 550 W h m^{-2}) showed considerable differences in the thermal behaviour from that of the original drug (see **Section 7.1**). The DSC and the TG curves, for the dark control samples, which were shielded from irradiation under aluminium foil, did not show any significant changes from those of the pure drug. The products of photodegradation either catalyze the thermal decomposition of FR in the solid state or lower the melting point of FR so that thermal decomposition in the melt is enhanced.

8.5 Thermal behaviour of mixtures of FR with cyclodextrins

As expected, the kneading procedure, using ethanol as the solvent, produced mixtures that showed more reproducible behaviour than simple physical mixing of the samples. The ethanol treatment does not have much effect on the water content of the cyclodextrins.

A strong indication of inclusion of FR in the cyclodextrin cavity was observed in the 1:3 FR/GCD kneaded mixture, where the melting of furosemide was not observed at its normal temperature (i.e. 222-226) ^{0}C, but two endotherms around 237-255 ^{0}C were observed which were not in the DSC curves for GCD. Changes in the IR spectra supported the occurrence of inclusion. The XRD powder pattern of the 1:3 FR/GCD kneaded mixture was observed to be different from the patterns of the drug alone, of GCD and of the 1:3 FR/GCD physical mixture.

8.6 Photostability of mixtures of FR with cyclodextrins

Comparison of the results of irradiation of samples of the FR/cyclodextrin mixtures for 16 hours at 550 W h m^{-2}, with those for pure FR under the same conditions, shows that the mixtures with cyclodextrins have a decreased photostability. While pure FR degrades by about 11 %, the 1:3 FR/GCD kneaded mixtures showed 57 % degradation and the 1:3 FR/BCD kneaded mixture showed 21 % degradation.

The interaction between FR and GCD, indicated by the thermal and spectral results for the 1:3 FR/GCD kneaded mixture, does not stabilize the drug towards exposure to light. This may indicate that the light-sensitive moiety of the drug molecule is outside the CD cavity, even if a considerable portion of the molecule is included, and so mixing with the cyclodextrin may result in an increase in the photodegradation of the drug.

Even though a full molecular modelling study was not attempted, some qualitative conclusions can be drawn. The diameters of the cavities in the two cyclodextrins used were different: 0.8 nm for BCD and 1.0 nm for GCD. (See **Figure 8.2** [55] and also **Figures 4.1 and 4.2**) The crystal structure of FR has been reported by Al-Obaid et al. [3]. A diagram of the optimized molecular structure of FR, prepared using the semi-empirical PM3 approach in the Spartan molecular modelling program shown in **Figure 8.3**. Some of the major dimensions of the FR molecule are given in **Table 8.1** (based on the numbering given in **Figure 8.2**).

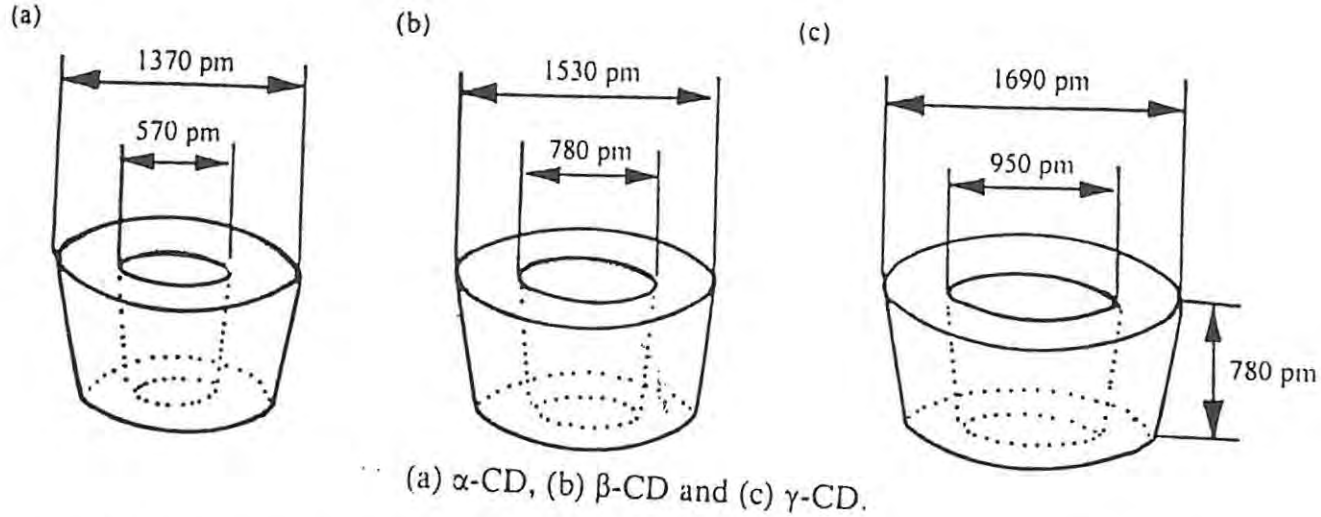

(a) α-CD, (b) β-CD and (c) γ-CD.

Figure 8.2 Illustration of the approximated diameters of beta-cyclodextrin and gamma-cyclodextrin cavities [55]

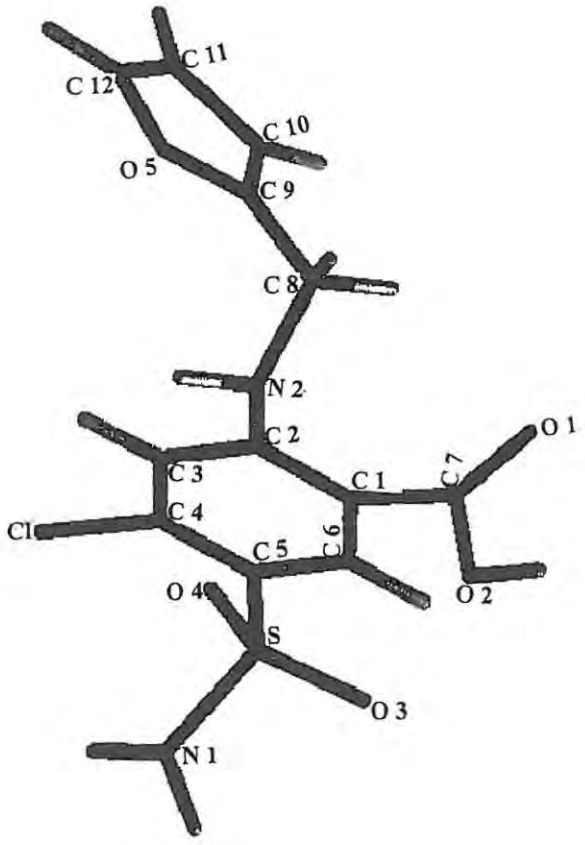

Figure 8.3 Optimized molecular structure of FR, prepared using the semi-empirical PM3 approach in Spartan molecular modelling program.

Table 8.1 Some of the major dimensions (in Å) of the FR molecule based on the numbering in **Figure 8.3**

C 11 to N 1	9.36
O 1 to C 1	6.80
N 2 to C 11	4.57
C 2 to C 11	4.90
N 2 to S	6.10

It would appear unlikely that the FR molecule would be totally included, even in the larger GCD cavity. The space available for inclusion is doubled in the head-to-head alignment of two CD molecules [85] (**Figure 8.4**) but, presumably, such an arrangement would require a more symmetrical guest molecule than that of FR.

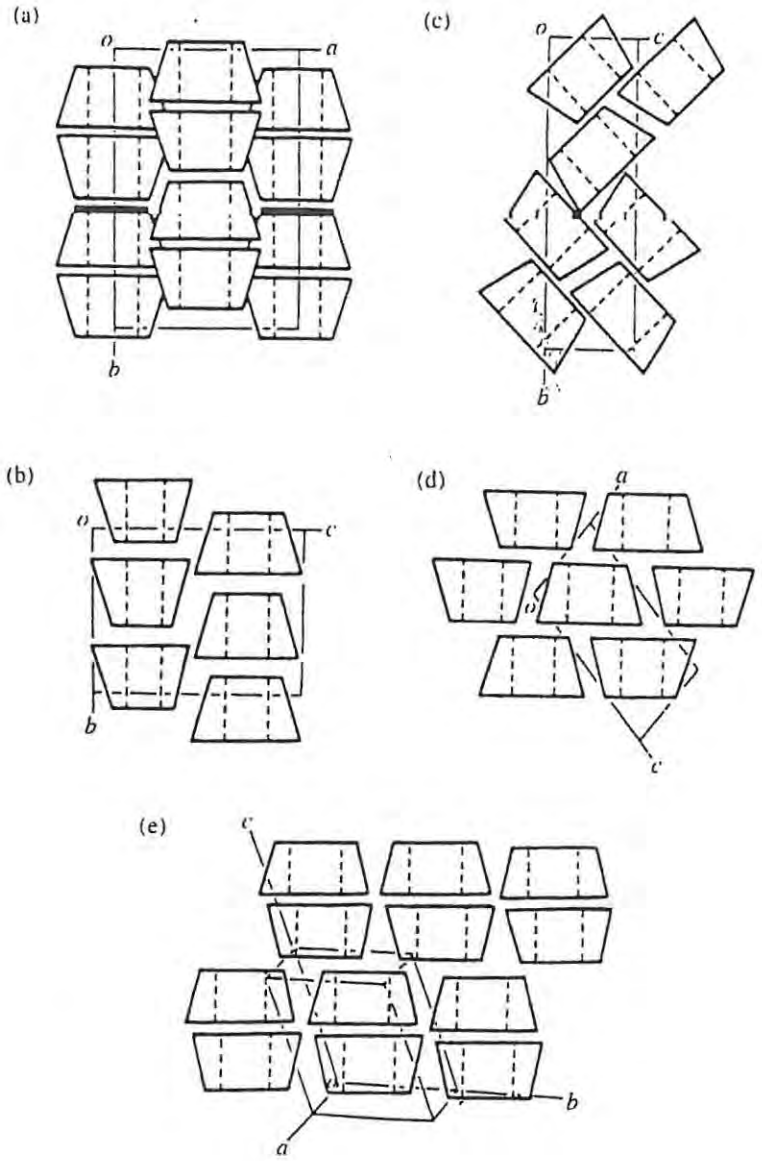

Figure 8.4 Schematic representation of the different packings of the structures of beta-cyclodextrin dimers, with (a) showing the head-to-head channel alignment, (b) head-to-channel-type, (c) the cage-type, (d) the layer-type and (e) the layer-type composed of BCD dimers [85].

Some of the possible modes of partial inclusion of large (and unsymmetrical) guest molecules are discussed by Osa and Suzuki [86]. Most of the examples quoted show ready inclusion of the phenyl ring.

REFERENCES

1. Micromedex Inc., 1974-1999, MICROMEDEX (R), Healthcare series, Vol. 102.
2. Http://www.marvistavet.com/html/body-furosemide.html,
3. M A. Al-Obaid, J.F. Al-Shammary, K. A.M. Al-Rashood and M S. Mian, "Analytical Profiles of Drug Substances", Academic Press, Inc., New York,Vol.18, 1989, p.156, 157, 161, 164, 169, 170, 171.
4. W.O. Faye, T.L. Lemke and D.A. Williams, " Principles of Medicinal Chemistry", 4th Edn, William and Wilkins Publishers, Baltimore, 1995, p. 412.
5. Martindale, " The Extra Pharmacopoeia", 26th Edn, (Eds N. H. Blacow and A.Wade), Pharmaceutical Press, London,1972.
6. O. Abdulla, Z.A. El-Gholmy, M. El-Massik and Y. Hammouda, *Acta Pharm. Technol.*, 35 (1989) 25.
7 A.G. Gilman, L.S. Goodman and A.Gilman, "The Pharmacological Basis of Therapeutics", 6th Edn, Macmillan Publishing Co., New York, 1990, p. 904.
8. V.K. Prasad, R.S. Rapaka, P.W. Knight and B.E. Cabana; *Int. J. Pharm.*, 11 (1982) 81.
9. "The United States Pharmacopoeia", 19th Edn, Mack Publishing Company, Easton, PA,1975.
10. L. L. B. Ponto and R. D. Schoenwald, *Clin. Pharmacokin.*, 18 (1990) 381.
11. V.S. Chungui L.W. Dittert and R.B. Smith, *Int. J. Pharm.*,4 (1979) 27.
12. J.E. Cruz, D.D. Maness and G.J. Yakatan, *Int. J. Pharm.*, 2 (1979) 25.
13. E.Spamer, MSc. Thesis, Potchefstroom University, 2000, p. 7.
14. M. Kingsford, N.J. Eggers, G. Soteros, T.J.B. Maling and R.J. Shirkey, *J. Pharm. Pharmacol.*, 36 (1984) 536.

15. S. G. Proudfoot, "Pharmaceutics: the Science of Dosage Form Design" (Ed M. E. Aulton), Churchill Livingstone, Edindurgh,1988, p. 135-173.

16. K. Sturm, W. Siedel, R. Weyer and H. Rusching, *Chem. Ber.*, 99 (1966) 328.

17. H. Bundgaard, T. Nørgaard and N.M. Nielsen, *Int. J. Pharm.* 42 (1988) 217.

18. H. Beyers, S.F. Malan, J.G. van der Watt, and M.M. de Villiers, *Drug Dev. Ind. Pharm.*, 26 (2000)1077.

19. C.Doherty and P. York, *Int.J.Pharm.*, 47 (1988) 141.

20. Y. Matsuda and E. Tatsumi, *Int. J. Pharm.*, 60 (1990) 11.

21. S.R. Byrn, R.R. Pfeiffer and J.G. Stowell, "Solid-State Chemistry of Drugs", 2 nd Edn, SSCI Inc., West Lafeyette, Indiana, 2000, p. 202-205.

22. T.L. Cottrell, "The Strength of Chemical Bonds ", Butterworths, London, 1954, p.310.

23. J.Lamotte, L. Campsteyn, L. Dupont, and M.Vermere, *Acta Crystallogr.*, 34 (1978) 1657.

24. P.C. Rowbotham, J.B. Stanford and J.K. Sugden, *Acta Pharm. Helv.*, 51 (1976) 304.

25. D.E. Moore and S.R. Tamat, *J. Pharm. Pharmacol.*, 32 (1980) 172.

26. D.E. Moore and V. Sithipitaks, *J. Pharm. Pharmacol.*, 35 (1983) 489.

27. A.M. Yahya, J.C. McElnay and P.F. D'Archy, *Int. J. Pharm.*, 31 (1986) 56.

28. J. M. Neil, A.F. Fell and G. Smith, *Int. J. Pharm.*, 22 (1984) 105.

29. N. Özdermir and S. Ordu, *Drug Dev. Ind. Pharm.*, 24 (1998) 19.

30. S.R. Byrn, "Solid State Chemistry of Drugs", Academic Press, New York, 1982, p. 47.

31. G. van der Plaats, "The Practice of Thermal Analysis", Mettler-Toledo,Switzerland, 1991, p. 9.

32. M. E. Brown, "Introduction to Thermal Analysis ", Chapman and Hall, London, 1988, p. 43, 50, 71.

33. J. Mullens, "Handbook of Thermal Analysis and Calorimetry", Vol.1, (Ed M.E.Brown), Elsevier, Amsterdam, 1998, p. 518, 528.

34. E. Kaisersberger and E.Post, *Thermochim. Acta* 295 (1997) 73, 75,78,90, 93.

35. V. Berbenni, A. Marini, G. Bruni and T. Zerlia, *Thermochim. Acta,* 258 (1995) 125.

36. W.C. McCrone, "Proc. ESTA 1", (Ed. D. Dollimore), Heyden, London, 1976, p. 63.

37. J. L. Ford and R. Willson, "Handbook of Thermal Analysis and Calorimetry ",Vol.4, (Ed. R. B. Kemp), Elsevier, Amsterdam, 1999, p.923-964.

38. J.L. Ford and P. Timmins, "Pharmaceutical Thermal Analysis, Techniques and Applications", Ellis Horwood, New York, 1989, p. 26, 201-210.

39. E.S Basle and J.de B. Shcwerzenbach, "Collected Applications of Thermal Analysis: Pharmaceuticals", Mettler- Toledo, Switzerland, 1998, p. 4, 11.

40. D. Giron, *J. Pharm. Biomed. Anal.*, 6 (1986) 757.

41. P. Enghag, B. Haglund and T. Luks, *Proc. Annu. Conv. Wire Assoc. Int.*, 55 (1985) 113.

42. A.S. Alam and E.L. Parrot, *J. Pharm.Sci.*, 60 (1971) 263.

43. L. Parnetti, *Clin. Pharmacokin*, 2 (1995) 110.

44. D.D. Wirth, S.W. Baertschi, R.A. Johnson, S.R. Maple and S.M. Gregg, *J. Pharm. Sci.*, 87 (1998) 31.

45. J.T. Carstensen, "Drug Stability, Principles and Practices ", Marcel Dekker, Inc., New York and Basel, 1990, p. 134, 155.

46. K. Umprayn and R.W. Mendes, *Drug Dev. Ind. Pharm.*, 13 (1987) 653.

47. J.T. Carstensen, "Drug stability, Principles and Practices ", Marcel Dekker, Inc. New York and Basel, 1990, p. 165, 166, 168, 207.

48. G. Edgar and W.O. Swan, *J. Amer. Chem. Soc.*, 44 (1922) 570.

49. A.S. Mikulinskii and R.I. Rubinshstein, *J. Phys. Chem.*, 9 (1937) 431. (Ref. from Chem. Abstr.,33:61266, (in K. Umprayn and R.W. Mendes, *Drug Dev. Ind. Pharm.*, 13 (1987) 654)).

50. W.C. Griffin, R.W. Behrens and S.T. Scot, *J. Soc. Cosmet. Chem.*, 3 (1952) 5.

51. H.Czetsch-Lindenwald, *Oesterr. Apoth. Ztg.*, 17 (1963) 553.

52. J. T. Carstensen, E. Aron, D. Spera and J.J. Vance, *J. Pharm. Sci.*, 55 (1966) 561.

53. P. Admirat and J.C. Grenier ; *J. Rech. Atmos.*, 9 (1975) 97.

54. K.A.Connors, G.L. Amidon and V.J. Stella, "Chemical Stability of Pharmaceuticals, A Handbook for Pharmacists ", John Wiley and Sons, New York, 2 nd Edn, 1985, p. 126-129.

55. J. Szejtli and L, Szente, "Comprehensive Supramolecular Chemistry: Cyclodextrins "(Eds. J.L.Atwood, J.E.D. Davies, D.D.Macnicol and F.Vôgtle), Pergamon, New York, Vol. 3, 1996, p. 12, 17, 20, 21, 243, 245.

56. D. Duchene and D. Wouessidjewe, *Drug Dev. Ind. Pharm.*, 16 (1990) 2488.

57. J. Szejtli, "Cyclodextrins and their Inclusion Complexes ", Akademiai Kiado, Budapest, 1982, p. 243-248.

58. J.S. Pagington, *Perfum. Flav. Int.*, 11 (1986) 49.

59. M.E. Brewester J.W. Simpkins, M.S. Hora, W.C. Stern and N. Bodor, *J. Par. Sci. Tech.*, 43 (1989) 231,233,237.

60. J. Pitha; *Life Sciences*, 29 (1981) 307.

61. Http://www.cyclodex.com/cgi-bin/NCE1/p-info1. html.

62. S.G. Frank, *J. Pharm. Sci.*, 64 (1975) 1585.

63. H. Coetzee, M.Sc. Thesis, University of Port Elizabeth, 1992, p. 23-35.

64. F. Cramer, W. Saenger, and H.C.H. Spatz, *J. Amer. Chem. Soc.*,89 (1967) 14.

65. O. Bekers, E.V. Uijtendaal, J.H. Beijnen, A. Bult and W.J.M. Underberg, *Drug Dev. Ind. Pharm*, 17 (1991) 1503.

66. A.R. Rajewski and J.V. Stella, *J. Pharm. Sci.*, 85 (1996) 1142.

67. A.R. Hedges, Chem. Rev. 98 (1998) 2035.

68. G. Les Bas, N. Rysanek, G. Tsoucaris,"Minutes of the 5th International Symposium on Cyclodextrins"(Ed D. Duchéne), Edition de Sante,Paris,1990, p. 114.

69. K. Griez, E. Fenyvesi, M.Molnar and B. Horvath, "Proceedings of the Eighth International Symposium on Cyclodextrins", (Eds. J.Szjetli and L.Szente), Kluwer Academic Publishers:Dordrecht, The Netherlands, 1996, p. 547.

70. H.J. Buschman, "Proceedings of the Eighth International Symposium on Cyclodextrins", (Eds. J.Szjetli and L.Szente), Kluwer Academic Publishers: Dordrecht, The Netherlands, 1996, p. 609.

71. W. Lau and B.M. Shah, *U. S. Patent*, (1994) 376, (in A.R. Hedges, *Chem. Rev.*, 98 (1998) 2042).

72. P.J. Lentini and J.R. Zecchino, *U. S. Patent*, (1996) 367, (in A.R. Hedges, *Chem. Rev.*, 98 (1998) 2042).

73. K.B. Hicks, R.M. Haines, C.B.S. Tong, G.M. Sapers, Y. El-Atawy, P.L. Irwin and P.A.J. Seib, *J. Agric. Food Chem.*, 44 (1996), 2591.

74. R.H. Pierson, A.N. Fletcher and E. St. Clair Gahtz, *Anal. Chem.*, 28 (1956) 1218.

75. T. Loftssen and M.J. Brewster, *Pharm. Sci.*, 85 (1996) 1017,1019,1020,1024,1025.

76. E.M. Antunes, M.Sc. Thesis, Rhodes University, 1999, p. 142.

77. A.R. Fassihi and P.H.R. Persicaner, *Int. J. Pharm.*, 37 (1987) 167.

78. D.Duchéne and D. Wouessidjewe, *Drug Dev. Ind. Pharm.*, 16 (1990) 2487.

79. K. Uekama, F. Hiryama and T. Irie, *Chem. Rev.*, 98 (1998) 2055.

80. Y. Matsuda, M. Otsuka, M. Onoe and E. Tatsumi, *J. Pharm. Pharmacol.*, 44 (1992) 627.

81. M. Bilal, C. de Braner, P. Claudy, P. Gerseain and J. M. Létoffé, *Thermochim. Acta*, 249 (1995) 63.

82. D. Duchéne, "Cyclodextrins and their Industrial Uses ", Editions de Santé, France, 1987, p. 157.

83. M.M. De Villiers, J.G. van der Watt and A.P. Lötter, *Int. J. Pharm.*, 88 (1992) 280.

84. P.M. Drummond, Honours Thesis, Rhodes University, 1994, p. 25.

85. K. Harata "Comprehensive Supramolecular Chemistry: Cyclodextrins "(Eds. J.L.Atwood, J.E.D. Davies, D.D.Macnicol and F.Vôgtle), Pergamon, New York, Vol. 3, 1996, p. 287.

86. T. Osa and I. Suzuki, "Comprehensive Supramolecular Chemistry: Cyclodextrins "(Eds. J.L.Atwood, J.E.D. Davies, D.D.Macnicol and F.Vôgtle), Pergamon, New York, Vol. 3, 1996, p. 369-395.